SATBAYEV UNIVERSITY

ISSN 2959-2348 (Online)

ENGINEERING JOURNAL of Satbayev University

Volume 147 (Issue 4)
August 2025

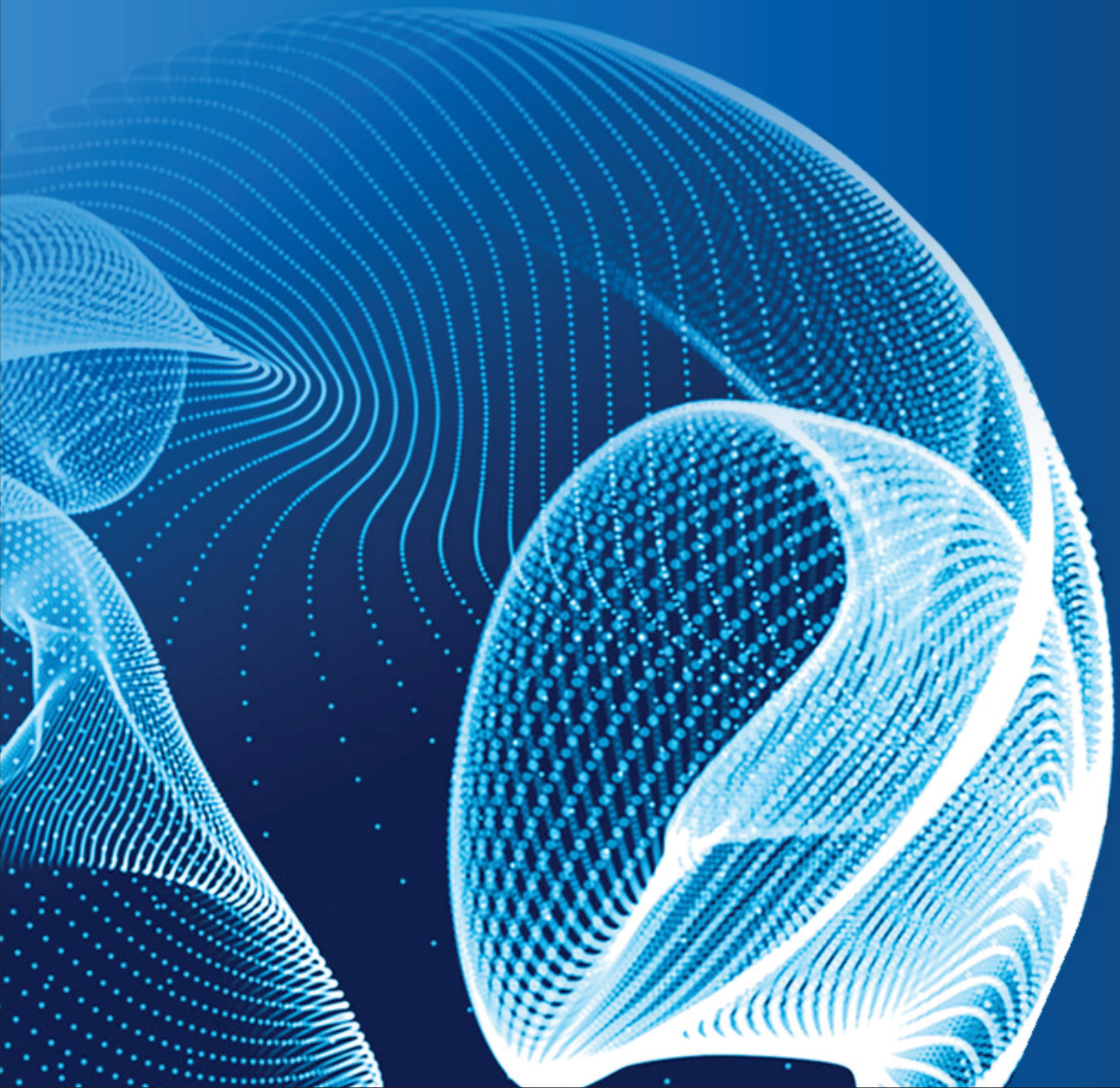

eISSN 2959-2348

eISSN 2959-2348

eISSN 2959-2348

SATBAYEV UNIVERSITY

Engineering Journal of Satbayev University

Volume 147 (2025), Issue 4, 1-8

https://doi.org/10.51301/ejsu.2025.i4.01

Thermodynamic calculations and construction of Ellingham and phase stability diagrams for the W-Ti-C-Co system

A.M. Alimzhanova[1], B.T. Sakhova[1,2*], A.Zh. Terlikbaeva[1], A.A. Mukhametzhanova[1], G.K. Maldybaev[1,3], N.M. Seidakhmetova[1], S.A. Vorotilo[4], G.M. Koishina[2]

[1]*National Center for Integrated Processing of Mineral Raw Materials of the Republic of Kazakhstan, Almaty, Kazakhstan*
[2]*Satbayev University, Almaty, Kazakhstan*
[3]*Kazakh-British Technical University, Almaty, Kazakhstan*
[4]*King Abdullah University of Science and Technology, Thuwal, Saudi Arabia*

**Corresponding author: banu_st@mail.ru*

Abstract. This study provides a thermodynamic analysis of phase equilibria and compound stability in the W–Ti–C–Co system using ab initio modeling, the Materials Project database, and HSC Chemistry 6. The focus is on identifying stable and metastable phases relevant to composite materials based on refractory metals and carbon with cobalt and titanium as alloying elements. Calculations yielded a list of characteristic phases, quaternary and ternary phase diagrams (Ti–W–C, Co–Ti–C, Co–W–C), Ellingham-type stability diagrams, and interfacial reaction maps. Mechanical properties were assessed via bulk and shear moduli, showing WC as the hardest and TiCo as the most ductile phase. The study predicts the likely formation of ternary carbides (W–Co, W–Ti), which strongly influence material properties. Fourteen interfacial reactions were identified, including carbide and intermetallic formation. Ellingham analysis showed Co_2C is unstable above ~400°C, and Co_7W_6 is unfavorable at all temperatures, while WC remains stable up to ~1400°C, beyond which W2C dominates. These results deepen the understanding of phase behavior in multicomponent metal – carbon systems and support the development of thermally stable, mechanically optimized materials.

Keywords: *thermodynamic modeling, phase diagram, Ellingham diagram, refractory materials, phase stability, bulk modulus, shear modulus.*

Received: 06 May 2025
Accepted: 15 August 2025
Available online: 31 August 2025

1. Introduction

In the context of increasing operational demands on cutting and forming tools, there is a growing need to develop new types of hard alloys with enhanced strength, thermal stability, and wear resistance [1, 2]. Among these, particular attention is given to dual-carbide cemented carbides based on the W–C–TiC–Co system, which are distinguished by their combination of high hardness and thermochemical stability [3]. However, the development of new compositions requires a deep understanding of phase equilibria and interfacial interactions in multicomponent systems, including rare and metastable compounds.

Of special interest is thermodynamic modeling and the construction of phase stability diagrams (Ellingham diagrams) and phase dominance maps for systems involving transition metals and carbon. The application of density functional theory (DFT) methods allows for a quantitative assessment of formation energies and the construction of highly accurate phase diagrams. These approaches have been successfully implemented in systems analogous to W–Ti–C–Co [4, 5], while the Materials Project database [6] offers a comprehensive platform for automated access to thermodynamic and structural properties of compounds based on ab initio calculations.

Previous studies have shown that W–Ti systems exhibit pronounced asymmetry in mixing energies and limited mutual solubility, particularly in the BCC lattice structure [7]. These features significantly affect phase stability and the formation of intermetallic compounds. At the same time, experimental investigations into Co–Ti and Co–W interactions have enabled the construction of isothermal sections and the identification of stable phases at temperatures ranging from 1273 to 1473 K [8].

In the W–C–Ti–Co system, carbide phases such as WC, TiC, and complex carbides of the (Ti,W)C type play a key role. These compounds are characterized by high cohesive energy, low self-diffusion coefficients, and increased metastability, making them especially relevant for high-temperature applications [9]. Furthermore, the stability of phase boundaries critically determines the reliability and service life of cemented carbides. To analyze interfacial interactions, phase reaction and phase dominance diagrams are constructed using computational tools based on the Materials API [6, 10].

The objective of this study is to construct phase diagrams and evaluate the thermodynamic stability of phases in the W–C–Ti–Co system using quantum mechanical modeling, machine learning, and statistical analysis.

aliyuchca@mail.ru; banu_st@mail.ru; alma_terlikbaeva@mail.ru; narike.91@mail.ru; galimjan_87@mail.ru; erkej@mail.ru; stepan.vorotylo@gmail.com; gulzada.koishina@mail.ru
Engineering Journal of Satbayev University. eISSN 2959-2348. Published by Satbayev University

2. Materials and methods

To construct the phase diagram and analyze phase equilibria in the quaternary W–C–Ti–Co system, a comprehensive approach based on ab initio modeling within the framework of density functional theory (DFT) was employed. The primary source of input data was the Materials Project database [10, 11, 5], which contains structural and energetic characteristics for over 100,000 inorganic compounds obtained through standardized DFT calculations.

To improve the accuracy of the electronic state descriptions for the transition metals W, Ti, and Co, formation enthalpy calculations were carried out using a hybrid GGA/GGA+U scheme. The use of GGA+U potentials allowed for correction of d-electron delocalization and ensured a more reliable assessment of compound stability [1]. The U parameters were selected in accordance with semi-empirically calibrated values provided by the Materials Project [10].

Phase diagrams were generated using the PDApp software, a component of the Materials API–a REST-based interface providing access to data on energies, compositions, and crystal structures [2, 7]. The calculations were based on the convex hull method, which made it possible to identify thermodynamically stable and metastable phases at a given temperature. Structural data were primarily sourced from the ICSD database, which contains experimentally validated lattice parameters, symmetries, and atomic coordinates [13].

To predict not-yet-discovered but potentially stable compounds, the modeling incorporated a machine learning–based approach [4]. This method combined data from known phases with DFT results, allowing for an expanded exploration of the phase space in the W–C–Ti–Co system. Probabilistic models were used to evaluate the stability of hypothetical compounds, enabling the prediction of possible stable phases not represented in experimental databases.

The morphology of interfacial boundaries and the evolution of phases under non-equilibrium conditions were studied using phase-field modeling [14], which accounted for kinetic aspects of phase transformations at high temperatures. This was especially relevant for assessing the stability of carbides, known for their high cohesive energy and metastability. According to [9], at 0 K, the median metastability of carbides reaches 144 meV/atom, compared to only about 20 meV/atom for most other compounds.

The methodology applied in this work provides high accuracy in constructing phase stability diagrams, identifying stable phases, and analyzing the behavior of the W–C–Ti–Co system under conditions that closely resemble those of real-world hard alloy synthesis.

3. Results and discussion

3.1. Thermodynamic modeling of phase equilibria and construction of the phase diagram for the W–C–Ti–Co system

The phase diagram of the quaternary W–C–Ti–Co system was constructed based on data obtained using the PDApp software and the Materials Project database. The analysis focused on thermodynamic stability, metastability, and potential decomposition pathways of compounds, carried out through the construction of phase stability diagrams and convex hull projections in composition space.

The resulting phase diagram reflects the thermodynamic stability of compounds in the W–C–Ti–Co system at temperatures up to 1000 K (Figure 1). The diagram's nodes are color-coded according to stability: green indicates thermodynamically stable phases, while yellow and red denote metastable compounds, whose degree of instability is defined by their positive energy deviation from the convex hull surface. The color of the rhombus overlaid on each node represents the magnitude of this deviation, ranging from moderate (yellow) to high (red) metastability.

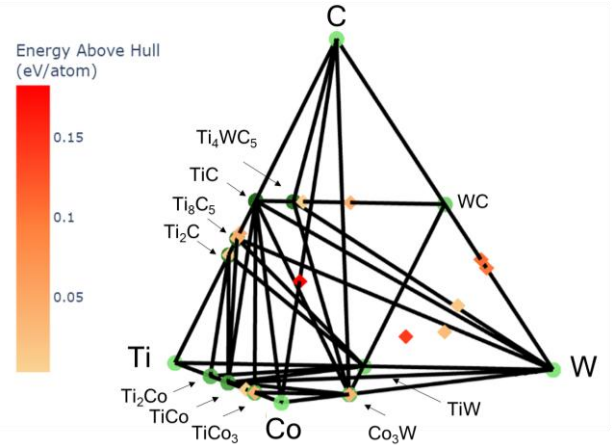

Figure 1. Phase diagram of the W–Ti–C–Co system

The black lines connecting the nodes represent projections of the Maxwell convex hull onto the compositional space. These connections form what are known as Gibbs triangles, with each vertex corresponding to a stable phase. Any point within such a triangle can be described as a mixture of the three phases located at its vertices. The phase composition and ratios of this mixture are determined by the lever rule, applied here in a higher-dimensional compositional space.

Special attention is given to green nodes overlaid with colored rhombuses, which indicate the presence of metastable «satellite» phases that share similar chemical compositions with certain «primary» stable compounds but differ in crystal structure. Examples of such systems include Co_3W, Ti_2C, Ti_8C_5, and $TiCo_3$. The existence of competing structural modifications can have important implications for synthesis conditions and the thermal history of the material.

To assess the potential mechanical properties of the compounds shown in the diagram, Table 1 presents their formation and decomposition energies, shear modulus, bulk modulus, and Pugh's ratio (G/B) [3]. Pugh's ratio serves as an indicator of a material's tendency toward plastic or brittle behavior: values below 0.5 suggest ductility, while values above this threshold indicate brittleness. The elastic modulus values were derived using machine learning algorithms trained on large DFT-based datasets [15].

The TiCo phase exhibits the lowest Pugh's ratio (G/B) among all compounds considered in the W–Ti–C–Co system, indicating its highest propensity for plastic deformation. In contrast, the WC phase displays the highest elastic moduli, reflecting its exceptional stiffness and potential brittleness under mechanical loading. Below are the crystal structures and brief descriptions of the equilibrium and metastable phases identified through the modeling of the system.

Table 1. Stable and metastable phases in the W–Ti–C–Co system

Stable Phases				
Phase	Formation energy, eV/atom	Shear modulus G, GPa	Bulk modulus B, GPa	Pugh's ratio (G/B)
Co_3W	- 0.084	140	179	0.782
Ti_2C	- 0.644	78	139	0.561
Ti_2Co	- 0.285	74	154	0.481
Ti_8C_5	- 0.719	115	170	0.676
TiC	- 0.81	176	253	0.696
TiCo	- 0.401	61	163	0.374
$TiCo_3$	- 0.262	83	194	0.428
TiW	- 0.02	94	206	0.456
WC	- 0.123	279	385	0.725
Co_2W_4C	- 0.067	130	320	0.406
Metastable Phases				
Phase	Decomposition energy, eV/atom	Decomposes into	Shear modulus G, GPa	Bulk modulus B, GPa	Pugh's ratio (G/B)
Co_2C	0.108	C + Co	110	257	0.428
Co_3W_3C	0.089	Co_3W + WC + W	129	308	0.419
$Co_6W_{20}C_7$	0.018	Co_3W + WC + W	141	330	0.427
Ti_3C_2	0.05	Ti_8C_5 + TiC	130	194	0.670
Ti_3WC_4	0.025	WC + TiC	184	280	0.657
Ti_4WC_5	0.019	WC + TiC	183	274	0.668
$TiCo_2$	0.006	$TiCo_3$ + TiCo	90	204	0.441
$TiWC_2$	0.07	WC + TiC	187	304	0.615
W_2C	0.065	WC + W	167	334	0.500
W_9C_4	0.072	WC + W	149	337	0.442

Cobalt carbide Co_2C

The compound Co_2C crystallizes in the orthorhombic crystal system, space group Pnnm, and adopts a hydrophilite-type structure (Figure 2).

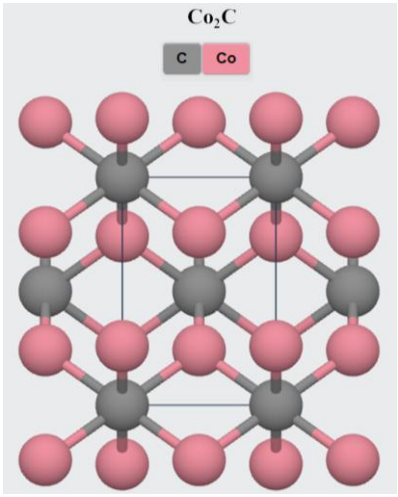

Figure 2. Crystal structure of the Co_2C phase

Its crystal structure is three-dimensional. Co^{2+} ions are in a trigonal planar coordination with three equivalent C^{4-} atoms; all Co–C bond lengths are 1.90 Å. Each carbon atom (C^{4-}) is surrounded by six equivalent Co^{2+} atoms, forming CCo_6 coordination octahedra that share edges and corners. The octahedral tilt angles are approximately 52°, indicating a distortion from ideal geometry and reflecting specific bonding features within this phase.

Titanium-cobalt intermetallics

The Ti_2Co phase crystallizes in the cubic space group Fd-3m and features a three-dimensional crystal structure (Figure 3).

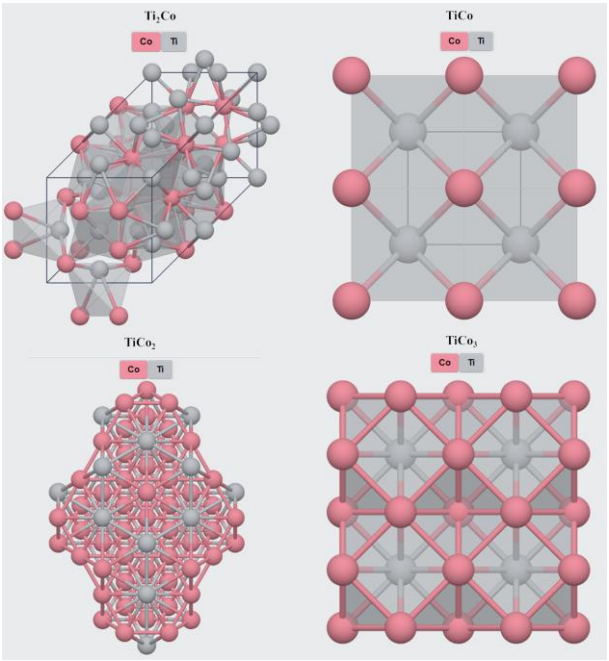

Figure 3. Crystal structures of titanium–cobalt intermetallics: Ti_2Co, TiCo, $TiCo_2$, $TiCo_3$

Two crystallographically distinct Ti positions are present. In the first site, the Ti atom is in a 12-fold coordination with six equivalent Co atoms; all Ti–Co bond lengths are 2.49 Å. In the second site, the Ti atom displays a distorted fourfold coordination with Co, comprising two shorter Ti–Co bonds at 2.53 Å and two longer ones at 2.87 Å. Co atoms are situated in a 9-fold coordination environment, each surrounded by nine Ti atoms.

The TiCo compound adopts the tetraauricupride-type structure and crystallizes in the cubic space group Pm-3m. The crystal structure is three-dimensional. Ti atoms occupy body-centered cubic positions and are coordinated by eight equivalent Co atoms, with uniform Ti–Co bond lengths of 2.58 Å. Likewise, Co atoms are in a body-centered cubic coordination, each surrounded by eight equivalent Ti atoms.

The $TiCo_2$ phase crystallizes in the hexagonal space group $P\bar{6}3/mmc$ and adopts a hexagonal Laves-type structure. The structure is three-dimensional and includes five crystallographically distinct titanium atomic sites. At each site, a titanium atom is coordinated in a 12-fold geometry with four titanium atoms and twelve cobalt atoms. In the first site, there is one shorter Ti–Ti bond (2.83 Å) and three longer ones (2.89 Å). The Ti–Co bond lengths range from 2.75 to 2.77 Å. In the second site, the bonding pattern is similar, with one shorter (2.83 Å) and three longer (2.89 Å) Ti–Ti bonds, and Ti–Co bond distances also ranging from 2.75 to 2.77 Å. At the third site, all Ti–Ti bond lengths are 2.89 Å, with Ti–Co distances again falling within 2.75–2.77 Å. In the fourth and fifth sites, all Ti–Ti bonds measure 2.89 Å. The Ti–Co bonds consist of six shorter (2.75 Å) and six longer (2.76 Å) distances.

Cobalt atoms occupy three crystallographically distinct sites. In the first and second sites, each cobalt atom is surrounded by six titanium and six cobalt atoms, forming mixed $CoTi_6Co_6$ cuboctahedra sharing faces, edges, and vertices. In the first cobalt site, there are three shorter (2.36 Å) and three longer (2.37 Å) Co–Co bonds; in the second site, all Co–Co bonds are 2.35 Å. In the third site, the local structure is simi-

lar, though the Co–Co bonds include two shorter (2.29 Å) and two longer (2.41 Å) distances, indicating some anisotropy in the coordination environment.

The compound Co_3Ti adopts the uranium silicide structure type and crystallizes in the cubic space group Pm–3m. The structure features a three-dimensional coordination network. Titanium atoms are coordinated by twelve equivalent cobalt atoms, forming $TiCo_{12}$ cuboctahedra. These polyhedra are interconnected: they share vertices with twelve equivalent $TiCo_{12}$ units, edges with twenty-four equivalent $CoTi_4Co_8$ cuboctahedra, and faces with six $TiCo_{12}$ and twelve $CoTi_4Co_8$ units. All Ti–Co bond lengths are 2.55 Å.

Cobalt atoms, in turn, are coordinated by four equivalent titanium atoms and eight cobalt atoms, forming $CoTi_4Co_8$ cuboctahedra. These structures share vertices with twelve similar $CoTi_4Co_8$ units, edges with eight $TiCo_{12}$ and sixteen $CoTi_4Co_8$ units, and faces with twelve $TiCo_{12}$ and four $CoTi_4Co_8$ cuboctahedra. All Co–Co bond distances are also 2.55 Å.

Ternary tungsten–titanium carbides

Ti_4WC_5 adopts the caswellsilverite-type structure ($NaCrS_2$) and crystallizes in the trigonal space group R–3m (Figure 4).

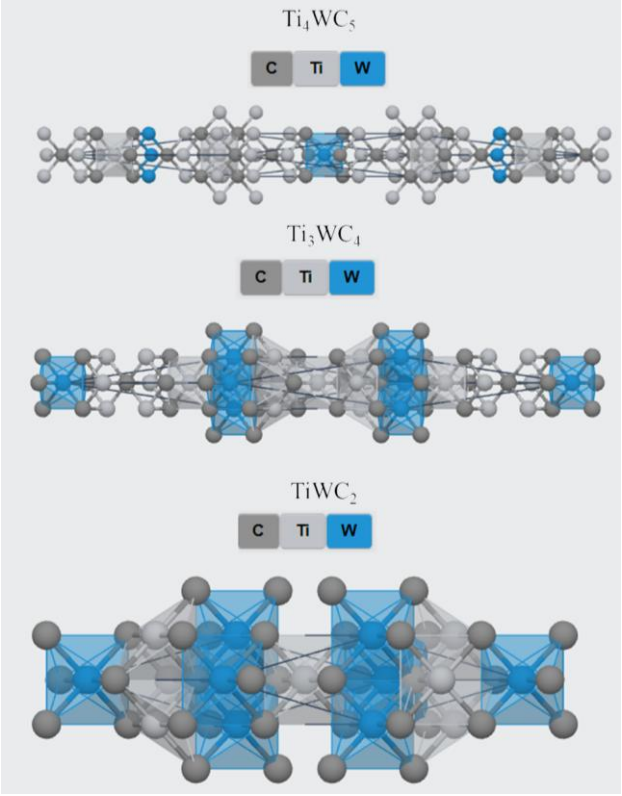

Figure 4. Crystal structures of ternary tungsten–titanium carbides: Ti_4WC_5, Ti_3WC_4, $TiWC_2$

The structure is three-dimensional and features two crystallographically distinct Ti^{4+} sites. In the first site, the Ti^{4+} ion is coordinated by six C^{4-} atoms, forming TiC_6 octahedra. These octahedra are corner-sharing with three equivalent TiC_6 octahedra and three WC_6 octahedra, and edge-sharing with three WC_6 and nine other TiC_6 octahedra. The tilt angles between corner-sharing octahedra range from 0° to 1°. Ti–C bond lengths vary slightly, with three shorter bonds at 2.16 Å and three longer ones at 2.18 Å.

In the second Ti^{4+} site, the ion is also surrounded by six C^{4-} atoms, forming TiC_6 octahedra that are connected via both corner- and edge-sharing. The tilt angles between adjacent octahedra also fall within the 0 e-1° range, and Ti–C bond lengths measure 2.17 Å and 2.18 Å. The W^{4+} ion is coordinated by six equivalent C^{4-} atoms to form regular WC_6 octahedra. These octahedra share corners with six TiC_6 octahedra and edges with six TiC_6 and six WC_6 octahedra. The tilt angles are 0°, and all W–C bond lengths are 2.17 Å.

There are three crystallographically distinct C^{4-} sites. In the first site, the C^{4-} atom is bonded to six Ti^{4+} ions, forming CTi_6 octahedra that share edges and corners. Tilt angles range from 0° to 1°. In the second site, the C^{4-} atom is also coordinated by six equivalent Ti^{4+} ions, forming a similar environment with no observable tilt (0°). In the third site, the C^{4-} ion is coordinated by three Ti^{4+} and three W^{4+} ions, forming CTi_3W_3 octahedra that share both edges and corners, with tilt angles also in the range of 0° to 1°.

$WTiC_2$ also crystallizes in the caswellsilverite-type structure (R–3m) and exhibits a three-dimensional framework. The Ti^{4+} ion is coordinated by six equivalent C^{4-} atoms, forming TiC_6 octahedra. These polyhedra share corners with six WC_6 octahedra and edges with six TiC_6 and six WC_6 octahedra. The tilt angles are 0°, and Ti–C bond lengths are 2.17 Å. The W^{4+} ion is likewise coordinated by six equivalent C^{4-} atoms in WC_6 octahedra. These are corner-sharing with six TiC_6 octahedra and edge-sharing with six TiC_6 and six WC_6 octahedra. The octahedra are nearly ideal, with 0° tilt angles and W–C bond lengths of 2.18 Å. Each C^{4-} ion is bonded to three equivalent Ti^{4+} and three equivalent W^{4+} ions, forming mixed CTi_3W_3 octahedra that are interconnected via shared edges and corners. The tilt angles are 0°, indicating high symmetry and a highly regular crystal structure.

3.2. Calculation of stability and phase dominance diagrams in the W–Ti–C–Co system

To analyze phase interactions at the interface between primary and secondary phases, interfacial reaction diagrams were constructed using the Interface Reaction App software.

Figure 5 shows the interaction diagram between the WC and Co phases. Only a single reaction (Reaction 1) is possible between them. The interaction between tungsten carbide and cobalt can lead to the formation of the intermetallic compound Co_3W and elemental carbon.

$$0.75Co+0.25WC \rightarrow 0.25Co_3W+0.25C \quad (E= -2.222\ kJ/mol). \quad (1)$$

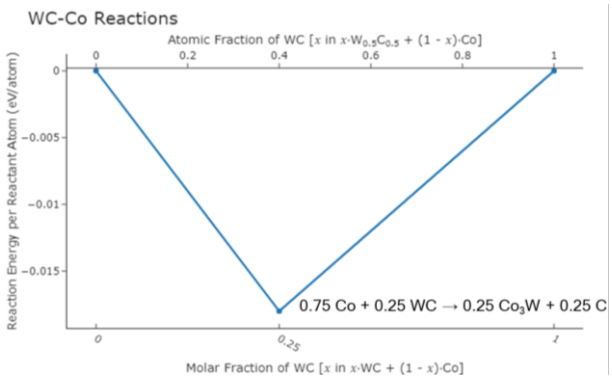

Figure 5. Interfacial reaction diagram between WC and Co phases

Figure 6 presents the interaction diagram between the WC and Ti phases. Four possible reactions (Reactions 2-5) can occur between them. The interaction of tungsten carbide with titanium may lead to the formation of the intermetallic compound TiW, titanium carbides Ti_2C, Ti_8C_5, and TiC, as well as elemental tungsten.

$0.75Ti+0.25WC \rightarrow 0.25TiW+0.25Ti_2C$ (E = -41.64 kJ/mol); (2)

$0.667Ti+0.333WC \rightarrow 0.333Ti_2C+0.333W$ (E = -54.23 kJ/mol); (3)

$0.615Ti+0.385WC \rightarrow 0.077Ti_8C_5+0.385W$ (E = -60.28 kJ/mol); (4)

$0.5Ti+0.5WC \rightarrow 0.5W+0.5TiC$ (E = -66.32 kJ/mol). (5)

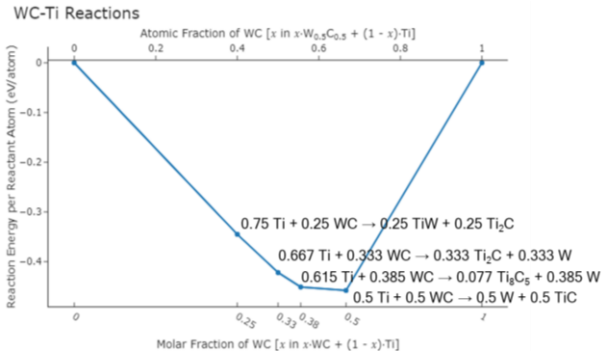

Figure 6. Interfacial reaction diagram between WC and Ti phases

Figure 7 presents the interaction diagram between the Co_3W and Ti phases. Four possible reactions (Reactions 6-9) can occur between them. The interaction between the intermetallic compound Co_3W and titanium may lead to the formation of intermetallics $TiCo_3$, Ti_2Co, TiCo, TiW, as well as elemental tungsten.

$0.125Co_3W+0.875Ti \rightarrow 0.375Ti_2Co+0.125TiW$ (E = -27.34 kJ/mol); (6)

$0.143Co_3W+0.857Ti \rightarrow 0.429Ti_2Co+0.143W$ (E = -30.69 kJ/mol); (7)

$0.25Co_3W+0.75Ti \rightarrow 0.75TiCo+0.25W$ (E = - 49.83 kJ/mol); (8)

$0.5Co_3W+0.5Ti \rightarrow 0.5TiCo_3+0.5W$ (E = -34.22 kJ/mol). (9)

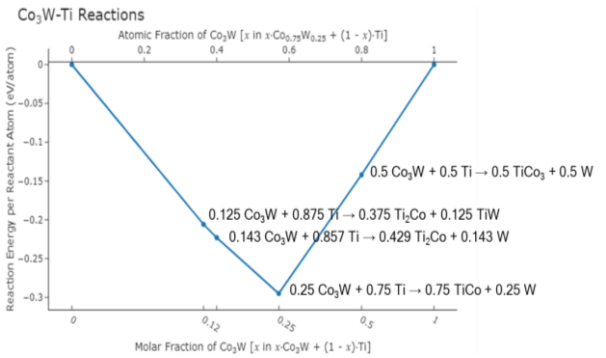

Figure 7. Interfacial reaction diagram between Co_3W and Ti phases

$0.9Co+0.1Ti_8C_5 \rightarrow 0.3TiCo_3+0.5TiC$ (E = -18.26 kJ/mol); (10)

$0.75Co+0.25Ti_8C_5 \rightarrow 0.75TiCo+1.25TiC$ (E= -27.86 kJ/mol). (11)

Figure 8 presents the interaction diagram between the Ti_8C_5 and Co phases. Two possible reactions (Reactions 10–11) can occur between them.

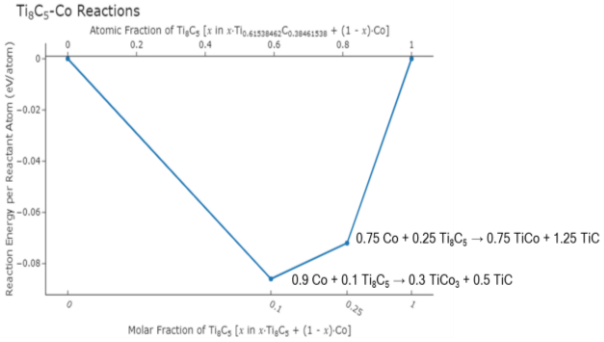

Figure 8. Interfacial reaction diagram between Ti_8C_5 and Co phases

The interaction of Ti_8C_5 carbide with cobalt may lead to the formation of the intermetallic compounds $TiCo_3$ and TiCo, as well as TiC carbide.

Analysis of the interfacial reaction diagrams indicates that a variety of chemical transformations are possible within the W–Ti–C–Co system, resulting in the formation of intermetallic compounds and carbides. The most energetically favorable reactions occur between WC and Ti (particularly those forming TiC and W), as well as between Co_3W and Ti.

Figure 9 shows the phase stability diagram (Ellingham diagram) for the W–Ti–Co–C system, constructed using the HSC Chemistry 6 software package. The diagram illustrates the change in Gibbs free energy (ΔG) of formation for various compounds as a function of temperature. It should be noted that the diagram includes only those phases for which data are available in the HSC Chemistry 6 database. Specifically, information is lacking on Ti–W and Ti–Co intermetallics, as well as on lower titanium carbides and ternary carbides based on tungsten and cobalt.

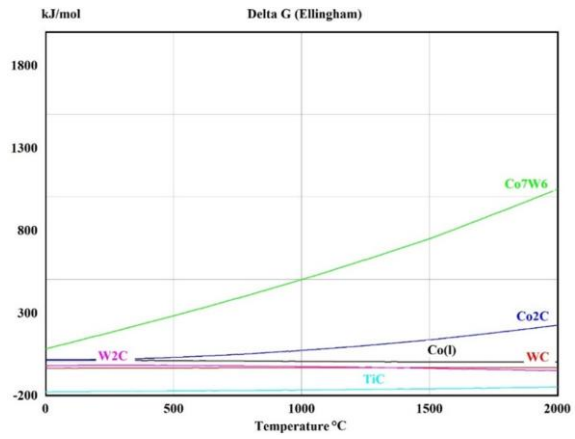

Figure 9. Ellingham-type phase stability diagram for the W–Ti–Co–C system

Based on the phase stability diagram, it can be concluded that Co_2C is thermally unstable at temperatures above approximately 400°C, which limits its applicability in high-temperature processes. Metallic cobalt (Co^0) retains moderate stability but does not form stable carbides at elevated temperatures. Tungsten carbide (WC) remains stable up to ~1400°C; above this temperature, the more stable subcarbide W_2C be-

comes dominant. The compound Co_7W_6 is thermodynamically unstable across the entire temperature range ($\Delta G > 0$).

The phase dominance diagrams shown in Figure 10 were constructed using the HSC Chemistry 6 software package.

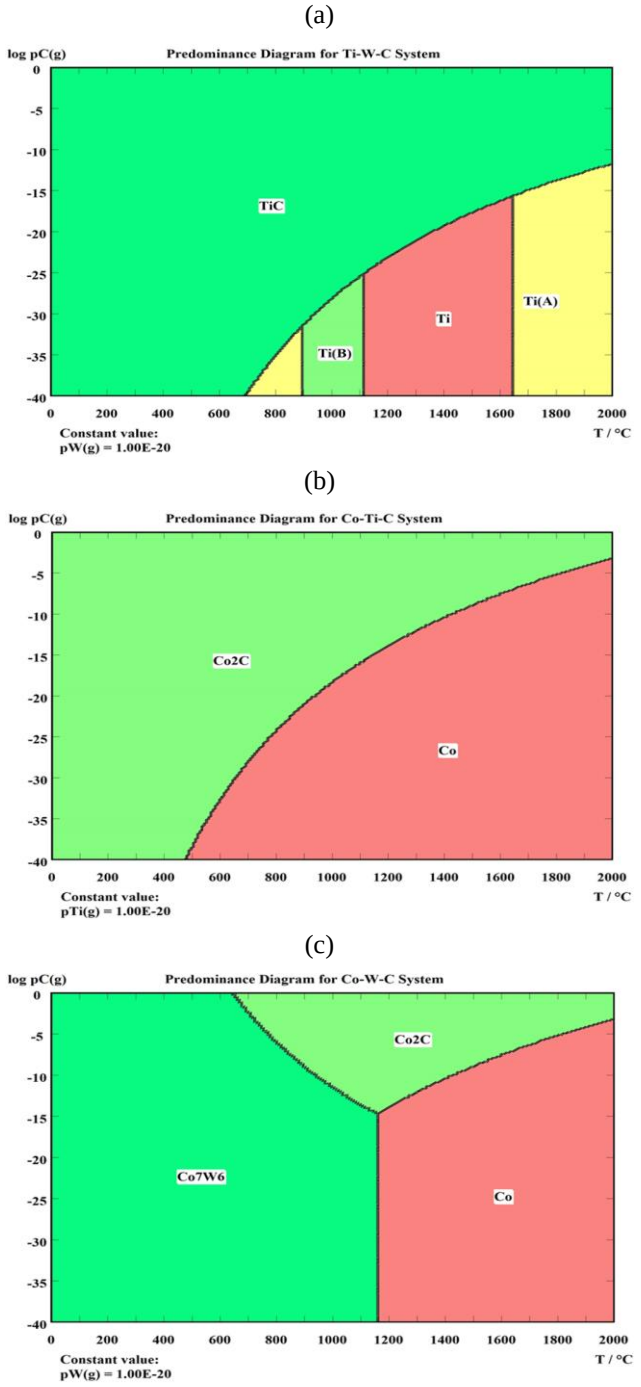

Figure 10. Phase dominance diagrams for ternary systems: (a) – Ti–W–C, (b) – Co–Ti–C, (c) – Co–W–C

These diagrams reflect the thermodynamically most stable phases in the corresponding ternary systems at a given temperature and the partial pressure of one component, assuming the vapor pressure of the second component remains constant. The diagrams were constructed for the Ti–W–C (Figure 10a), Co–Ti–C (Figure 10b), and Co–W–C (Figure 10c) systems. The obtained data enable assessment of the phase stability under conditions approximating real-world processes and contribute to a deeper understanding of phase transformations in multiphase metal – carbon systems.

4. Conclusions

As a result of the conducted research using thermodynamic modeling and the Materials Project ab initio database, a comprehensive analysis of phase equilibria and compound stability in the multiphase W–Ti–C–Co system has been carried out. Based on the calculations, a list of stable and metastable phases characteristic of the system was compiled, and a corresponding quaternary phase diagram was constructed. For each identified phase, bulk and shear moduli were calculated, enabling a comparative analysis of their mechanical properties. It was established that tungsten carbide (WC) is the hardest compound in the system, while the intermetallic TiCo exhibits the highest ductility.

The analysis confirmed the possibility of forming several stable ternary carbide phases, particularly tungsten–cobalt and tungsten–titanium compounds, both in stable and metastable forms. The constructed Ellingham phase stability diagrams, interfacial reaction diagrams, and phase dominance diagrams for the ternary subsystems Ti–W–C, Co–Ti–C, and Co–W–C demonstrated the thermodynamic feasibility of new phase formation at interfaces between components. Fourteen potential reactions were identified, indicating the potential for a wide range of intermetallic and carbide compounds to form as a result of interactions between primary and secondary phases.

Thus, the obtained results not only expand current understanding of phase transformations in refractory metal – carbon systems, but also provide a foundation for the targeted selection of composite materials with tailored mechanical properties, as well as for optimizing synthesis and heat treatment parameters.

Author contributions

Conceptualization: AMA, BTS, NMS; Data curation: AMA, BTS, AAM; Formal analysis: GKM, SAV; Funding acquisition: AZT, GMK; Investigation: AMA, BTS, AAM; Methodology: AMA, SAV, NMS; Project administration: AZT; Resources: AMA, GMK, NMS, GKM; Software: AMA, BTS, AAM; Supervision: AMA, AZT; Validation: SAV, AAM; Visualization: BTS, GKM; Writing – original draft: AMA, BTS, AAM; Writing – review & editing: AMA, BTS, SAV, GMK. All authors have read and agreed to the published version of the manuscript.

Funding

This research received no external funding.

Acknowledgements

The authors express their sincere gratitude to the editor and anonymous reviewers for their constructive comments and valuable suggestions, which have significantly improved the quality of this manuscript.

Conflicts of interest

The authors declare no conflict of interest.

Data availability statement

The original contributions presented in this study are included in the article. Further inquiries can be directed to the corresponding author.

References

[1] Fal'kovskii, V.A., & Kliachko, LI. (2005). Hard alloys. *Moscow: Ruda i metally*

[2] Andrievskii, R.A., & Ragulia, A.V. (2005). Nanostructured materials. *Moscow: Akademiia*

[3] Pugh, S.F. (1954). XCII. Relations between the elastic moduli and the plastic properties of polycrystalline pure metals. *The London, Edinburgh, and Dublin Philosophical Magazine and Journal of Science, 45(367), 823-843.* https://doi.org/10.1080/14786440808520496

[4] Hautier, G., Fischer, C.C., Jain, A., Mueller, T. & Ceder, G. (2010). Finding nature's missing ternary oxide compounds using machine learning and density functional theory. *Chemistry of Materials, 22(12), 3762-3767.* https://doi.org/10.1021/cm100795d

[5] Ong, S.P., Jain, A., Hautier, G., Kang, B. & Ceder, G. (2010). Thermal stabilities of delithiated olivine MPO4 (M = Fe, Mn) cathodes investigated using first principles calculations. *Electrochemistry Communications, 12(3), 427-430.* https://doi.org/10.1016/j.elecom.2010.01.010

[6] Ong, S.P., Cholia, S., Jain, A., Brafman, M., Gunter, D., Ceder, G. & Persson, K.A. (2015). The Materials Application Programming Interface (API): A simple, flexible and efficient API for materials data based on Representational State Transfer (REST) principles. *Computational Materials Science, 97, 209-215.* https://doi.org/10.1016/j.commatsci.2014.10.037

[7] Ångqvist, M.A., Rahm, J.M., Gharaee, L., &Erhart, P. (2019). Phase diagram of the Ti–W system from first-principles. *arXiv preprint. arXiv:1904.04814.* https://arxiv.org/abs/1904.04814

[8] Shi, Y., Guo, C., Li, C., Du, Z., & Hu, D. (2022). Experimental investigation of isothermal sections in the Co–Ti–W system. *Frontiers in Materials, (9), 880143.* https://doi.org/10.3389/fmats.2022.880143

[9] Bartel, C.J., Millican, S.L., Deml, A.M., Rumptz, J. R., Tumas, W., Weimer, A.W., & Holder, A.M (2018). Physical descriptor for the Gibbs energy of inorganic crystalline solids and temperature-dependent materials chemistry. *Nature Communications, (9), 4168.* https://doi.org/10.1038/s41467-018-06682-4

[10] Jain, A., Hautier, G., Ong, S. P., Moore, C., Fischer, C.C., Persson, K.A. & Ceder, G. (2011). Formation enthalpies by mixing GGA and GGA+U calculations. *Physical Review B, 84(4), 045115.* https://doi.org/10.1103/PhysRevB.84.045115

[11] Ong, S.P., Wang, L., Kang, B. & Ceder, G. (2008). The Li–Fe–P–O2 phase diagram from first principles calculations. *Chemistry of Materials, 20(5), 1798-1807.* https://doi.org/10.1021/cm702327g

[12] Richards, W.D., Miara, L.J., Wang, Y., Kim, J.C. & Ceder, G. (2016). Interface stability in solid-state batteries. *Chemistry of Materials, 28(1), 266-273.* https://doi.org/10.1021/acs.chemmater.5b04082

[13] Belsky, A., Hellenbrandt, M., Karen, V.L. & Luksch, P. (2002). New developments in the Inorganic Crystal Structure Database (ICSD): Accessibility in support of materials research and design. *Acta Crystallographica Section B: Structural Science, 58(3), 364–369.* https://doi.org/10.1107/S0108768102006948

[14] Folch, R., Plapp, M. (2005). Quantitative phase-field modeling of two-phase growth. *Physical Review E, 72(1), 011602.* https://doi.org/10.1103/PhysRevE.72.011602

[15] De Jong, M., Chen, W., Notestine, R., Persson, K., Ceder, G., Jain, A., Asta, M. & Gamst, A. (2016). A statistical learning framework for materials science: Application to elastic moduli of k-nary inorganic polycrystalline compounds. *Scientific Reports, (6), 34256.* https://doi.org/10.1038/srep34256

W–Ti–C–Co жүйесі үшін эллингемнің фазалық тұрақтылық диаграммасы мен фазалық басымдық диаграммасын құру және термодинамикалық есептеулер

А.М. Алимжанова[1], Б.Т. Сахова[1,2*], А.Ж. Терликбаева[1], А.А. Мухаметжанова[1], Г.К. Малдыбаев[1,3], Н.М. Сейдахметова[1], С.А. Воротыло[4], Г.М. Койшина[2]

[1]*Қазақстан Республикасының минералдық шикізатты кешенді қайта өңдеу жөніндегі ұлттық орталығы, Алматы, Қазақстан*
[2]*Satbayev University, Алматы, Қазақстан*
[3]*Қазақстан-Британ техникалық университеті, Алматы, Қазақстан*
[4]*Король Абдалла атындағы ғылыми-технологиялық университеті, Тувал, Сауд Арабиясы*

**Корреспонденция үшін автор: banu_st@mail.ru*

Аңдатпа. Осы зерттеуде W–Ti–C–Co жүйесіндегі фазалық тепе-теңдік пен қосылыстардың тұрақтылығына термодинамикалық талдау жасалды. Зерттеу ab initio модельдеу, Materials Project дерекқоры және HSC Chemistry 6 бағдарламалық пакеті негізінде жүргізілді. Негізгі мақсат - кобальт пен титан легирлеуші элементтер ретінде қолданылатын отқа төзімді металлдар мен көміртекке негізделген композициялық материалдарда түзілуі мүмкін тұрақты және метастабильді фазаларды анықтау. Есептеулер нәтижесінде жүйеге тән фазалардың тізімі, төрт компонентті және үш компонентті фазалық диаграммалар (Ti–W–C, Co–Ti–C, Co–W–C), Эллингем типті тұрақтылық диаграммалары мен фазалық өзара әрекеттесу карталары жасалды. Фазалардың механикалық қасиеттері көлемдік және ығысу модульдері арқылы бағаланды: ең қаттысы – вольфрам карбиді (WC), ал ең иілгіш қосылыс – TiCo интерметаллиді. Зерттеу барысында W–Co және W–Ti құрамды үштік карбидтердің түзілу ықтималдығы жоғары екені анықталды, бұл материал қасиеттеріне айтарлықтай әсер етеді. Барлығы 14 ықтимал фазалық өзара әрекеттесу реакциясы анықталды, олардың ішінде әртүрлі интерметалдық және карбидтік қосылыстар бар. Эллингем диаграммасына сәйкес, Co_2C ~400°C жоғары температурада термиялық тұрақсыз, ал Co_7W_6 барлық температурада термодинамикалық тұрғыдан тұрақсыз. WC ~1400°C дейін тұрақты болып қала береді, одан жоғары температурада W_2C басым фазада болады. Бұл нәтижелер металл-көміртек көпкомпонентті жүйелеріндегі фазатүзілуді терең түсінуге және жылу тұрақтылығы мен механикалық қасиеттері жоғары жаңа материалдарды жобалауға негіз болады.

Негізгі сөздер: *термодинамикалық модельдеу, фазалық диаграмма, Эллингем диаграммасы, отқа төзімді материалдар, фаза тұрақтылығы, көлемдік серпімділік модулі, ығысу модулі.*

Термодинамические расчеты и построение диаграмм фазовой стабильности Эллингхема и фазового доминирования для системы W–Ti–C–Co

А.М. Алимжанова[1], Б.Т. Сахова[1,2*], А.Ж. Терликбаева[1], А.А. Мухаметжанова[1], Г.К. Малдыбаев[1,3], Н.М. Сейдахметова[1], С.А. Воротыло[4], Г.М. Койшина[2]

[1]*Национальный центр по комплексной переработке минерального сырья Республики Казахстан, Алматы, Казахстан*
[2]*Satbayev University, Алматы, Казахстан*
[3]*Казахстанско-Британский технический университет, Алматы, Казахстан*
[4]*Научно-технологический университет имени короля Абдаллы, Тувал, Саудовская Аравия*

**Автор для корреспонденции: banu_st@mail.ru*

Аннотация. В настоящем исследовании представлен термодинамический анализ фазовых равновесий и устойчивости соединений в системе W–Ti–C–Co с использованием ab initio моделирования, базы данных Materials Project и программного комплекса HSC Chemistry 6. Основное внимание уделено выявлению стабильных и метастабильных фаз, характерных для композиционных материалов на основе тугоплавких металлов и углерода с добавками кобальта и титана. Проведенные расчеты позволили определить перечень характерных фаз, построить четвертичную и тройные фазовые диаграммы (Ti–W–C, Co–Ti–C, Co–W–C), диаграммы устойчивости типа Эллингема и карты межфазных реакций. Механические свойства оценивались по значениям объемного и сдвигового модулей: карбид вольфрама (WC) оказался самым твердым, а интерметаллид TiCo – наиболее пластичным. Установлена высокая вероятность образования тройных карбидов (W–Co, W–Ti), существенно влияющих на свойства материала. Выявлены 14 возможных межфазных реакций, включая образование карбидов и интерметаллидов. Анализ диаграммы Эллингема показал, что соединение Co_2C термически неустойчиво выше ~400°C, а Co_7W_6 термодинамически невыгоден во всем температурном диапазоне. WC стабилен до ~1400°C, после чего доминирует W_2C. Результаты исследования способствуют углубленному пониманию фазообразования в многокомпонентных металл-углеродных системах и формируют научную базу для создания термостойких материалов с заданными механическими свойствами.

Ключевые слова: *термодинамическое моделирование, диаграмма фазовых состояний, диаграмма Эллингема, огнеупорные материалы, фазовая стабильность, модуль объёмной упругости, модуль сдвига.*

SATBAYEV UNIVERSITY

Engineering Journal of Satbayev University

Volume 147 (2025), Issue 4, 9-15

https://doi.org/10.51301/ejsu.2025.i4.02

Thermomechanical processing of HSLA steels: Overview

U.K. Kakimov*, A.A. Kaipova

Satbayev University, Almaty, Kazakhstan

**Corresponding author: u.kakimov@satbayev.university*

Abstract. Thermomechanical processing of steels is an advanced process for producing high-strength steels. Low-alloy high-strength steel grades have a wide range of applications in the production of large-diameter pipes for transporting oil and gas. The application of API grades like X70 steels in pipe rolling production has led to a reduction in metal consumption and energy expenses for their production. Warm rolling or controlled rolling is one of the advanced technological modes of steel processing, which is described in this article. Therefore, it needs to be emphasized that high-strength low-alloy (HSLA) steels have gained significant attention due to their superior mechanical properties and cost-effectiveness in various industrial applications. Thermomechanical processing (TMP) plays a crucial role in optimizing the microstructure and mechanical performance of these steels. This paper explores the fundamental principles of TMP, including controlled rolling, accelerated cooling, and precipitation strengthening. The impact of processing parameters on grain refinement, phase transformations, and mechanical properties is discussed. Advances in TMP techniques, such as direct quenching and ultra-fast cooling, are also highlighted. Understanding these processes enables the development of HSLA steels with enhanced strength, toughness, and weldability. The paper also contains experimental part regarding to plane strain compression test results, which is modelling thermomechanical processing of HSLA steels.

Keywords: *HSLA steels, thermomechanical processing, microstructure, controlled rolling, accelerated cooling, phase transformation, precipitation strengthening.*

Received: 12 May 2025
Accepted: 15 August 2025
Available online: 31 August 2025

1. Introduction

The rapid development of the oil and gas industry has led to an increase in hydrocarbon consumption and, accordingly, to the construction of main oil and gas pipelines. Accordingly, there was a need to produce large diameter pipes. The development of steel grades from the X50 to X100 series has led to a decrease in metal consumption and an increase in strength characteristics.

High-strength low-alloy (HSLA) steels are a class of steel designed to provide improved mechanical properties compared to conventional carbon steels while maintaining cost efficiency. These steels achieve their superior strength and toughness through microalloying and TMP. The key to optimizing HSLA steel properties lies in carefully controlling deformation and thermal cycles during processing [1].

This paper provides an in-depth analysis of TMP, including its effects on grain refinement, precipitation strengthening, and phase transformations. The latest advancements in processing techniques are also discussed.

TMP combines mechanical deformation with controlled thermal treatments to manipulate the microstructure of HSLA steels. It includes grain refinement to enhance strength and toughness, controlled phase transformations for microstructural optimization and precipitation strengthening through microalloy additions such as Nb, Ti, and V etc. [2-7].

TMP typically involves the following key stages [8]:

1. Controlled rolling, where deformation is applied at specific temperature ranges to control recrystallization and grain size.
2. Accelerated cooling, when rapid cooling rates adjust phase transformations, refining microstructure and enhancing strength.
3. Precipitation hardening, the controlled formation of fine precipitates to improve yield strength.

1.1 Effects of TMP on microstructure and properties

One of the primary benefits of TMP is its ability to refine grain structure. Fine-grained microstructures enhance yield strength, toughness, and resistance to brittle fracture. The application of controlled rolling below the recrystallization temperature suppresses grain growth, resulting in finer structures [8-10].

The microstructural evolution during TMP significantly affects the final properties of HSLA steels. The key phase transformations include ferrite formation at high temperatures, improving ductility; bainitic or martensitic transformation in accelerated cooling, enhancing strength; retained austenite stabilization for improved toughness.

Microalloyed HSLA steels contain Nb, Ti, or V, which form fine precipitates during processing (Figures 1, 2). These precipitates hinder dislocation movement, improving yield strength without compromising ductility. The precise control of precipitation kinetics is essential for achieving the desired mechanical performance.

u.kakimov@satbayev.university; a.kaipova@satbayev.university
Engineering Journal of Satbayev University. eISSN 2959-2348. Published by Satbayev University

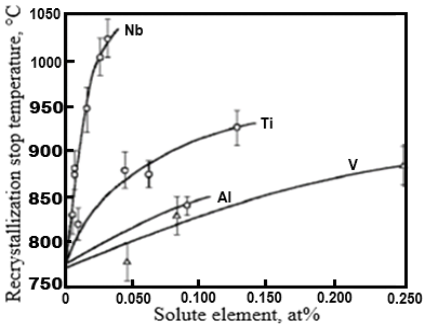

Figure 1. Influence of microalloying elements on recrystallization stop temperature in steel 0.07C-0.225Si-1.40Mn [2]

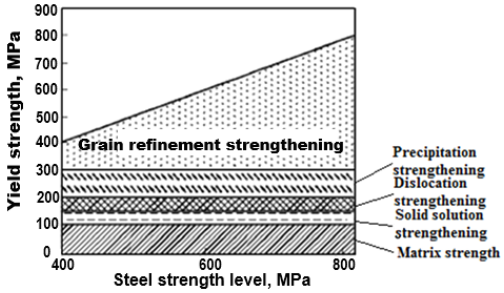

Figure 2. Effects of different strengthening mechanisms [2]

Grain refinement is a strengthening mechanism that provides the advantage of high strength combined with a low impact transition temperature (ITT). Unlike other strengthening methods, grain refinement improves or maintains toughness without compromising it.

In ferritic steels, grain refinement is typically achieved through thermomechanical processing. This involves precise control over austenite grain growth, which is suppressed using microalloying elements such as titanium (Ti) and niobium (Nb) during the reheating and rough rolling stages. These elements form stable precipitates that pin the grain boundaries of austenite, preventing excessive grain growth.

As a result, the austenite grains become pancaked-flattened due to deformation – by the end of the rolling process. Upon cooling, the transformation from austenite (γ) to ferrite (α) leads to the formation of fine ferrite grains, thereby achieving the desired grain refinement.

Another key parameter associated with grain refinement is the interfacial boundary area (S_v) of ferrite grains. It is necessary to highlight that a higher S_v, resulting from austenite pre-transformation, contributes significantly to ferrite grain refinement. For this reason, the steel is reheated above the austenite recrystallization temperature (T_{RXN}) and then subjected to rolling, promoting the formation of fine, equiaxed grains compared to the basic coarser structure. Consequently, the decrease in grain size leads to rise significantly of grain boundary area, thereby enhancing the S_v value simultaneously.

1.2. Advanced thermomechanical processing techniques

Recent advancements in TMP have led to novel techniques designed to further enhance HSLA steel properties. Some notable developments include Direct quenching (DQ), rapid quenching immediately after controlled rolling improves hardness and strength; Ultra-fast cooling (UFC), extreme cooling rates enhance the formation of bainitic and martensitic microstructures; Thermal-mechanical control processing (TMCP) (Figure 3), an optimized combination of rolling and controlled cooling enhances strength-toughness balance [3].

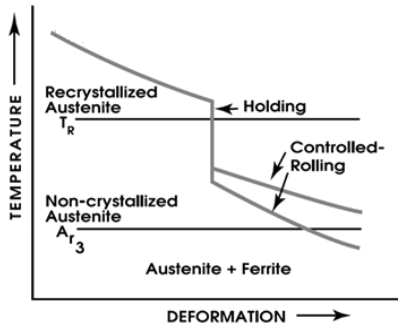

Figure 3. Schematic diagram of controlled rolling [5]

A major difference between thermomechanical processing (TMP) and conventional hot rolling (CHR) lies in the reheating, rough rolling, and final rolling temperatures, which are generally higher in CHR than in TMP. Moreover, TMP employs a faster cooling rate following the finishing rolling stage compared to CHR, contributing to significant differences in microstructural evolution.

Further development in this field led to the improvements of recrystallization-controlled rolling (RCR) – a variant of CR. In RCR, both rough and finishing rolling passes are carried out above the austenite recrystallization temperature (T_{RXN}), ensuring the formation of fine, equiaxed austenite grains. During cooling, these transform into fine ferrite grains, thereby enhancing the mechanical properties of the final steel product.

The advent of controlled rolling (CR) marked a pivotal development in steel processing, with its primary objective being the precise control of microstructure evolution during deformation. This is achieved by conducting rolling operations within the non-recrystallized austenite region, which promotes the formation of refined ferrite grains upon transformation.

1.3. Applications of thermomechanical processed HSLA steels

HSLA steel processed via TMP are widely used in industries requiring high strength and toughness, including lightweight components with high crash resistance in automotive industry, structural beams and bridges with superior load-bearing capacity in construction; high-strength, weldable steels for oil and gas transportation in pipeline industry; tough and corrosion-resistant materials for marine environments in shipbuilding. In automotive industry in terms of weight reduction enables lighter vehicle designs while maintaining safety and performance, in shipbuilding considering weight saving TMP improves fuel efficiency without compromising structural integrity.

2. Materials and methods

2.1. Sample preparation and characterization procedure

Experimental samples (60×30×10 mm) are machined and prepared in form of rolled plates of steel grade S460, similar to X70 [11-13]. The composition of the steel is shown in Table 1. Evaluated region of samples is rolling-transverse direction. Therefore, deformed samples were cut along in longitudinal direction and the cross section of transverse direction was assessed for microstructural analysis. Then samples were mounted, grounded manually, polished down to 1μm and etched in 2% nital for 20 sec. The samples dimensions are schematically shown in Figure 4.

Table 1. Chemical composition for plate steel S460

Alloying element	%
C	0.13
Si	0.49
Mn	1.49
Ni	0.019
Cu	0.012
Cr	0.061
Mo	0.002
V	0.071
Nb	0.035
Ti	0.003
Al	0.039

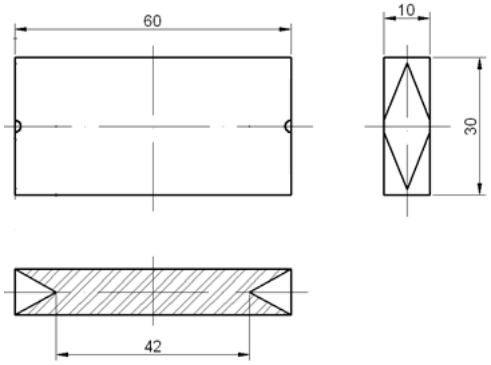

Figure 4. Experimental sample dimensions [4]

2.2. Plain strain compression test

Samples were deformed at four temperatures: 800°C, 750°C, 725°C and 700°C. Chosen temperatures considered as intercritical region on Fe_3C diagram and employed as finishing rolling temperature range for thermomechanical processing. Tools of deformation is shown in Figure 5.

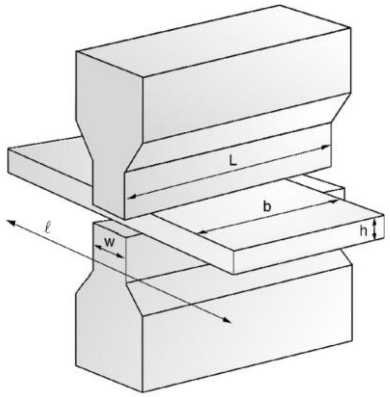

Figure 5. Deformation tool for plane strain compression test [5]

PSC test started with heating of the sample at a rate of 13°C/s up to 1050°C in two minutes. Then the sample was cooled down to the temperature of intercritical region and held up to 250 seconds. Then samples were deformed at $\varepsilon = 0.3$ and further subjected to accelerated cooling (10°C/s) down to room temperature. In Figure 6 PSC test is shown schematically.

2.3. Metallographic analysis

Samples were observed on a light microscope with magnification of 50× and 100×. Each of the micrographs taken was assessed by quantitative method to carry out the metallographic analysis to define ferrite grain size [13].

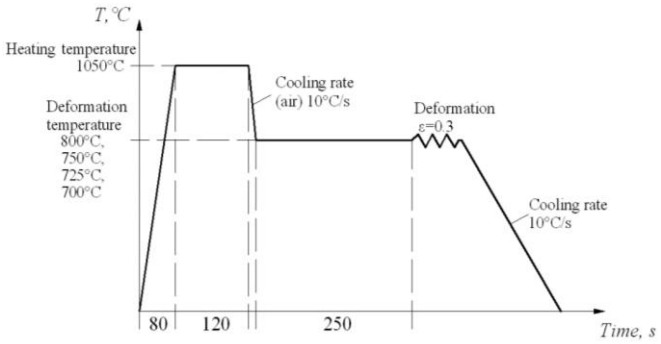

Figure 6. Schematic diagram of PSC test

2.4. Measurement of hardness

Measurement of the hardness of deformed and non-deformed regions of the samples, the Vickers hardness test was employed [14-15]. A measured hardness data is shown in Table 1.

3. Results and discussion

3.1. Modelling of flow stress

The flow stress of samples was measured according to the good practice guideline [5]. The flow stress curves are shown in Figure 7. The maximum stress value (σ = 310 MPa) was indicated at 700°C, whereas the minimum stress value (σ = 255 MPa) was at 750°C. The deformation at 800°C shows stress value equal to 264 MPa.

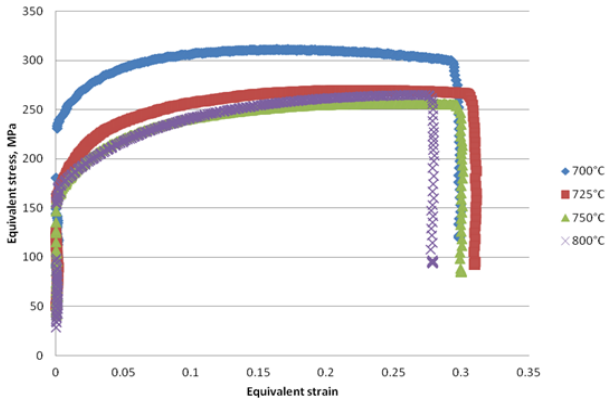

Figure 7. Equivalent stress vs. equivalent strain curve at different deformation temperature range

The flow stress curves of four samples show different yield points. The maximum value was observed at 700°C (σ = 230 MPa), whereas the minimum value was at 800°C (σ = 130 MPa). Nevertheless, the yield point of the deformed specimen at 750°C was higher than that at 725°C, measuring 160 MPa and 155 MPa, respectively.

Static recovery is the primary mechanism and can be applicable in explaining all the observed flow stress curves. The initial rise in stress during work hardening persists until it reaches a stable level, where the increased dislocation density is counterbalanced by dynamic recovery (Figure 7). This is evident in the steady-state strain, which is followed by a constant flow curve. Such mechanism is usual for metals having high staking fault energy [16].

3.2. Microstructural analysis

In the Figure 8(a) the grain size of ferrite in the deformed zone is nearly half that of the undeformed zone, while the volume fraction of ferrite remains approximately the same in both regions (Table 2). The grain size of ferrite in Figure 8(b) of deformed zone is decreased to 38% and the volume fraction is raised approximately to 10% comparing to undeformed zone.

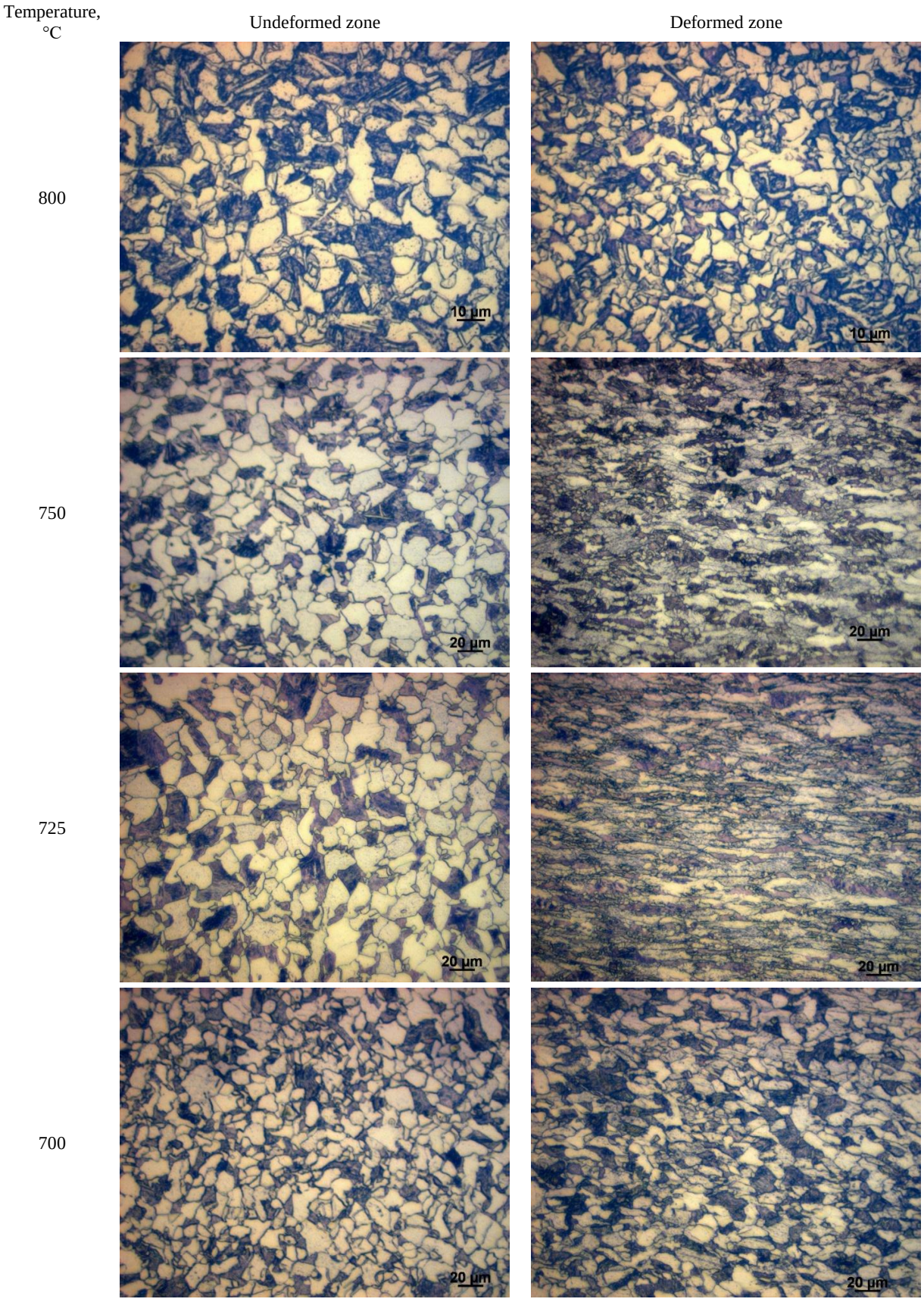

Figure 8. Microstructure of undeformed (left) and deformed (right) zones of the sample at deformation temperature

Table 2. Results of quantitative analysis of micrographs

No. of a sample and deformation temperature	Grain size, $L \pm (t_{0.95,\,n-1}) \cdot s(L)$, μm		Volume fraction of ferrite, V_V, %	
	Deformed	Undeformed	Deformed	Undeformed
Sample 1 (800°C)	3.5±0.16	6.2±0.25	56.1±3.045	51.7±2.44
Sample 2 (750°C)	7.1±0.37	11.4±0.52	62.6±2.77	57.5±3.31
Sample 3 (725°C)	8.7±0.35	10.4±0.36	66.3±2.30	60.7±3.71
Sample 4 (700°C)	8.7±0.41	9.5±0.41	66.2±2.61	60.6±3.20

The deformation at 725°C shows flattened grains according to the microstructure in Figure 8(c). Nevertheless, the ferrite grain refinement as well as the volume fraction has no significance. There are some coarse ferrite grains in deformed zone after treatment at 700°C Figure 8(d). The ferrite grain refinement and the ferrite volume fraction of undeformed and deformed zones are insignificant according to Table 2.

The deformation at 800°C indicates a tremendous ferrite grain refinement compared to other deformation temperatures. As is shown in Table 2, the difference between the ferrite grain sizes deformed at 800°C (~3.5 μm) approximately three times less than at 700°C (~8.7 μm).

Typical characteristic of all microstructures in the undeformed zones is the presence of distinct ferrite grains with austenite islands, whereas the distribution of the two phases in the deformed zones follows a different pattern. Therefore, the microstructure of deformed zone at 800°C consists of refined ferrite grains along with fine residual austenite. Nevertheless, defamation at 750°C microstructure of the ferrite grains is elongated flattened shaped along the grain boundaries of the austenite-ferrite interface. Microstructure of deformed samples at 725°C and 700°C shows elongated ferrite grains with residual austenite in deformed zones.

The volume fraction of ferrite in the assessed microstructures ranges from 56.1% to 66.2% in the deformed zones and from 51.7% to 60.6% in the undeformed zones (Table 2). Generally, the difference in volume fraction between deformed and undeformed zones among all samples is approximately 5%. Nonetheless, theoretical calculation of ferrite and austenite volume fractions indicate that this difference changes depending on the deformation temperature. As shown in Table 2, the ferrite volume fraction at 800°C is around 65%, whereas at 725°C, it increases to 82%. These values are derived from the Fe-C phase diagram, which does not account for alloying elements. Alloying elements such as Mn, Co, and Ni influence phase transformation temperatures like Ar_1, suggesting that the ferrite volume fraction in the studied HSLA steel may deviate from theoretical predictions. Furthermore, the theoretical calculation of ferrite volume fraction does not consider the impact of deformation at specific temperatures.

3.3. Hardness

As shown in Table 3, the highest hardness (502.1 HV) was recorded in Sample 3 at 725°C, while the lowest hardness (332.7 HV) was observed in the deformed Sample 1 at 800°C. Notably, the hard difference between the deformed and undeformed zones of Sample 1 is minimal, measuring approximately 330 HV in both zones. However, in Samples 3 and 4, this difference is substantial, exceeding 40%. The significant increase in hardness following deformation at 700°C and 725°C can be attributed to the characteristics of the flow stress curves.

Table 3. Hardness of deformed and undeformed zones of the samples

Number of measurements	Hardness by Vickers, HV			
	Sample 1	Sample 2	Sample 3	Sample 4
Deformed zone				
1	352	407	452	532
2	330	378	434	474
3	321	389	507	438
4	348	389	612	413
5	313	401	506	482
Average	332.7	392.8	502.1	467.8
Undeformed zone				
1	304	254	339	245
2	329	297	313	245
3	329	329	317	259
4	348	276	269	290
5	329	283	239	259
Average	327.8	287.8	295.4	259.6

3.4. Summary of thermomechanical processing aspects

Thermomechanical processing is a critical technology for optimizing the properties of HSLA steels. By refining grain size, controlling phase transformations, and enhancing precipitation strengthening, TMP enables the production of steels with superior mechanical performance. Advances in TMP techniques continue to improve the efficiency and applicability of HSLA steels across various industries. Further research into innovative processing methods will pave the way for next-generation high-performance steels.

There was much research fulfilled corresponding to thermomechanical processing of HSLA steels. Plenty of success in this field was achieved by the University of Sheffield. It was found proper cooling rate and intercritical strain during processing to improve steel production performance and mechanical properties of HSLA steels [16, 17]. As it is mentioned in [15], implementing intermediate forced cooling (IFC) shortens the inter-pass holding time, which is a major drawback compared to conventional rolling process [16]. Nevertheless, applying this method in an industrial setting is considered challenging. Therefore, the research was conducted using a plane strain compression test, followed by modeling with the finite element method. The key distinction between this research and the present study is that the former examines the impact of IFC on mill productivity, whereas the current work focuses on microstructural evolution during intercritical processing.

4. Conclusions

To summarize this research, it needs to be emphasized that considerable grain refinement of the ferrite was observed during the deformation at 800 °C, with an average grain size of 3.6 μm. High ferrite volume fraction was assessed for sample 3 at 725°C and obtained 66.3%. The difference between theoretical and actual volume fractions can be explained by influence of alloying elements (Mn, Co and Ni). The highest value of macro hardness was observed in Sample 3 at 725°C (502.2 HV). Thus, hardness increases significantly just above the temperature of Ar_1.

The modelling of flow stress curves shows remarkable increase in stress at intercritical temperatures, influenced by initial work hardening followed by dynamic recovery. Therefore, during intrcritical processing dynamic recrystallization process is not preferred. Deformation in intercritical regions

is beneficial for the ferrite grain refinement to obtain ultrafine ferrite grains. Corresponding results suggest warm deformation at 800°C to achive required grain refinement, whereas benefits in hardness can be obtained at 725°C. Therefore, indicated temperatures need to be considered critical during thermomechanical processing.

Author contributions

Conceptualization: UKK; Data curation: UKK, AAK; Formal analysis: UKK; Funding acquisition: UKK; Investigation: UKK, AAK; Methodology: UKK, AAK; Project administration: UKK; Resources: UKK; Software: UKK; Supervision: UKK; Validation: UKK; Visualization: UKK, AAK; Writing – original draft: UKK, AAK; Writing – review & editing: UKK, AAK. All authors have read and agreed to the published version of the manuscript.

Funding

This research received no external funding.

Acknowledgements

The authors would like to thank Prof. E.J. Plmiere from the University of Sheffield for his support during their master's program studies.

Conflicts of interest

The authors declare no conflict of interest.

Data availability statement

The original contributions presented in this study are included in the article. Further inquiries can be directed to the corresponding author.

References

[1] DeArdo, A.J., Garcia, C.I. & Palmiere, E.J. (1991). Thermomechanical processing of steel Metals. 10th edition. *Materials park, OH: ASM International*

[2] Weng, Y. (2009). Ultra-fined grained steels. *Metallurgical industry press, Beijing*

[3] Kakimov, U.K., & Kaipova, A.A. (2022). Sovremennoe razvi-tie termomehanicheskoj obrabotki vysokoprochnyh nizkolegirovannyh stalej tipa H70-H100. *Trudy mezhdunarodnoj nauchno-prakticheskoj konferencii «Satpaevskie chtenija – 2022. Trendy sovremennyh nauchnyh issledovanij.*

[4] Sampath, K. (2006). An understanding of HSLA-65 plate steels. *Journal of Materials Engineering and Performance*, (15), 32-40. http://dx.doi.org/10.1361/105994906X83439

[5] Opiela, M. (2014). Effect of thermomechanical processing on the microstructure and mechanical properties of Nb-Ti-V microalloyed steel. *Journal of Materials Engineering and Performance*, *23*(9), 3379-3388. http://dx.doi.org/10.1007/s11665-014-1111-8

[6] Zhandar, E.E., Kaipova, A.A. & Kakimov, U.K. (2021). Ylken diametrli құbyrlardy өndiru үshin bolatty termomehani-kalyқ өңdeu tehnologijasyna sholu. *Trudy Satpaevskih chtenij «Satpaevskie chtenija – 2021», Almaty*

[7] Abdusajtov, S.E., Kaipova, A.A. & Kakimov, U.K. (2021). Termomehanikalyқ өңdeu kezinde az legirlengen bolattar-dyң zhoғary beriktigin zertteu. *Trudy Satpaevskih chtenij «Satpaevskie chtenija – 2021», Almaty*

[8] Kakimov, U.K., & Altynbek, R. (2015). Bolattardy termomehanikalyk ondeu processterine sholu. *Vestnik nauki KazATU, 3(86), 72-77*

[9] Bodin, A. (2002). Intercritical deformation of low alloy steels. *Corus Technology BV, Netherlands*

[10] Song, R., Ponge, D., Raabe, D., Speer, J.G. & Matlock, D.K. (2006). Overview of processing, microstructure and mechanical properties of ultrafine grained bcc steels. *Materials Science and Engineering A, (441), 1-17*. https://doi.org/10.1016/j.msea.2006.08.095

[11] Hara, Y., & Rainford, S. (2009). Microstructural development of pipeline steel during thermomechanical processing. *MMet dissertation, The University of Sheffield*

[12] Loveday, M.S., Mahon, G.J., Roebuck, B., Lacey, A.J., Palmiere, E.J., Sellars, C.M. & van der Winden, M.R. (2008). Measurement of flow stress in hot plane strain compression tests. *Materials at high temperatures, 23(2), 85-118.* https://doi.org/10.1179/mht.2006.006

[13] Ohser, J., Mücklich, F. (2000). Statistical analysis of microstructures in materials science. *John Wiley & Sons, 1st edition*

[14] Tamura, I., Sekine, H., & Tanaka, T. (1988). Thermomechanical processing of high-strength low-alloy steels. *Butterworths, London*

[15] Hinton, J.S., Palmiere, E.J. & Rainforth, W.M. (2012). The effect of high temperature grain refinement on the isothermal ferrite grain growth kinetics in steel S460. *Materials science forum, 715*, 907-912. http://dx.doi.org/10.4028/www.scientific.net/MSF.715-716.907

[16] Xiao, B., Palmiere, E.J., Howe, A.A. & Carey, H.C. (2012). Multi-pass simulation of heavy plate rolling including intermediate forced cooling. *Advanced materials research, 409*, 443-448. https://doi.org/10.4028/www.scientific.net%2FAMR.409.443

[17] Cahn, R.W. (2007). Thermo-mechanical processing of metallic materials. *Pergamon materials series, Elsevier*

HSLA болаттарын термомеханикалық өңдеу: шолу

У.К. Какимов*, А.А. Каипова

Satbayev University, Алматы, Қазақстан

**Корреспонденция үшін автор: u.kakimov@satbayev.university*

Аңдатпа. Болаттарды термомеханикалық өңдеу – жоғары берік болаттарды алудың жетілдірілген процесі. Төмен легирленген беріктігі жоғары болат маркалары мұнай мен газды тасымалдауға арналған үлкен диаметрлі құбырларды өндіруде кең ауқымды қолдануға ие. Құбыр илемдеу өндірісінде X70 маркалы болаттарды қолдану металды тұтынуды және оларды өндіруге арналған энергия шығындарын азайтуға әкелді. Жылы илемдеу немесе бақыланатын илемдеу осы мақалада сипатталған болат өңдеудің озық технологиялық режимдерінің бірі болып табылады. Сондықтан, төмен легирленген беріктігі жоғары (HSLA) болаттар жоғары механикалық қасиеттеріне және әртүрлі өнеркәсіптік қолданбаларда үнемділігіне байланысты айтарлықтай назар аударғанын атап өткен жөн. Термомеханикалық өңдеу

(ТМӨ) осы болаттардың микроқұрылымын және механикалық өнімділігін оңтайландыруда шешуші рөл атқарады. Бұл жұмыс бақыланатын илемдеуді, қарқынды салқындатуды және тұнбаға түсумен беріктендіруді қоса алғанда, ТМӨ негізгі принциптерін зерттейді. Өңдеу параметрлерінің дәнді ұсақтауға, фазалық өзгерістерге және механикалық қасиеттерге әсері талқыланады. Тікелей шынықтыру және ультра қарқынды салқындату сияқты ТМӨ әдістерінің жетістіктері де атап өтілген. Бұл процестерді түсіну беріктігі, қаттылығы және пісірілу қабілеті жоғары HSLA болаттарын жасауға мүмкіндік береді. Сондай-ақ мақалада HSLA болаттарының термомеханикалық өңдеуін модельдейтін жазық деформацияны басу сынағы нәтижелеріне қатысты тәжірибелік бөлімі бар.

Негізгі сөздер: *HSLA болаттары, термомеханикалық өңдеу, микроқұрылым, бақыланатын илемдеу, қарқынды салқындату, фазалық түрлендіру, тұнбаға түсумен беріктендіру.*

Термомеханическая обработка сталей HSLA: Обзор

У.К. Какимов*, А.А. Каипова

Satbayev University, Алматы, Казахстан

**Автор для корреспонденции: u.kakimov@satbayev.university*

Аннотация. Термомеханическая обработка сталей является передовым процессом производства высокопрочных сталей. Низколегированные высокопрочные марки стали имеют широкий спектр применения в производстве труб большого диаметра для транспортировки нефти и газа. Применение сталей марки X70 в производстве трубопроката привело к снижению расхода металла и энергозатрат на их производство. Теплая прокатка или контролируемая прокатка является одним из передовых технологических методов обработки стали, который описан в данной статье. Поэтому необходимо подчеркнуть, что высокопрочные низколегированные (HSLA) стали привлекли значительное внимание благодаря своим превосходным механическим свойствам и экономической эффективности в различных промышленных применениях. Термомеханическая обработка (ТМО) играет решающую роль в оптимизации микроструктуры и механических характеристик этих сталей. В данной статье рассматриваются основные принципы ТМО, включая контролируемую прокатку, ускоренное охлаждение и дисперсионное упрочнение. Обсуждается влияние параметров обработки на измельчение зерна, фазовые превращения и механические свойства. Также освещаются достижения в технологиях ТМО, таких как прямая закалка и сверхбыстрое охлаждение. Понимание этих процессов позволяет разрабатывать стали HSLA с повышенной прочностью, вязкостью и свариваемостью. В статье также содержится экспериментальная часть, касающаяся результатов испытаний на сжатие при плоской деформации, которая моделирует термомеханическую обработку сталей HSLA.

Ключевые слова: *HSLA стали, термомеханическая обработка, микроструктура, контролируемая прокатка, ускоренное охлаждение, фазовое превращение, дисперсионное упрочнение.*

SATBAYEV UNIVERSITY

Engineering Journal of Satbayev University

Volume 147 (2025), Issue 4, 16-22

https://doi.org/10.51301/ejsu.2025.i4.03

Distribution of niobium during chlorine processing of various titanium-containing feedstocks

T.K. Sarsembekov[1*], T.A. Chepushtanova[1], Ye.S. Merkibayev[1], T.B. Yanko[2]

[1]*Satbayev University, Almaty, Kazakhstan*
[2]*UNDERSLAB LTD OOD, Burgas, Bulgaria*

**Corresponding author: t.sarsembekov@satbayev.university*

Abstract. This article presents the results of a study on the distribution of niobium during the chlorination processing of various titanium-containing feedstocks, including titanium slag from JSC «UK TMP», titanium slag from the Norwegian company TiZir Titanium & Iron AS, and their mixtures in different ratios. The titanium slag samples were ground and treated by chlorination using concentrated gaseous chlorine in a molten salt medium composed of alkali metal chlorides ($MgCl_2$, KCl, NaCl), with finely crushed anthracite as a carbon-based reducing agent. The process was conducted at temperatures from 700 to 820°C. The study focused on the distribution behavior of vanadium and niobium during the chlorination of blended titanium slags in proportions of 60/40, 50/50, and 30/70 (UK TMP/TiZir), as well as in 100% UK TMP slag. The results indicate that most of the niobium accumulates in the dump slag of the titanium chlorinator and in the slurry of the irrigated scrubber. It was also found that an increase in the initial niobium content in the feed leads to its higher concentrations in the sublimate of the dust chamber, in the melt of the salt bath dust-settling chamber, and in the scrubber slurry, while its share in the dump slag decreases.

Keywords: *titanium slag, vanadium, niobium, distribution, titanium, dump slag, chloride sublimates, chlorination, slag processing, niobium recovery.*

Received: 22 April 2025
Accepted: 15 August 2025
Available online: 31 August 2025

1. Introduction

Improving the comprehensiveness of raw material processing and increasing the recovery of valuable accompanying elements is one of the primary objectives in modern extractive metallurgy. This is particularly relevant for complex feedstocks that contain multiple strategic or rare elements, whose inefficient recovery can lead to significant economic and environmental losses. Among such materials, titanium-containing feedstocks – such as ilmenite concentrate and titanium slag are known to contain a range of valuable metals, including rare and dispersed elements such as vanadium, niobium, tantalum, scandium, and zirconium [1, 2]. However, only vanadium and scandium currently have established industrial-scale recovery processes in the titanium production chain, while other critical elements are typically lost in waste streams [3].

Niobium (Nb), a strategic refractory metal with an average crustal abundance of 2×10^{-3} wt.% [4], plays a vital role in a wide array of high-technology applications. These include the manufacture of advanced structural materials, catalysts, superconducting systems, and electronics. Its main commercially exploited minerals are pyrochlore and columbite-tantalite, although it is also present in smaller quantities in perovskite, loparite, and ilmenorutile [5]. In many titanium ores, particularly ilmenite, niobium occurs in isomorphous substitutional positions, replacing titanium or iron due to its similar ionic radius and valence states. This complicates selective extraction during both reductive smelting and chlorination processing stages.

As shown in Figure 1, the global production of primary niobium feedstocks (mostly pyrochlore concentrates from Brazil and Canada) has increased steadily between 2001 and 2014, reflecting growing demand for niobium-containing materials in structural alloys and high-performance steels. Secondary sources of niobium, such as tin slag and tantalum-bearing minerals, contribute only marginally to the overall global supply (Figure 2). This supply imbalance highlights the importance of developing technologies for niobium recovery from alternative and non-traditional sources, including titanium-bearing slags.

One of the unique geochemical properties of niobium is its pronounced affinity to titanium and iron, which leads to the formation of a range of complex oxide and oxide-fluoride phases during natural and industrial processes. This includes the development of solid solutions such as $FeNb_2O_6$ and $CaNb_2O_6$, as well as the stabilization of niobium within perovskite- and rutile-type crystal structures [6]. As a result, niobium is commonly encountered as a trace element in a variety of titanium ores, which are often processed without consideration for its recovery. This represents both a missed economic opportunity and a challenge for resource sustainability.

t.sarsembekov@satbayev.university; t.chepushtanova@satbayev.university; y.merkibayev@satbayev.university; titanlab3@ukr.net
Engineering Journal of Satbayev University. eISSN 2959-2348. Published by Satbayev University

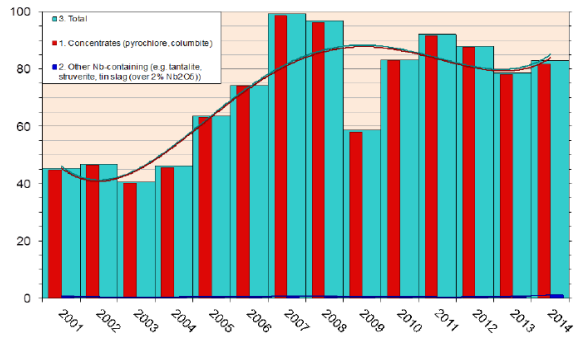

Figure 1. Production of primary niobium raw materials in 2001-2014

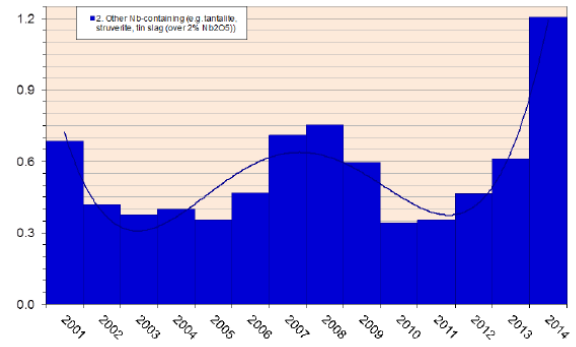

Figure 2. Production of secondary niobium raw materials in 2001-2014

Technologically, niobium is indispensable. It is widely used in the production of high-strength low-alloy (HSLA) steels, superconducting magnets (NbTi, Nb_3Sn), nuclear reactor components, aerospace alloys, electronics, and medical devices. As illustrated in Figure 3, approximately 87% of the global niobium consumption is in the form of steel-grade ferroniobium, which is added to microalloyed steels used in pipelines, automotive structures, and civil engineering. These steels typically contain ~0.05 wt.% Nb in HSLA grades and 0.04-0.08 wt.% in stainless steels. The remaining 13% of niobium is used in high-purity applications, including vacuum-grade alloys, chemicals (such as catalysts), and pure metal products [7].

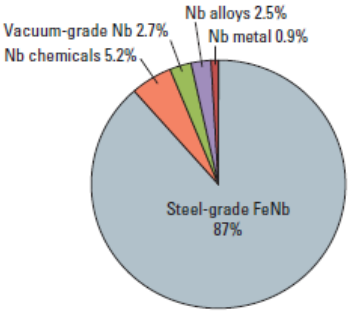

Figure 3. Niobium consumption by end-use sectors

The global niobium market is highly concentrated. Brazil accounts for approximately 90% of the total production, followed by Canada (~8%) (Figure 4). The world's leading producers CBMM (Companhia Brasileira de Metalurgia e Mineração), Mineração Catalão de Goias (both in Brazil), and IAMGOLD Corporation (Canada) dominate the supply chain and export primarily ferroniobium and niobium oxide products [8].

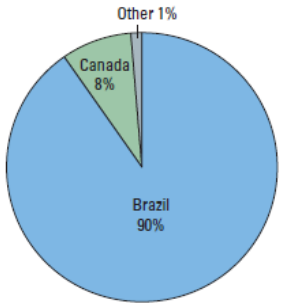

Figure 4. Niobium-producing countries

In 2012, the global output reached 53.5 thousand tonnes (Nb content), up from 52.2 thousand tonnes in 2011, reflecting a steady increase in demand from the steel and aerospace sectors [9].

Despite its strategic and economic importance, the industrial extraction of niobium from complex oxide matrices such as titanium slag remains challenging. Traditional pyrometallurgical or hydrometallurgical routes are not always viable, especially given niobium's high thermodynamic stability in refractory phases such as Nb_2O_5 and its low reactivity under standard chlorination conditions. In the presence of titanium oxides, niobium tends to be retained within solid solutions or form refractory compounds that resist volatilization or selective leaching. This makes it difficult to co-recover niobium during typical processing of titanium ores or slags.

The issue is particularly pronounced during the chlorination of titanium slag, a material produced from the reductive smelting of ilmenite concentrate. Depending on the origin and processing route, titanium slag may contain up to 0.12 wt.% Nb_2O_5, which corresponds to approximately 0.08 wt.% metallic niobium. While this may appear minor, in large-scale operations (20 thousand tonnes per year), this translates to potential niobium losses of 16 tonnes annually. Without targeted recovery, this valuable metal is lost with waste streams such as chlorinator dump slag, sublimates from the dust chambers, salt bath residues, and wet scrubber slurry.

Recent studies suggest that the behavior of niobium during slag chlorination is influenced by multiple factors, including temperature, partial pressure of chlorine, presence of reducing agents like carbon, slag composition, and the configuration of the chlorination system. In optimized systems that use molten salt media ($NaCl - KCl - MgCl_2$) and fine anthracite, partial conversion of niobium into volatile chlorides (NbC_5) and oxychlorides ($NbOCl_3$) becomes feasible. However, due to the relatively high Gibbs free energies of the required reactions, volatilization yields remain modest, and significant fractions of niobium persist in condensed phases.

Thus, to enable the recovery of niobium as a co-product during titanium tetrachloride ($TiCl_4$) production, it is essential to study its phase transformations and distribution across process streams in real industrial environments. Most prior research has focused on ilmenite concentrates and laboratory-scale experiments. There is a lack of data on industrial chlorination of titanium slag, especially from different geological and technological origins, and on the impact of feed blending on niobium recovery potential.

This study seeks to fill this knowledge gap by performing a comparative analysis of niobium distribution during the industrial chlorination of titanium slags from two different producers: JSC «UK TMP» (Kazakhstan) and TiZir Titanium & Iron AS (Norway). The research evaluates pure and blend-

ed feeds (100/0, 60/40, 50/50, and 30/70 ratios) under standardized chlorination conditions. The results provide a basis for understanding how feedstock composition, thermodynamic environment, and operational parameters influence niobium recovery.

The novelty of this research lies in the integration of industrial-scale experimental data with thermodynamic modeling to characterize niobium's phase behavior, chlorination kinetics, and final distribution. The insights gained can guide the development of selective co-recovery technologies for niobium and support more sustainable utilization of titanium-bearing feedstocks.

2. Materials and methods

The research utilized a variety of titanium-bearing raw materials and chlorination reagents. The primary materials were titanium slags obtained from two major industrial sources: JSC «UK TMP» (Kazakhstan) and TiZir Titanium & Iron AS (Norway). These slags were selected due to their distinct genesis and chemical composition, offering a representative spectrum for analyzing niobium distribution. The slags are formed via high temperature carbothermic reduction of ilmenite concentrates using anthracite as a carbonaceous reducing agent. Their physicochemical characteristics significantly influence the behavior of niobium and associated elements during chlorination [10-15].

The average chemical composition of the titanium slags is presented in Table 1. The Kazakh slag is notably rich in TiO_2 (85.12 wt.%) and contains elevated amounts of vanadium pentoxide (7.67 wt.%) and iron oxide (7.08 wt.%), while the Norwegian slag features a slightly lower TiO_2 content (84.79 wt.%) and significantly reduced vanadium (0.486 wt.%), making it suitable for comparative evaluation. Minor impurities such as Al_2O_3, CaO, MgO, Nb_2O_5, and trace quantities of rare-earth oxides (Sc_2O_3, Ta_2O_5, ZrO_2) were also recorded, reflecting the natural variability in ilmenite deposits.

Table 1. Average chemical composition of titanium slags (wt.%)

Type of slag	Average content, %													
	TiO_2	FeO	SiO_2	V_2O_5	Al_2O_3	CaO	MgO	Cr_2O_3	Sc_2O_3	Ta_2O_5	Nb_2O_5	MnO	S	ZrO_2
UK TMP	85.12	7.08	3.59	7.67	2.19	0.26	1.23	0.51	0.00	0.00	0.04	1.97	0.12	0.22
TiZir	84.786	7.854	2.292	0.486	2.006	0.125	1.3204	0.274	0.002	0.002	0.0602	1.666	0.0386	0.212

The chlorination reagents comprised AM-grade powdered anthracite and industrial-grade chlorine gas (minimum 90% vol. purity). These were selected based on compatibility with standard chlorinator systems used at titanium production facilities.

The experimental procedure consisted of a dual approach:

– thermodynamic modeling using HSC Chemistry 6.0 to simulate relevant chlorination reactions;

– validation through industrial-scale chlorination trials over the temperature range of 700-820°C.

Gibbs free energy (ΔG) values were calculated to assess the spontaneity and feasibility of reactions involving niobium- and titanium-containing phases, including the formation of volatile chlorides and intermediate oxychlorides.

The physical chlorination experiments were carried out using molten-salt chlorinators designed to simulate real production conditions. The chlorinator (Figure 5) was a cylindrical, steel-shelled, refractory-lined unit equipped with tuyeres for chlorine gas injection, upper and lower slag tapping ports, and a loading system for solid feedstock and reducing agent. The interior contained a melt of alkali metal chlorides (KCl, NaCl, $MgCl_2$) that served as both reaction medium and heat transfer agent. Slag samples were first crushed, milled to a particle size ≤0.16 mm, and dried before being introduced into the chlorinator alongside anthracite.

During operation, the chlorine gas was introduced through a tuyere system at the lower zone of the reactor, promoting chlorination within the molten salt bath. The process generated a vapor-gas mixture enriched in titanium tetrachloride ($TiCl_4$), volatile vanadium and niobium chlorides, and gaseous by-products. The gas phase was routed through a multistage condensation system consisting of a dust chamber, salt bath condenser, scrubber, and cryogenic condenser to selectively recover components based on their boiling points.

Uncondensed tail gases (CO, CO_2, Cl_2, O_2, N_2, HCl) were evacuated via exhaust fans and routed to a gas purification unit.

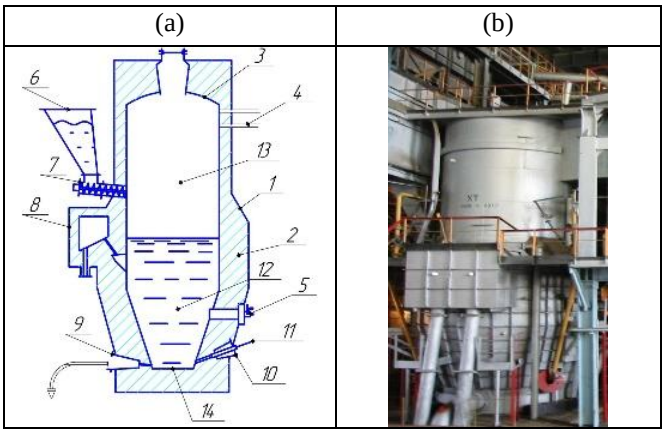

Figure 5. Chlorinator: (a) – schematic view; (b) – general view: 1 – shell; 2 – fireclay brick lining; 3 – dome; 4 – main gas duct; 5 – graphite electrode; 6 – intermediate feed bunker; 7 – screw feeder; 8 – upper slag tapping port; 9 – lower slag tapping port; 10 – tuyere assembly; 11 – chlorine pipeline; 12 – molten zone; 13 – vapor-gas zone; 14 – hearth

The condensation units were maintained at controlled temperatures to ensure selective separation:

– 400-600°C – dust chamber for solid sublimates ($NbOCl_3$, $VOCl_3$);

– 300-320°C – salt bath melt condenser for semi-volatile species;

– 100-160°C – scrubber system for soluble chlorides;

– <20°C – spray condenser for high-purity $TiCl_4$ recovery.

Sampling was performed at all process stages daily. Composite samples were prepared every 10 days for monthly analysis. The niobium content in raw slag was measured via atomic emission spectroscopy (AES) using a DFS-458 spectrometer, while chlorinator discharge slag, dust, salt bath residues, and scrubber slurries were analyzed by photometric methods involving niobium PAR complex formation in a tartaric-HCl medium, followed by absorbance quantification with a KFK-3 photocolorimeter [10].

Quantitative niobium distribution was assessed by recalculating its mass across process outputs per ton of feedstock, using monthly datasets collected from 2019 to 2024 across varying slag compositions and chlorination campaigns.

3. Results and discussion

3.1 Niobium occurrence in ilmenite and behavior in slag

Mineralogically, ilmenite ($FeTiO_3$) belongs to the subclass of complex oxides within the trigonal crystal system. It often serves as a primary source of titanium dioxide (TiO_2) for metallurgical and pigment applications. In addition to titanium and iron, natural ilmenite frequently contains trace elements such as vanadium, chromium, and particularly niobium, which can be present in varying amounts depending on the geological origin of the deposit.

The Nb_2O_5 content in natural ilmenite has been reported to vary significantly: from 0.26-1.44 wt.% in agpaitic pegmatites and from 0.93-1.55 wt.% in miaskitic pegmatites, both types of alkaline rocks associated with complex rare-element mineralization. These values suggest that certain ilmenite deposits may serve as secondary sources of niobium. Spectrochemical analysis of ilmenite from the Volnogorsk deposit (Ukraine) shows an average Nb_2O_5 content of approximately 0.034%, while in Satpayev ilmenite (Kazakhstan), the content is around 0.02%.

During carbothermic smelting of ilmenite concentrate at elevated temperatures (~1500-1700°C), most of the iron is reduced to metal or enters the slag as FeO, while titanium remains as TiO_2-rich slag. Niobium, being less reducible than titanium or iron, remains entirely in the oxide form and accumulates within the titanium slag phase. The Gibbs free energy (ΔG) for the reduction of Nb_2O_5 by carbon at 1500°C is +1564.6 kJ, indicating that the direct reduction of niobium pentoxide by carbon is thermodynamically unfavorable under standard metallurgical conditions. This explains its persistence in the slag phase post-smelting.

3.2 Thermodynamic considerations and chlorination environment

Chlorination experiments were performed on the titanium slag in a molten salt medium within a temperature range of 700-820°C. The salt composition typically included alkali and transition metal chlorides, approximated as (% wt.): NaCl – 19-24.5; KCl – 16.7-20; $MgCl_2$ – 1-11.7; $FeCl_2$ – 8-26; $FeCl_3$ – 0.8-2; $AlCl_3$ – 1.5-4. These chlorides served multiple roles: as a heat transfer medium, a diluent, and a reactive agent facilitating chlorination of refractory oxides.

According to literature, niobium in chloride melts can exist in various oxidation states and coordination environments. It is widely accepted that high-valent niobium, particularly Nb^{5+}, forms stable octahedral anionic complexes such as $[NbCl_6]^-$. In reducing environments or with high chloride activity, tetravalent complexes like $[NbCl_6]^{2-}$ and even lower-valent or cluster species can be stabilized. These species demonstrate different volatilities and reactivities, which is significant for understanding their behavior in the chlorination and condensation circuits.

Analytical monitoring of the chlorinator melts after prolonged operation revealed an average Nb_2O_5 concentration of ~0.05%. This suggests gradual but consistent enrichment of the melt in niobium-containing species during chlorination.

3.3 Reactions of niobium during chlorination

Niobium present in the titanium slag undergoes several thermodynamically favorable transformations in the presence of chlorine gas and carbon as a reducing agent. The primary reactions include:

$$2Nb_2O_5 + 6Cl_2 + 3C \rightarrow 4NbOCl_3 + 3CO_2, \quad (1)$$
$\Delta G = -594.8$ to -563.6 kJ.

$$2Nb_2O_5 + 10Cl_2 + 5C \rightarrow 4NbCl_5 + 5CO_2, \quad (2)$$
$\Delta G = -987.5$ to -974.9 kJ.

$$2Nb_2O_5 + 6Cl_2 + 5C \rightarrow 4NbCl_3 + 5CO_2, \quad (3)$$
$\Delta G = -527.2$ to -534.2 kJ.

These reactions illustrate the stepwise reduction and chlorination of niobium pentoxide to various chlorinated forms, depending on the redox conditions and chlorine partial pressure. Empirical studies [16] have shown that the chlorination of Nb_2O_5 typically results in a mixture of $NbOCl_3$ and $NbCl_5$, formed via the following overall reaction:

$$Nb_2O_5 + 4Cl_2 + 2C \rightarrow NbOCl_3 + NbCl_5 + 2CO_2, \quad (4)$$
$\Delta G = -395.8$ to -384.6 kJ.

Chlorinated niobium species enter the vapor phase and migrate downstream in the gas flow. $NbOCl_3$ sublimes at ~400°C, and $NbCl_5$ has a boiling point of 248.3°C, both well below the operating temperature of the dust chamber (500-600°C), ensuring they remain in the gas phase through this section.

3.4 Condensation and niobium concentration in slurry

Upon entering the salt bath condensation chamber (SBC), where the temperature is maintained at 300-350°C, $NbOCl_3$ condenses into the salt melt due to its lower volatility [17]. The concentration of niobium in the SBC melt, again expressed as Nb_2O_5, was found to be ~0.05%. $AlCl_3$ in the SBC reached up to 40 wt.%, influencing redox equilibria. Under these conditions, a secondary reaction proceeds:

$$NbOCl_3 + AlCl_3 \rightarrow NbCl_5 + AlOCl, \quad (1)$$
$\Delta G = -3.5$ to -3.2 kJ.

This transformation increases the concentration of volatile $NbCl_5$, which is more prone to carrying over into downstream zones. Observations revealed that dilution of the SBC melt (due to excess slag or scrubber return) led to reduced $AlCl_3$ concentrations and correspondingly lower niobium concentrations in the final slurry. Thus, maintaining high $AlCl_3$ levels appears beneficial for enhanced niobium transfer.

In the final condensation zone the irrigated scrubber, the gas stream is cooled below 125°C. Since $NbCl_5$ condenses at 248.3°C, complete condensation occurs here. Niobium precipitates in the $TiCl_4$ pulp as fine, yellowish, acicular crystals. The total solid content of the pulp may reach up to 100 g/L, with the niobium-rich fraction exceeding 20 wt.% as Nb_2O_5.

3.5 Industrial data and discussion

Between 2019 and 2024, a series of trials were conducted at titanium processing facilities using various combinations of titanium slag from JSC «UK TMP» (Kazakhstan) and TiZir Titanium & Iron AS (Norway). These experiments involved blending the slags in different ratios (100/0, 60/40, 50/50, 30/70) to observe changes in niobium behavior. The analysis showed that average Nb_2O_5 content ranged from 0.036-0.050% in UK TMP slag and 0.057-0.067% in TiZir slag. Table 2 summarizes the distribution of niobium across process streams.

Table 2. Distribution of niobium among process products

No.	Ti Slag Ratio (UK TMP /TiZir)	Average Nb_2O_5 Content, %	Distribution of Nb, %			
			Dump slag	Sublimates from the dust chamber	Melt from the salt-bath condensation chamber	Irrigated scrubber slurry
1	100/0	0.045	51.0	3.4	2.1	43.5
2	60/40	0.049	46.8	4.5	2.9	45.8
3	50/50	0.052	45.1	4.2	2.1	48.6
4	30/70	0.058	42.7	2.0	1.3	54.0

The data suggest that higher proportions of TiZir slag, which contains more Nb, promote niobium enrichment in volatile and condensable fractions (dust, melt, slurry), while decreasing its retention in the dump slag. This trend is consistent with the formation of more volatile niobium chlorides under higher Nb feed conditions. Therefore, from a process engineering standpoint, the increase in TiZir slag fraction enhances niobium recovery in downstream process products, especially in the slurry where its selective extraction may be most feasible.

4. Conclusions

Thus, during the chlorination of titanium-containing feedstock in the presence of a reducing agent such as carbon, niobium initially retained in oxide form within the titanium slag undergoes chemical transformation into volatile chlorinated species. Specifically, niobium transitions into oxychloride forms such as $NbOCl_3$ and, under favorable conditions particularly in the presence of aluminum trichloride, converts to niobium pentachloride ($NbCl_5$). These processes are facilitated by the molten salt medium used during chlorination, which provides a chemically active and heat-stable environment conducive to complex reaction pathways.

Thermodynamic analysis based on calculated Gibbs free energy (ΔG) values confirms the feasibility and spontaneity of these transformations within the temperature range of 700-820 °C. The experimental findings align with theoretical predictions and with published literature data, reinforcing the understanding of niobium's behavior under industrial chlorination conditions.

Experimental methods, including chemical analysis of solid and liquid process streams, were employed to determine the average niobium content in both the raw feedstock and the intermediate products formed throughout the titanium tetrachloride production cycle. The results demonstrate the complex migration behavior of niobium, indicating that it does not remain inert within the slag but instead redistributes across several phases depending on reaction conditions and equipment configuration.

Industrial-scale trials involving the processing of titanium slags from two different sources JSC «UK TMP» (Kazakhstan) and TiZir Titanium & Iron AS (Norway) in various mass ratios (100/0 to 30/70) have shown clear trends in niobium distribution. Most of the niobium was found to accumulate in two main fractions: the dump slag from the chlorinator and the solid phase of the scrubber slurry, where temperatures are conducive to condensation and precipitation. Notably, as the initial content of niobium in the feed increases particularly with the use of higher TiZir slag proportions, the concentration of niobium in downstream products (dust chamber sublimates, salt bath melt, and scrubber slurry) also increases, while its content in the dump slag decreases. This redistribution pattern can be attributed to the formation of more volatile and thermodynamically stable niobium chlorides under higher feed concentrations.

These findings suggest that the most promising direction for the development and implementation of niobium recovery technology within titanium tetrachloride production lies in the targeted extraction from the dump slag and scrubber slurry. These process streams consistently demonstrate the highest concentrations of niobium and offer opportunities for selective recovery using hydrometallurgical or combined techniques. The data obtained from both laboratory and industrial experiments may therefore serve as a foundation for future technological solutions aimed at enhancing the overall efficiency of rare metal utilization in the titanium industry.

Author contributions

Conceptualization: TKS, TAC; Data curation: YEM, TKS; Formal analysis: YEM, TBY; Funding acquisition: TKS, TAC; Investigation: YEM, TBY; Methodology: TKS, TAC; Project administration: TKS, TAC; Resources: TAC, YEM; Software: YEM, TBY; Supervision: TKS, TAC; Validation: TKS, TAC; Visualization: YEM, TBY; Writing – original draft: TKS, TBY; Writing – review & editing: TKS, TAC. All authors have read and agreed to the published version of the manuscript.

Funding

This research was funded by the Committee of Science of the Ministry of Education and Science of the Republic of Kazakhstan under grant No. AP22686490.

Acknowledgements

The authors express their sincere gratitude to the editor and anonymous reviewers for their constructive comments and valuable suggestions, which have significantly improved the quality of this manuscript.

Conflicts of interests

The authors declare no conflict of interest.

Data availability statement

The original contributions presented in this study are included in the article. Further inquiries can be directed to the corresponding author.

References

[1] Shikika, A., Sethurajan, M., Muvundja, F., Mugumaoderha, M.C. & Gaydardzhiev, St. (2020). A review on extractive metallurgy of tantalum and niobium. *Hydrometallurgy, 198. 105496.* https://doi.org/10.1016/j.hydromet.2020.105496

[2] Sarsembekov, T.K. & Chepushtanova, T.A. (2019). Distribution of niobium and vanadium in industrial products during titanium tetrachloride production. *Non-ferrous Metals, (8), 55-60.* https://doi.org/10.17580/tsm.2022.08.07

[3] Sarsembekov, T.K., Yanko, T.B., Sidorenko, S.A. & Pylypenko, M.M. (2020). Concomitant extraction process of niobium at the titanium tetrachloride production. *Problems of Atomic Science and Technology, 1, 173-177*. http://doi.org/10.46813/2020-125-173

[4] Nico, C., Monteiro, T. & Graça, M.P.F. (2016). Niobium oxides and niobates physical properties: Review and prospects. *Progress in Materials Science, 80, 1-37*. https://doi.org/10.1016/j.pmatsci.2016.02.001

[5] Timofeev, A. & Williams-Jones, A.E. (2015). The origin of niobium and tantalum mineralization in the Nechalacho REE deposit, NWT, Canada. *Economic Geology, 110(7), 1719-1735*. https://doi.org/10.2113/econgeo.110.7.1719

[6] Mitchell, R.H. (2015). Primary and secondary niobium mineral deposits associated with carbonatites. *Ore Geology Reviews, 64, 626-641*. https://doi.org/10.1016/j.oregeorev.2014.03.010

[7] Mackay, D., & Simandl, G. (2014). Geology, market and supply chain of niobium and tantalum – a review. *Mineralium Deposita, 49, 1025-1047*. http://doi.org/10.1007/s00126-014-0551-2

[8] de Oliveira Cordeiro, P.F., Brod, J.A., Palmieri, M., de Oliveira, C.G., Rocha Barbosa, E.S., Santos, R.V., Gaspar, J.C. & Assis, L.C. (2011). The Catalão I niobium deposit, central Brazil: Resources, geology and pyrochlore chemistry. *Ore Geology Reviews, 41(1), 112-121*. https://doi.org/10.1016/j.oregeorev.2011.06.013

[9] Boyarko, G.Yu. (2019). Dynamics of global production and trade flows of niobium raw materials. Bulletin of Tomsk Polytechnic University. *Geo Resources Engineering, 330(10), 216-229*. https://doi.org/10.18799/24131830/2019/10/2318

[10] Federal Scientific and Methodological Center for Laboratory Research and Certification of Mineral Raw Materials «VIMS». (2007). Methodology for determining the mass fraction of tantalum and niobium by photometric method with crystal violet or rhodamine-6Zh and sulfochlorophenol-S in rocks, ores and minerals. *Ministry of Natural Resources and Ecology of the Russian Federation, Moscow*

[11] Mukhamadieva, A.S. (2004). Electrolytic refining of niobium in chloride melts. Doctoral dissertation. *Yekaterinburg, Russia*

[12] Rosenkilde, C., Voyiatzis, G., Jensen, V.R., Ystenes, M. & Ostvold, T. (1995). Raman spectroscopic and ab initio quantum chemical investigations of molecules and complex ions in the molten system CsCl–NbCl5–NbOCl3. *Inorganic Chemistry, 34(17), 4360-4369*

[13] Polyakov, E.G. (1998). Niobium in molten salts: state and electrochemical behavior (review). *Journal of Applied Chemistry, 71(2), 181-193*

[14] Maslov, S.V. & Vasin, B.D. (1993). Spectroscopic study of (Na-Cs)Cl eutectic melts containing niobium. *Melts, (4), 37-40*

[15] Voyiatzis, G.A., Pavlatou, E.A., Papatheodorou, G.N., Bachtler, M. & Freyland, W. (1993). Reduction products of pentavalent niobium and tantalum in fused chloride solvents. Proceedings of the Electrochemical Society: *Molten Salt Chemistry and Technology, 9(93), 252-264*

[16] Maslov, A.A., Ostvald, R.V., Shagalov, V.V., Maslova, E.S. & Gorenyuk, Yu.S. (2010). Chemical technology of niobium and tantalum. *Tomsk: Publishing House of Tomsk Polytechnic University*

[17] Morozov, I.S. (1966). The use of chlorine in the metallurgy of rare and non-ferrous metals. *Moscow: Nauka*

Хлорлау өңдеу процесінде ниобийдің әртүрлі титанды құрамды шикізаттарда таралуы

Т.К. Сарсембеков[1*], Т.А. Чепуштанова[1], Е.С. Меркібаев[1], Т.Б. Янко[2]

[1]*Satbayev University, Алматы, Қазақстан*
[2]*UNDERSLAB LTD OOD, Бургас, Болгария*

**Корреспонденция үшін автор: t.sarsembekov@satbayev.university*

Аңдатпа. Бұл мақалада «ӨТМК» АҚ (Қазақстан) компаниясының титан шлактары, норвегиялық TiZir Titanium & Iron AS компаниясының титан шлактары және олардың әртүрлі қатынастағы қоспалары сияқты әртүрлі титанды құрамды шикізатты хлорлау арқылы өңдеу барысында ниобийдің таралуын зерттеу нәтижелері ұсынылған. Титан шлак үлгілері ұсақталып, сілтілі металл хлоридтерінен ($MgCl_2$, KCl, NaCl) тұратын балқытылған тұз ортасында, қалпына келтіруші ретінде ұнтақталған антрацитпен бірге, концентрленген хлор газы арқылы хлорланды. Процесс 700-820°C температурада жүргізілді. Зерттеу барысында титанды шлактарды 60/40, 50/50 және 30/70 (ӨТМК/TiZir) қатынастарда, сондай-ақ 100% ӨТМК шлагында хлорлау кезінде ванадий мен ниобийдің таралу заңдылықтары анықталды. Зерттеу нәтижелері бойынша ниобийдің негізгі бөлігі титан хлораторынан шыққан шлакте және оросительді скруббер пульпасында жиналатыны анықталды. Сондай-ақ бастапқы шикізаттағы ниобий мөлшері артқан сайын оның шаң камерасындағы сублиматта, тұзды ваннаның шаңтұндыру камерасындағы балқымасында және скруббер пульпасындағы концентрациясы артып, ал хлоратор шлагындағы үлесі төмендейтіні байқалды.

Негізгі сөздер: *титан шлактары, ванадий, ниобий, таралу, титан, хлоратор шлактары, хлорлы сублиматтар, хлорлау, шлактарды өңдеу, ниобийді алу.*

Распределение ниобия при хлорной переработке различного титансодержащего сырья

Т.К. Сарсембеков[1*], Т.А. Чепуштанова[1], Е.С. Меркибаев[1], Т.Б. Янко[2]

[1]*Satbayev University, Алматы, Казахстан*
[2]*UNDERSLAB LTD OOD, Бургас, Болгария*

**Автор для корреспонденции: t.sarsembekov@satbayev.university*

Аннотация. В данной статье представлены результаты исследования распределения ниобия при хлорной переработке различных титансодержащих сырьевых материалов, включая титановые шлаки АО «УК ТМК», титановые шлаки норвежской компании TiZir Titanium & Iron AS, а также их смеси в различных соотношениях. Образцы титанового шлака были измельчены и подвергнуты хлорированию с использованием концентрированного хлорного газа в расплаве солей щелочных металлов ($MgCl_2$, KCl, NaCl), при этом в качестве восстановителя использовался тонкоизмельчённый антрацит. Процесс проводился при температуре 700-820°C. Основное внимание в исследовании было уделено поведению ванадия и ниобия при хлорировании смешанных шлаков в соотношениях 60/40, 50/50 и 30/70 (АО «УК ТМК»/TiZir), а также в 100 % шлаке АО «УК ТМК». Результаты показали, что основное количество ниобия накапливается в отвальном шлаке титаново-хлорирующей установки и в пульпе оросительного скруббера. Также установлено, что с увеличением исходного содержания ниобия в сырье возрастает его концентрация в возгонах пылевой камеры, в расплаве солевой пылеосадительной камеры и в пульпе скруббера, тогда как его доля в отвальном шлаке снижается.

Ключевые слова: *титановые шлаки, ванадий, ниобий, распределение, титан, отвальный шлак, хлоридные возгоны, хлорирование, переработка шлаков, извлечение ниобия*.

Publisher's note

All claims expressed in this manuscript are solely those of the authors and do not necessarily represent those of their affiliated organizations, or those of the publisher, the editors and the reviewers.

SATBAYEV UNIVERSITY

Engineering Journal of Satbayev University

Volume 147 (2025), Issue 4, 23-29

https://doi.org/10.51301/ejsu.2025.i4.04

Assessment of industrial waste disposal practices in the mining sector of Uzbekistan

A.T. Nizamova*, A.Kh. Rasulov, D.R. Maxmadiyev

Tashkent State Technical University named after Islam Karimov, Tashkent, Uzbekistan

**Corresponding author: at.nizamova@gmail.com*

Abstract. As a result of the intensive development of the mining and metallurgical industry, the volume of industrial waste continues to grow year after year. These wastes contain highly toxic heavy metals, aggressive chemical reagents, and other environmentally hazardous components threatening the environment and human health. Among the mining sector's most dangerous yet critical infrastructural elements are tailings storage facilities structures designed to accumulate industrial waste (specifically slurry) and typically built from earthen materials. Such facilities' planning, construction, and operation often lack sufficient technical and financial resources, rendering them high-risk structures. Foundation settlement, internal erosion, filtration, breach risk, and seismic instability are all factors that necessitate continuous monitoring to ensure the safety of these storage facilities. Traditional geodetic and mine surveying techniques provide insufficient monitoring capabilities. In current conditions, these methods must be supplemented by geoinformation technologies (GIS, remote sensing, UAVs), which offer spatial coverage, rapid data acquisition, and the capacity for integrated analysis. This paper presents a detailed analysis of the structure, risk level, and monitoring methods of various waste storage facilities operated by the Navoi Mining and Metallurgical Combinat (NMMC), utilizing GIS technologies.

Keywords: *mining and metallurgical waste, geoinformation technologies, GIS, remote sensing, tailings storage, uncrewed aerial vehicles, environmental risk, spatiotemporal analysis.*

Received: 04 June 2025
Accepted: 15 August 2025
Available online: 31 August 2025

1. Introduction

In recent decades, the rapid expansion of the mining and metallurgical industry has been accompanied by a sharp increase in its associated environmental risks. In particular, the continuous growth in industrial waste volumes and the presence of highly toxic heavy metals, aggressive chemical reagents, and radioactive components make this issue one of the most pressing scientific and practical problems, posing significant threats to environmental and public health.

Typically, such waste accumulates over large areas near mining sites, where special hydraulic structures, tailings and sludge storage facilities are constructed for containment and management. These facilities are intended for the temporary or permanent storage of liquid or semi-liquid residues from ore processing and often suffer from inadequate stability, seismic resilience, and operational reliability. Their insufficient investment support and failure to meet modern engineering standards frequently make them some of the mining infrastructure's most vulnerable and hazardous elements. Consequently, they are susceptible to internal erosion, settlement, filtration, flooding, and seismic impacts, requiring continuous monitoring [1, 2].

In recent years, geoinformation technologies (GIS), Earth remote sensing (ERS), uncrewed aerial vehicles (UAVs), digital elevation models (DEMs), and global navigation satellite systems (GNSS) have emerged as promising supplements to traditional mine surveying methods. GIS capabilities, in particular, enable the analysis of the spatiotemporal dynamics of waste distribution, risk zone modeling, real-time warning system development, and interactive visualization of monitoring results.

2. Materials and methods

Uzbekistan’s mining and industrial sector includes numerous sites that warrant special attention to environmental safety and waste management systems. These sites are primarily located in the Navoi, Samarkand, Jizzakh, and Khorezm regions, serving as accumulation points for various waste generated through industrial activity (Figure 1). These include slurries (pulp), solid and liquid household waste, non-toxic and non-radioactive industrial waste, and sludges containing suspended substances in wastewater. Each site has distinct parameters, location, surface area, commissioning date, and waste storage capacity, requiring tailored scientific and practical analysis for effective environmental monitoring and regional safety policy development.

This approach enables a comprehensive assessment of potential environmental risks, forming state and corporate ecological oversight priorities, and the development of effective measures to prevent emergencies.

at.nizamova@gmail.com; abdulladjanrasulov1995@gmail.com; dmaxmadiyev@gmail.ru
Engineering Journal of Satbayev University. eISSN 2959-2348. Published by Satbayev University

Specifically, the pulp storage facilities located in the «Muruntau» industrial zone of the Navoi region, under the jurisdiction of the Central Mining Administration (2nd Processing Plant), are among the largest tailings repositories in Uzbekistan. These facilities began operating in 1969 and 1975 and now span over 3,452 hectares. Over 2.5 million tons of industrial slurry have been accumulated there. In the nearby «Besapan» industrial zone, a centralized landfill for solid household and industrial waste is also active, containing approximately 79,000 tons. Both sites have been designated 300-meter sanitary protection zones as necessary epidemiological and environmental safety buffers.

Additionally, waste storage sites operated by the Northern Mining Administration in the Uchkuduk district are of significant ecological concern. These include pulp accumulation areas and industrial waste burial sites commissioned in 1995 and 2000. They hold over 142,000 tons of slurry and over 400 tons of industrial waste. Sanitary protection zones of up to 1,000 meters have been established around these facilities, which is critical in limiting harmful environmental impacts.

Furthermore, three waste storage sites operated by the 1st Mining Administration (Processing Plant) in Navoi city are major accumulation centers for mining industry waste (Figure 2). These facilities, active since 1964, store radioactive, toxic, and non-toxic industrial waste, construction debris, household garbage, and metal residues recovered from industrial filters. In certain sections, over 85,000 tons of trash are stored, with sanitary protection zones reaching up to 800 meters, an essential safeguard due to their proximity to urban areas.

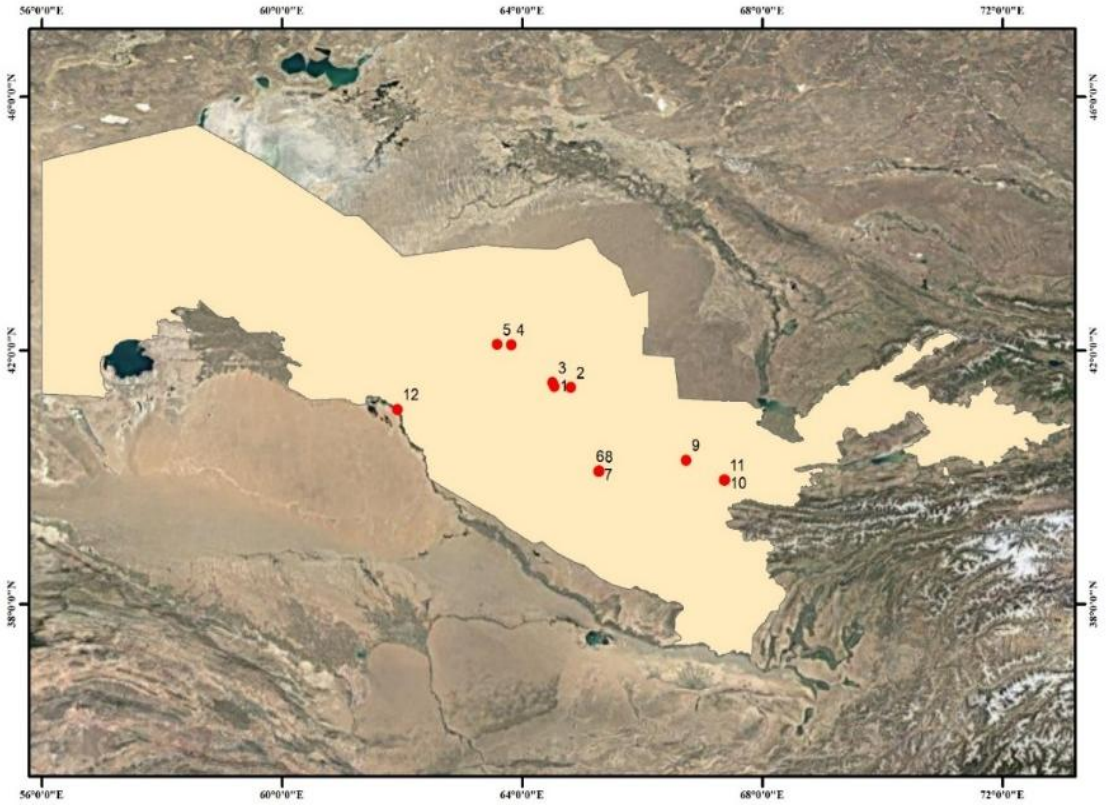

Figure 1. Location of the NMMC tailings facility in the Republic of Uzbekistan. 1 – first-stage tailings accumulation site (tailings storage); 2 - second-stage tailings accumulation site (tailings storage); 3 - centralized landfill for disposal and storage of solid household and industrial waste located in the Besapan industrial area; 4 – 3-HMP tailings accumulation site (tailings storage); 5 – Industrial waste burial site; 6 – 1st «HMP» mining administration industrial waste storage section; 7 – 1st «HMP» mining administration industrial waste storage section; 8 – 1st «HMP» mining administration industrial waste storage section; 9 – 4th «HMP» mining administration industrial waste storage section; 10 – Marjonbuloq waste storage section; 11 – Marjonbuloq old waste storage section (tailings storage); 12 – central mining administration sludge storage site of the industrial area; HMP – hydrometallurgical plant

The Southern Mining Administration's sites, located in Samarkand and Jizzakh regions, are relatively new, having been commissioned between 2017 and 2020. In particular, the «Marjonbulok» industrial zone facilities meet modern environmental standards. They store approximately 35,000 tons of waste and have a 100-meter sanitary protection zone, allowing them to be categorized as relatively safe (Figure 3).

Another ecologically significant site is located in the Tuproqqala district of the Khorezm region. Managed by the Central Mining Administration, this site has been used since 1986 to store sludge from sedimented particles in the Amu Darya River water. The facility covers 15 hectares and contains around 15,000 tons of waste. Such sites are crucial in preserving water resources and preventing hydrosphere contamination.

The state of tailings and sludge storage facilities in these areas is regularly and reliably monitored under existing regulatory guidelines [3], primarily using traditional methods. The main objective is to detect geodynamic processes that could compromise dam stability.

Such facilities' planning, construction, and operation often lack sufficient technical and financial resources, rendering them high-risk structures. Foundation settlement, internal erosion, filtration, breach risk, and seismic instability are all factors that necessitate continuous monitoring to ensure the safety of these storage facilities.

Figure. 2. Tailings facility for industrial waste, Mining Administration No. 4 «Processing Plant»

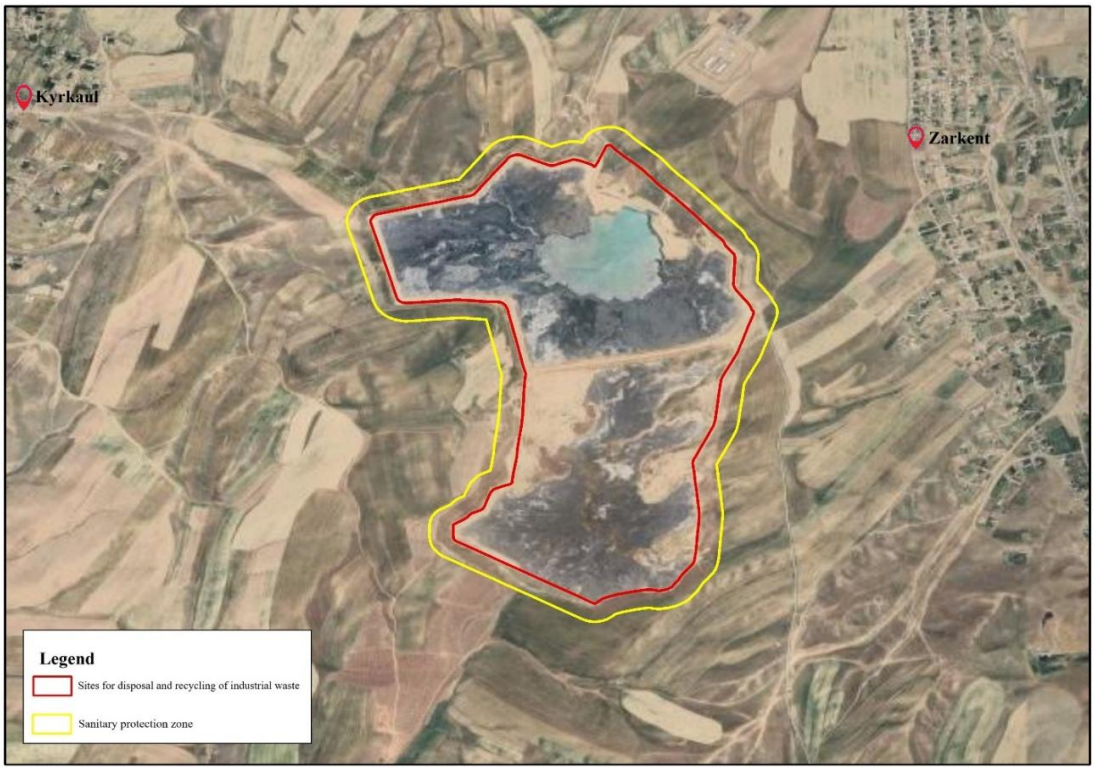

Figure 3. Tailings facility for industrial waste, Mining Administration No. 1 «Processing Plant»

Traditional geodetic and mine surveying techniques provide insufficient monitoring capabilities. In current conditions, these methods must be supplemented by geoinformation technologies (GIS, remote sensing, UAVs), which offer spatial coverage, rapid data acquisition, and the capacity for integrated analysis. This paper presents a detailed analysis of the structure, risk level, and monitoring methods of various waste storage facilities operated by the Navoi Mining and Metallurgical Combinat (NMMC), utilizing GIS technologies [4-6]

This monitoring includes surveying the vertical and horizontal displacements of dam structures. Effective and targeted observation of deformation processes requires thorough preliminary analysis of project documentation, geotechnical conditions (engineering geology and hydrogeology), and structural geometry. These assessments help determine dam stability levels and identify the most deformation-prone areas, guiding the placement of measurement instruments and observation points.

Control points are established in deformation-free zones, considering the maximum dimensions of each structure. Benchmark markers are installed on each moist layer, aligned with longitudinal and cross-sectional profiles. The spacing between markers is determined based on geological, hydrogeological, and technological factors to ensure sufficient data collection on deformation processes.

Field studies indicate that in high-risk areas, this spacing is approximately 50 meters, while in peripheral areas it ranges from 150 to 200 meters.

The geometric leveling method is the most widely used technique for measuring the settlement of engineering structures. The accuracy of third-class leveling is defined by closure discrepancies in leveling loops not exceeding ± 10 mm $\times \sqrt{L}$, where L is the length of the run-in kilometers. High-precision or precision levels in this class typically ensure a mean square error of no more than 2.5-3 mm per kilometer of leveling.

The trigonometric leveling method is employed when it is necessary to determine the settlement of points located at significantly different elevations or in hard-to-reach areas. When using optical or electronic instruments with an angular measurement error not worse than 2 seconds, the vertical elevation accuracy ranges from 0.3 mm to 8 mm for distances up to 500 meters. However, this accuracy rapidly decreases as distance increases beyond 1 kilometer; only decimeter-level precision is achievable.

The alignment method (or collimation method) is most commonly applied in hydro-engineering and irrigation infrastructure to monitor displacements. It is viable where working benchmarks can initially be placed in a straight line and approximately at the same elevation. However, implementing this for tailings dam monitoring is nearly impossible due to the deformations inherent in such structures [7, 8].

Angular or linear resection methods are used when it is possible to place observation benchmarks within line-of-sight from two baseline points situated on elevations. Horizontal and vertical angles are measured in these linear-angular networks and resections using high-precision electronic-optical instruments.

In all observation methods, it is advisable to use electronic distance meters (EDMs), which ensure high accuracy in distance measurements. For example, modern EDMs and electronic total stations can provide measurement accuracy defined as:

– $m_L = 1 + 1 \cdot 10^{-6} L$, mm (for short baselines);

– $m_L = 5 + 1 \cdot 10^{-6} L$, mm (for general applications).

Satellite coordinate determination methods, utilizing modern GPS equipment, offer extremely high measurement accuracy:

– $m_L = 5 + 1 \cdot 10^{-6} L$, mm for single-frequency,

– $m_L = 3 + 1 \cdot 10^{-6} L$, mm for dual-frequency systems.

3. Results and discussion

Measurements of baselines up to 2 km using GPS show discrepancies of less than 1 mm. However, due to certain limitations (signal obstructions, time requirements), GPS cannot entirely replace traditional observation methods. Instead, GPS is more appropriate for tracking reference (baseline) points.

Many countries have implemented large-scale research and practical systems for monitoring mining and metallurgical waste alongside traditional methods. Adopting geoinformation technologies in geotechnical risk analysis, environmental monitoring, and remote waste management has significantly changed the industry.

International experience highlights the importance of integrating geoinformation technologies in the monitoring, assessment, and risk management of mining waste. Adapting technologies like UAVs, remote sensing, and digital modeling to national contexts can significantly improve waste storage safety [9, 10]

A detailed comparison of traditional mine surveying methods and modern GIS-based approaches reveals distinct strengths and limitations, as outlined in Table 1.

Table 1. Key comparative parameters

Criterion	Traditional mine surveying methods	Modern GIS-based approaches
Coordinate accuracy	Millimeter-level precision, but limited to localized points	High accuracy via GNSS; lower with satellite data (10–30 m for Sentinel-2)
Area coverage	Limited; requires on-site visits for each location	Broad area coverage (up to 1,000 km² per satellite image)
Operational timeliness	Monitoring requires field expeditions; frequency is monthly or yearly	Sentinel-2: every 5 days; UAVs: real-time, frequent and automated
Data analysis	Manual or Excel-based; lacks spatial analysis	Multi-layer spatial analysis, 3D modeling, spatiotemporal trend detection
Environmental risk analysis	Subjective; based on visual on-site inspection	Analysis via spectral indices (NDWI, SAVI, MSI) for dust, moisture, and vegetation changes
Subsurface deformation detection	Only surface-level deformation is detectable.	InSAR technology enables the detection of profound structural shifts (foundation settlement)
Cost and resources	Initially low cost, but time and labor-intensive	High initial investment, but long-term efficiency via automation and speed
Visualization and reporting	2D graphs and printed maps	Interactive Web-GIS, 3D visualization, real-time dashboards
Human factor dependency	High, prone to error and subjectivity	Low; automation reduces subjectivity
Monitoring frequency	Periodic (monthly or quarterly), bureaucratically constrained	Weekly, daily, or near real-time

The methodological analysis conducted as part of this study highlights that the effectiveness of monitoring techniques for industrial waste depends on the purpose, geophysical conditions, complexity of the sites, and level of anthropogenic risk. The research compared traditional geodetic and mine surveying approaches with modern GIS-based methods, evaluating their responsiveness and applicability (Figure 4).

Traditional geodetic techniques offer high-precision measurements of physical surface changes and are particularly useful for local site-specific monitoring and structural deformation assessment. However, they are limited in tracking spatiotemporal dynamics, real-time monitoring, and environmental evaluation [11-13].

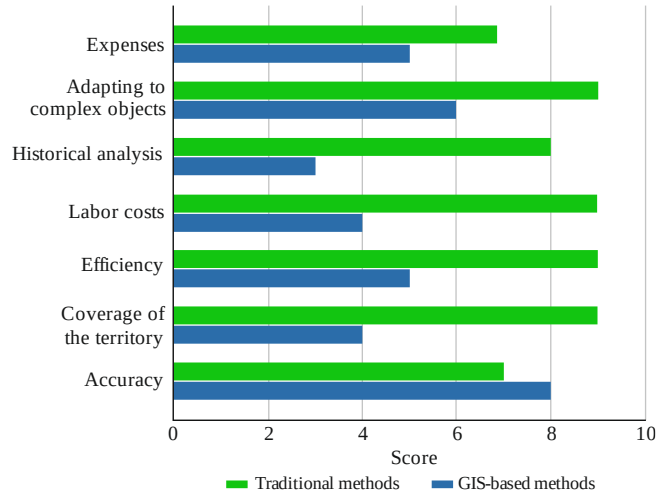

Figure 4. Comparison of traditional and GIS-based monitoring in the mining and metallurgical sector

In contrast, modern tools, including GIS, remote sensing (RS), UAVs, DEMs, and GNSS, elevate monitoring to a new level. These technologies provide broad temporal and spatial coverage; enable digital modeling, automated analysis, forecasting, and integration with management systems. GIS tools are especially indispensable for identifying risk zones involving slurry and toxic waste, modeling geodynamics, and detecting seismic instability. Their implementation demands advanced technical infrastructure, skilled personnel, and financial investment.

Traditional mine surveying methods provide accurate local data but are reactive and fragmented. They are not efficient for rugged or environmentally sensitive areas. GIS technologies significantly enhance monitoring by automating processes, visualizing spatial-temporal dynamics, forecasting risk factors, and integrating with management systems.

The most effective approach is a hybrid monitoring system**,** combining the precision of traditional methods with the coverage, efficiency, and analytical depth of GIS technologies (Table 2).

Table 2. Functional Logic of the Hybrid Model

Component	Function
Traditional Measurements	Localized accuracy and registration of primary deformations
UAV + DEM	Detection of surface-level changes and subsidence
GNSS	High-precision geolocation of dynamic points
GIS + RS	Spatiotemporal threat analysis
InSAR + IoT	Monitoring of subsurface pressures and oscillations
Visualization Tools	Web-GIS, 3D maps, real-time risk dashboards

Such a system is essential for ensuring industrial waste's safe and efficient monitoring, enabling real-time detection of subsidence, deformation, and other hazards in mining zones [14, 15].

The hybrid monitoring model combines both traditional and modern technologies. Classical methods include surface displacement monitoring using theodolites, levels, and total stations and surveying deformation benchmarks. Sequential measurements within a network of reference points remain essential, along with regular visual inspections at fixed intervals, which ensure localized accuracy and direct observation of critical areas.

At the same time, modern technologies significantly expand the scope and efficiency of monitoring. GIS systems allow advanced spatial analysis and the creation of detailed risk maps, while remote sensing provides valuable data through spectral indices such as NDWI, SAVI, and MSI from satellites like Sentinel-2 and Landsat. UAVs enhance the process by enabling 3D terrain modeling and detection of surface changes, and GNSS ensures precise geolocation of shifting points. In addition, InSAR technology makes it possible to identify deep subsurface deformations by analyzing radar signals, which adds a crucial predictive dimension to hazard monitoring.

4. Conclusions

Amid growing global environmental concerns, the issue of identifying and managing risks associated with industrial waste in the mining and metallurgical sector has become increasingly urgent. Based on the Navoi Mining and Metallurgical Combinat (NMMC) example, this study demonstrated that although traditional mine surveying methods offer high precision, they lose effectiveness in large-scale spatial monitoring. This limitation significantly hampers the assessment of safety conditions and the ability to generate real-time forecasts.

In contrast, modern geoinformation technologies such as GIS, remote sensing (RS), UAVs, digital elevation models (DEMs), and GNSS have ushered in a qualitatively new phase of monitoring for industrial infrastructure. These technologies enable spatiotemporal analysis of changes, risk zone detection, interactive visualization, and integration with environmental management systems.

Based on the conducted analysis, a hybrid monitoring model was proposed, combining the accuracy of conventional geodetic methods with the extensive capabilities of GIS. This model allows for assessing tailings dam stability through field observations and advanced digital analytical tools in near real-time. Furthermore, drawing on international experience, integrating Digital Twin platforms and automated Web-GIS systems can provide high safety and efficiency for environmental monitoring within Uzbekistan's mining infrastructure.

Thus, the outcomes of this research offer scientifically grounded, technologically advanced, and practically significant solutions for managing industrial waste in the mining and metallurgical sector. These findings contribute to developing long-term strategies for ecologically sustainable industrial growth.

Author contributions

Conceptualization: ATN; Data curation: AKR; Formal analysis: AKR, DRM; Funding acquisition: AKR; Investigation: DRM; Methodology: ATN; Project administration: ATN, AKR; Resources: DRM; Software: DRM; Supervision: ATN; Validation: ATN; Visualization: ATN; Writing – original draft: ATN, AKR; Writing – review & editing: ATN, AKR. All authors have read and agreed to the published version of the manuscript.

Funding

This research was carried out as part of the research plan of Tashkent State Technical University on the topic: «Scientific Foundations of Mine Surveying for Rational, Comprehensive, and Safe Mining and Subsoil Protection».

Acknowledgements

The authors express their sincere gratitude to the editor and anonymous reviewers for their constructive comments and valuable suggestions, which have significantly improved the quality of this manuscript.

Conflicts of interest

The authors declare no conflict of interest.

Data availability statement

The original contributions presented in this study are included in the article. Further inquiries can be directed to the corresponding author.

References

[1] Clarkson, L. (2021). Comprehensive Monitoring Strategy for Tailings Dams. *University of Queensland*

[2] Steven, G.V. (1990). Planning, Design, and Analysis of Tailings Dams. *BiTech Publishers, Limited*

[3] Cabinet of Ministers of the Republic of Uzbekistan. (2018). Regulation on enhancing geological management and environmental control (Resolution No. 983).

[4] Rauhala, A., Tuomela, A., Davids, C., & Rossi, P.M. (2017). UAV Remote Sensing Surveillance of a Mine Tailings Impoundment in Sub-Arctic Conditions. *Remote Sensing, 9(12), 1318.* https://doi.org/10.3390/rs9121318

[5] Nie, W., Luo, M., Wang, Y. & Li, R. (2022). 3D Visualization Monitoring and Early Warning System of a Tailings Dam–Gold Copper Mine Tailings Dam in Zijinshan, Fujian, China. *Frontiers in Earth Science, (10), 1-14.* https://doi.org/10.3389/feart.2022.800924

[6] Sayyidqosimov, S.S. (2021). Geo-information Systems in Mine Surveying. *Textbook, Tashkent*

[7] Kuldeev, E.I., Nurpeisova, M.B. & Kyrgizbaeva, G.M. (2021). Subsoil Development and Environmental Safety. *Germany: LAR Lambert Academic Publishing*

[8] Scaioni, M., Marsella, M., Crosetto, M., Tornatore, V. & Wang, J. (2018). Geodetic and Remote-Sensing Sensors for Dam Deformation Monitoring. *Sensors, 18(11), 3682.* https://doi.org/10.3390/s18113682

[9] National Committee. (2025). National Statistics Committee of the Republic of Uzbekistan. *Retrieved from*: https://stat.uz/ru/

[10] Rojas, L., Peña, Á. & Garcia, J. (2024). A Framework for Monitoring Stability of Tailings Dams in Realtime Using Digital Twin Simulation and Machine Learning. *Procedia Computer Science, 232(3), 2279-2288.* https://doi.org/10.1016/j.procs.2024.02.047

[11] Rojas, L., Peña, Á. & Garcia, J. (2025). AI-Driven Predictive Maintenance in Mining: A Systematic Literature Review on Fault Detection, Digital Twins, and Intelligent Asset Management. *Applied Sciences, 15(6), 3337.* https://doi.org/10.3390/app15063337

[12] Nurpeisova, M.B., Salkynov, A.T., Soltabayeva, S.T. & Miletenko, N.A. (2024). Patterns of development of geomechanical processes during hybrid open pit/underground mineral mining. *Eurasian mining, (1), 7-11*. https://doi.org/10.17580/em.2024.01.02

[13] Digital Twins for Tailings Dams. (2025). Water Power Magazine. *Retrieved from:* https://www.waterpowermagazine.com/analysis/digital-twins-for-tailings-dams

[14] Nurpeisova, M., Dzhangulova, G., Kurmanbaev, O., Sarsembekova, Z. & Ormanbekova, A. (2024). Creation of geodetic reference network for monitoring transport interchanges in seismic. *News of the National Academy of Sciences of the Republic of Kazakhstan series of geology and technical, (4), 209-223.* https://doi.org/10.32014/2024.2518-170X.4364

[15] Don, M.G., Wanasinghe, T.R., Gosine, R. & Warrian, P.J. (2025). Digital Twins and Enabling Technology Applications in Mining: Research Trends, Opportunities and Challenges. *IEEE Access, 13, 6945-6963.* https://doi.org/10.1109/ACCESS.2025.3526881

Өзбекстанның тау-кен секторындағы өнеркәсіптік қалдықтарды кәдеге жарату тәжірибесін бағалау

А.Т. Низамова*, А.Х. Расулов, Д.Р. Махмадиев

Ислам Каримов атындағы Ташкент мемлекеттік техникалық университеті, Ташкент, Өзбекістан

**Корреспонденция үшін автор: at.nizamova@gmail.com*

Аңдатпа. Тау-кен және металлургия өнеркәсібінің қарқынды дамуы нәтижесінде өнеркәсіптік қалдықтардың көлемі жылдан жылға өсуде. Бұл қалдықтардың құрамында өте улы ауыр металдар, қатты химиялық реагенттер және қоршаған ортаға және адам денсаулығына қауіп төндіретін басқа да экологиялық қауіпті компоненттер бар. Тау-кен өнеркәсібі инфрақұрылымының аса қауіпті және аса маңызды элементтерінің қатарына өнеркәсіптік қалдықтарды (атап айтқанда, шламдарды) жинақтауға арналған және әдетте жер материалдарынан салынған қалдық қоймалары жатады. Мұндай нысандарды жоспарлау, салу және пайдалану көбінесе жеткілікті техникалық және қаржылық ресурстарды қамтамасыз ету үшін жеткіліксіз, бұл оларды жоғары қауіпті құрылымдарға айналдырады. Іргетас шөгінділері, ішкі эрозия, сүзу, бұзылу қаупі және сейсмикалық тұрақсыздық – бұл қоймалардың қауіпсіздігін қамтамасыз ету үшін үнемі бақылауды қажет ететін факторлар. Дәстүрлі геодезиялық және маркшейдерлік әдістер жеткілікті бақылау мүмкіндіктерін қамтамасыз етпейді. Қазіргі жағдайда бұл әдістер кеңістіктік қамтуды, деректерді жылдам жинауды және кешенді талдау мүмкіндігін қамтамасыз ететін геоақпараттық технологиялармен (ГАЖ, қашықтықтан зондтау, ҰҰА) толықтырылуы тиіс. Бұл мақалада ГАЖ технологияларын қолдана отырып, Навои тау-кен металлургия комбинатының (НГМК) қалдықтарын сақтаудың әртүрлі объектілерінің құрылымын, тәуекел деңгейін және мониторинг әдістерін егжей-тегжейлі талдау ұсынылған.

Негізгі сөздер: *тау-кен металлургия өндірісінің қалдықтары, ГАЖ, қашықтықтан зондтау, қалдық қоймалары, ұшқышсыз ұшу аппараттары, экологиялық тәуекел, кеңістіктік-уақыттық талдау.*

Оценка практики утилизации промышленных отходов в горнодобывающем секторе Узбекистана

А.Т. Низамова*, А.Х. Расулов, Д.Р. Махмадиев

Ташкентский государственный технический университет имени Ислама Каримова, Ташкент, Узбекистан

**Автор для корреспонденции: at.nizamova@gmail.com*

Аннотация. В результате интенсивного развития горнодобывающей и металлургической промышленности объём промышленных отходов продолжает расти из года в год. Эти отходы содержат высокотоксичные тяжёлые металлы, агрессивные химические реагенты и другие экологически опасные компоненты, представляющие угрозу окружающей среде и здоровью человека. К числу наиболее опасных и критически важных элементов инфраструктуры горнодобывающей отрасли относятся хвостохранилища, предназначенные для накопления промышленных отходов (в частности, шламов) и, как правило, построенные из земляных материалов. Планирование, строительство и эксплуатация таких объектов зачастую недостаточны для обеспечения достаточных технических и финансовых ресурсов, что делает их высокорискованными сооружениями. Осадка фундаментов, внутренняя эрозия, фильтрация, риск прорыва и сейсмическая нестабильность – всё это факторы, требующие постоянного мониторинга для обеспечения безопасности этих хранилищ. Традиционные геодезические и маркшейдерские методы не обеспечивают достаточных возможностей мониторинга. В современных условиях эти методы должны быть дополнены геоинформационными технологиями (ГИС, дистанционное зондирование, БПЛА), которые обеспечивают пространственный охват, быстрый сбор данных и возможность комплексного анализа. В данной статье представлен подробный анализ структуры, уровня риска и методов мониторинга различных объектов хранения отходов Навоийского горно-металлургического комбината (НГМК) с использованием ГИС-технологий.

Ключевые слова: *отходы горно-металлургического производства, ГИС, дистанционное зондирование, хвостохранилища, беспилотные летательные аппараты, экологический риск, пространственно-временной анализ.*

Publisher's note

All claims expressed in this manuscript are solely those of the authors and do not necessarily represent those of their affiliated organizations, or those of the publisher, the editors and the reviewers.

SATBAYEV UNIVERSITY

Engineering Journal of Satbayev University

Volume 147 (2025), Issue 4, 30-36

https://doi.org/10.51301/ejsu.2025.i4.05

Geodynamics of the Shu-Ile ore zone: integration of geophysical, geochemical and cosmogeological methods

A.B. Baibatsha[1], M.K. Kembayev[1*], S.E. Rais[1], W. Yan[2], A.K. Amantayev[1], Y.T. Biyakyshev[1]

[1]*Satbayev University, Almaty, Kazakhstan*
[2]*University of Houston, Texas, USA*

**Corresponding author: m.kembayev@satbayev.university*

Abstract. The article presents the results of a comprehensive study of the Shu-Ile metallogenic zone using modern geophysical, geochemical methods and technologies of remote sensing of the Earth. The purpose of the study was to establish patterns of ore deposits within the zone based on new geodynamic approaches and the integration of multidisciplinary geological data. The relevance of the work is determined by the need to create sound predictive models of mineral deposits, including gold, polymetals and related elements, in conditions of a complicated geological situation and the exhaustion of lightly explored resources. During the research, data from gravimetry, magnetic surveying, electromagnetic sensing and remote sensing data, as well as geochemical characteristics of ore-bearing formations, were analyzed. These data were compared with the results of field observations, stratigraphic and tectonic constructions. A comprehensive analysis made it possible to identify zones of active interaction between the mantle and the earth's crust, manifested in the form of deep faults, subvertical conductive structures and tectonically weakened zones that play a key role in the formation of ore nodes. Based on a set of geophysical and geochemical features, a new approach to forecasting gold-sulfide and polymetallic mineralization is proposed. It involves modeling deep structures and assessing the degree of their influence on the surface manifestations of ore mineralization. The results obtained are of great practical importance: They can be used to optimize exploration activities, increase the efficiency of drilling programs, and minimize financial costs. The proposed methodology can be successfully applied in other metallogenic provinces of Central Asia, which emphasizes the versatility and practical significance of the work performed.

Keywords: *geodynamics, geophysical anomalies, ore-forming fluids, cosmogeological mapping, mantle plumes.*

Received: 29 April 2025
Accepted: 15 August 2025
Available online: 31 August 2025

1. Introduction

The Shu-Ile ore zone in South Kazakhstan is one of the key geological structures in the region due to its rich ore resources. Deposits of gold (Akbakai ore field), copper, uranium and other minerals have been found in this zone, making it an important target for geological research and exploration. Traditional models of plume-tectonics, widely used to study geotectonics and geodynamics, are not always able to explain the peculiar geological structure of the area, including the mosaic of the lithosphere and the diversity of tectonic structures.

In recent decades, the concept of plume tectonics, which links geodynamic processes with upward convective flows of the mantle (mantle plumes), has become increasingly popular [1-6]. This model represents an alternative view on the formation of tectonic structures and ore zones. It assumes that mantle plumes play a key role in the uplift of matter from the Earth's depths, enriching the crust with metals and creating conditions for mineralization. In the case of the Shu-Ile zone, plume tectonics helps explain the presence of ring structures, deep fault zones, and the associated magmatism and ore deposits.

Studies and analysis of the geological structure and geodynamics of the Shu-Ile ore zone from the position of plume-tectonics showed its practical significance for predicting new promising areas. For this purpose, we used an integrated approach, including geological mapping, geophysical studies and remote sensing. A review of the literature data was carried out, which emphasizes the importance of works on the study of geodynamics from a new position and adaptation of the plume-tectonic model of Kazakhstan to assess the influence of plumes on the formation of mineral provinces.

1.1. Geological and tectonic context

The Shu-Ile ore zone is located within Southern Kazakhstan, which can be considered as an element of the Central Asian orogenic belt. This belt was formed as a result of a long geological evolution starting from the Neoproterozoic, which continued into the Paleozoic and ended in the Mesozoic-Cenozoic [7]. The zone is characterized by a complex system of faults, the development of magmatism and sedimentary basins, reflecting its multistage development.

a.baibatsha@satbayev.university; m.kembayev@satbayev.university; s.rais@stud.satbayev.university; wyan3@uh.edu; abylay.amantayev99@gmail.com; Biyakyshev.Y@stud.satbayev.university
Engineering Journal of Satbayev University. eISSN 2959-2348. Published by Satbayev University

1.2. Historical overview of studies

Geological studies of the Shu-Ile Zone began in the third half of the twentieth century, when ideas about the formation of its mineral potential were established. In the 1980s, the fundamental series of works «Geology of the Shu-Ile region» was published, where the main tectonic elements of the zone were described [8]. However, this very valuable series of works was based on the ideas of the outdated paradigm and it needs to be interpreted on the basis of new theoretical ideas, which are confirmed in the practice of geological works. Modern studies have shifted the focus of geodynamics of the region to plume-tectonic concepts. The new model shows that the territory of Kazakhstan during the Paleozoic was affected by an active mantle plume, which influenced geotectonics and mineral formation [9].

1.3. Tectonic Features

The Shu-Ile zone includes several key structures:

– The Shu-Ile suture is a zone of deep faulting and crushing that has experienced vertical displacements. Along the faults, the fragmented blocks, depending on their inclination directions and vertical displacement amplitude, experienced compression and decompression, respectively, which led to local changes in the material composition of the geologic structures of this zone.

– The ring structures testify to the progressive influence of the mantle plume into the lithosphere during the Paleozoic, which is accompanied by active manifestations of magmatism and metasomatism [10].

– Deep faults served as channels for the uplift of mantle matter and its derivatives controlling ore mineralization [11].

As field geological studies show, these features of geodynamics of this zone are well connected with the provisions of the plume-tectonic concept and localization of ore mineralizations.

2. Materials and methods

The geological analysis of the Shu-Ile ore zone employed a comprehensive suite of methods to investigate both near-surface and deep-seated processes, integrating field observations, laboratory analyses, geophysical surveys, and remote sensing technologies. The methodology was designed to elucidate the complex geodynamic processes governing the formation of the Shu-Ile metallogenic zone, with a focus on plume-tectonic mechanisms. The study area, located within the early Caledonian zone of Kazakhstan and intersecting the Jalaiyr-Naiman geosuture, necessitated a multi-scale and multi-source data integration approach to delineate crustal structures and assess their metallogenic potential. The following methods were employed, building upon and extending previous research frameworks, including those outlined by Baibatsha et al. [3].

2.1 Geologic mapping

Geologic mapping formed the cornerstone of field-based investigations, involving systematic collection of data on the rocks composing tectonic structures, their age, composition, and spatial distribution. Fieldwork included detailed documentation of metamorphic, sedimentary, and magmatic complexes, with samples collected for petrographic and mineralogical analysis. These samples were examined in their natural occurrences and under laboratory conditions using optical microscopy to characterize mineral assemblages and textural relationships. The resulting data facilitated the construction of detailed geologic maps and cross-sections, providing a robust foundation for interpreting the structural and lithological framework of the Shu-Ile zone. Mapping efforts focused on identifying key tectonic features, such as the Shu-Ile suture, ring structures, and deep faults, which are critical for understanding ore localization.

2.2. Geophysical studies

Geophysical methods were employed to probe the subsurface structure of the Shu-Ile ore zone, complementing surface geological observations. These methods included gravimetry, magnetometry, and seismic profiling, each targeting specific aspects of the lithospheric architecture.

2.2.1. Gravimetry

Gravimetric surveys analyzed residual gravity anomalies to identify zones of increased or decreased density, which are indicative of subsurface lithological variations and structural discontinuities. Data were collected through ground-based measurements and supplemented by aerial surveys, processed using specialized software to generate anomaly maps. These maps revealed positive anomalies associated with ultramafic intrusions and negative anomalies corresponding to sedimentary basins, providing insights into the distribution of dense and less dense geological bodies.

2.2.2. Magnetometry

Magnetometric studies focused on mapping magnetic field variations to delineate buried intrusions and tectonic faults. High-resolution aerial surveys and ground measurements were conducted, with data processed to produce magnetic anomaly maps. These maps highlighted linear and isometric magnetic anomalies, reflecting the presence of magnetized bodies such as basic-ultrabasic formations and granitic intrusions. The Kypshakbay Allochthon, for example, was mapped with high-intensity linear magnetic anomalies exceeding +1000 nT, indicative of its ultramafic composition.

2.2.3. Seismic reflection profiling

Deep seismic sounding was applied to examine subhorizontal tectonic flow zones and their connections to crustal anisotropy and slip surfaces. Seismic reflection profiling, using the reflection wave method (RWM), captured intracrustal tectonic stratification, identifying subhorizontal and gently inclined flow zones within the crust. These zones, detected at depths of 10-15 km, divide the crust into upper and lower parts, with notable discontinuities along the boundary between the Early Precambrian basement and the Paleozoic cover. Steep suture zones, while not directly imaged by RWM, were inferred from surface outcrops and correlated with geophysical data, revealing their extension into the mantle. The Kendyktas profile, reaching depths of up to 50 km, underscored the central role of southwest-dipping structures in the Shu-Ile ore belt's crustal architecture.

2.3. Remote sensing

Remote sensing techniques utilized satellite imagery from Landsat ETM+ and ASTER to identify tectonic structures and ore-controlling factors. Image processing was performed using ERDAS IMAGINE and ArcGIS, enabling the detection of over 1800 linear structures, 119 ring structures, and numerous areal intrusive bodies [12]. The spectral characteristics of Landsat ETM+ (15-60 m resolution, with four visible, two near-infrared, and one thermal band) and ASTER (15-90 m resolution, with four visible, six near-infrared, and five thermal bands) provided high-fidelity data for structural mapping.

Digital elevation models (DEMs) based on SRTM (90 m resolution) and ASTER GDEM (25 m resolution) were integrated to enhance topographic and structural interpretations.

Cosmogeological mapping, a key component of remote sensing, involved the interpretation of satellite imagery to produce cosmostructural maps at a 1:200000 scale. These maps identified linear, ring, and arc structures, as well as areal bodies, across two structural levels of different ages. Over 3000 linear structures were identified, with geological interpretations provided for more than 1800, including fault disruptions, layering elements, acidic dykes, and geological boundaries. Faults were classified as primary (northwest-trending with significant right-lateral displacements), significant (subparallel with smaller displacements), and secondary (shorter, sub-vertical structures). Ring structures, totaling 119, ranged in diameter from 1.5 to 190 km and were categorized as metamorphogenic, magmatogenic (plutonogenic and hypabyssal), and tectonogenic, reflecting their diverse endogenous origins. Areal bodies, comprising over 450 magmatic rock bodies, included ultramafic and acidic intrusions, with their orientations and thermal alteration halos providing clues to their emplacement mechanisms.

2.4. Structural-geological mapping

Structural-geological mapping integrated surface geological data with satellite imagery analysis to classify tectonic units. Major structural elements, such as the Jalaiyr-Naiman megasynclinorium and Bolattau meganticlinorium, were delineated, reflecting first-rank tectonic features. This method combined field observations of outcrops with remote sensing data to map fault systems, fold structures, and intrusive bodies. The identification of layering elements and fault-associated cleavage highlighted folding structures, while acidic dykes were spectrally correlated with minor intrusions. This approach ensured a comprehensive understanding of the tectonic framework, particularly the role of northwest-oriented shear zones in controlling mineralization.

2.5. Stratigraphic correlation and petrological sampling

Stratigraphic correlation involved the study of sub-intrusive and intrusive sequences through fieldwork and laboratory analysis. SHRIMP zircon dating was applied to pinpoint key magmatic events in the Neoproterozoic and Paleozoic, providing temporal constraints on tectonic and mineralization processes. Petrological sampling focused on characterizing the mineralogical and petrographic properties of ore-bearing formations, with samples analyzed for their geochemical signatures to infer ore-forming processes.

2.6. Paleogeodynamic reconstruction

Paleogeodynamic reconstruction identified ancient rift zones, back-arc basins, and volcanic arcs instrumental in ore genesis. The study emphasized Ediacaran to Early Carboniferous tectonic regimes, reconstructing the geodynamic settings that facilitated mantle plume activity and crustal mineralization. This method integrated stratigraphic, geophysical, and remote sensing data to model the evolution of the Shu-Ile zone within the broader context of the Kazakh paleocontinent.

2.7. Interpretation of ophiolite complexes

The Shu-Balkhash ophiolite complex was evaluated for its metallogenic implications, with a focus on ophiolitic nappes and thrust sheets. Their structural evolution and mineral potential were assessed through field mapping and geophysical data, highlighting their role as conduits for ore-bearing fluids.

2.8. Data integration

The synthesis of geological, geophysical, and cosmogeological data enabled the construction of a three-dimensional geodynamic model of the Shu-Ile zone. This model integrated seismic profiles, gravity and magnetic anomaly maps, cosmostructural maps, and field observations to elucidate the interplay between mantle plume activity, crustal fault systems, and mineralization processes. The model highlighted the role of deep faults and ring structures as channels for mantle-derived melts, providing a predictive framework for identifying prospective ore deposits.

The methodology is built upon previous research on the Shu-Ile suture, extending earlier methods with additional material adapted from Baibatsha et al. (2024). By combining multi-scale data acquisition and advanced processing techniques, this study establishes a robust framework for understanding the geodynamic and metallogenic evolution of the Shu-Ile ore zone, with implications for regional mineral exploration.

3. Results and discussion

3.1. Geological structure

Analysis of available and obtained data has shown that the Shu-Ile zone is characterized by a mosaic structure with alternation of sedimentary basins, intrusions and tectonic blocks. Ring structures formed in the Neoproterozoic indicate the impact of the mantle plume accompanied by magmatic manifestation, and linear faults of the ring structure of northwest strike control the localization of ore formations.

3.2. Geophysical anomalies

Gravity and magnetic data revealed:

– Positive anomalies associated with ultramafic intrusions (Figure 1) [13,14];

– Negative anomalies corresponding to sedimentary basins (Figure 2) [15].

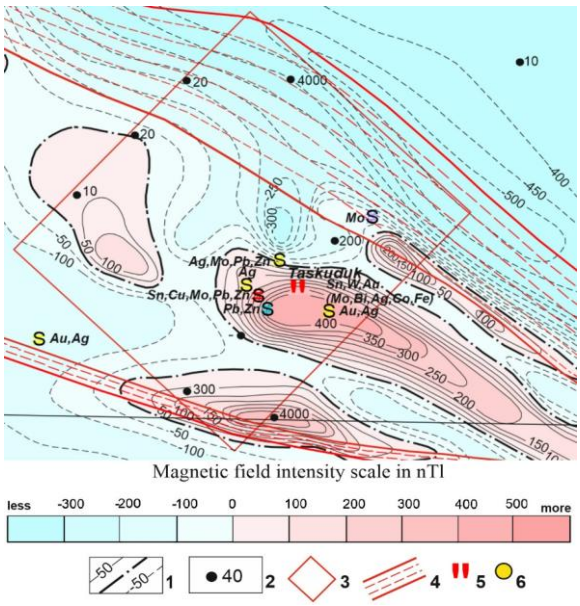

Figure 1. Residual anomalies map of the Ashyktas gold ore field: 1 - granitic (granite massifs are shown on the map of residual anomalies Δg: 1 – Mungli massif; 2 – Yergebulak massif deposits and occurrences of gold-secondary-quartzite type (in brackets – numbers on the maps): a - Ashyktas (4); b – Western Ashyktas (3); Eastern Ashyktas (5); 3 – small deposits and occurrences of gold-sulfide-quartz vein type: Ashyktas Zhilny (2), Kostakyr (6), Shubar (7), Khrustalnoye (8); 4 – Ashyktas gold ore field

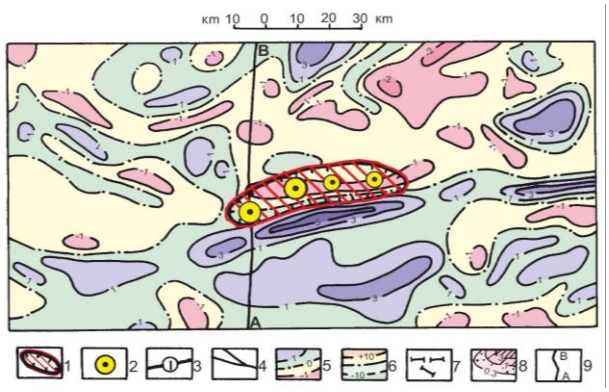

Figure 2. Scheme of the regional magnetic field of the Akbakai ore district: 1 – Kengir-Akbakai ore district; 2 – gold-sulfide-quartz deposits of Akbakai type (1 – large Akbakai, 2 – medium Svetinskoye, 3 – small Kengir, 4 – small Olimpiyskoye); 3 – deep faults separating structural-metallogenic zones; 4 – other faults; 5 – magnetic field isolines; 6 – isolines of residual gravity anomalies; 7 – reflecting sites according to seismic data; 8 – isolines of specific arsenic ore-bearing capacity (t/m/km^2); 9 – line of geological-geophysical section

3.3. Remote sensing

Space images have identified key structures (Figures 3-5) including shear zones and intrusions associated with the Akbakai and Ashiktas deposits [16].

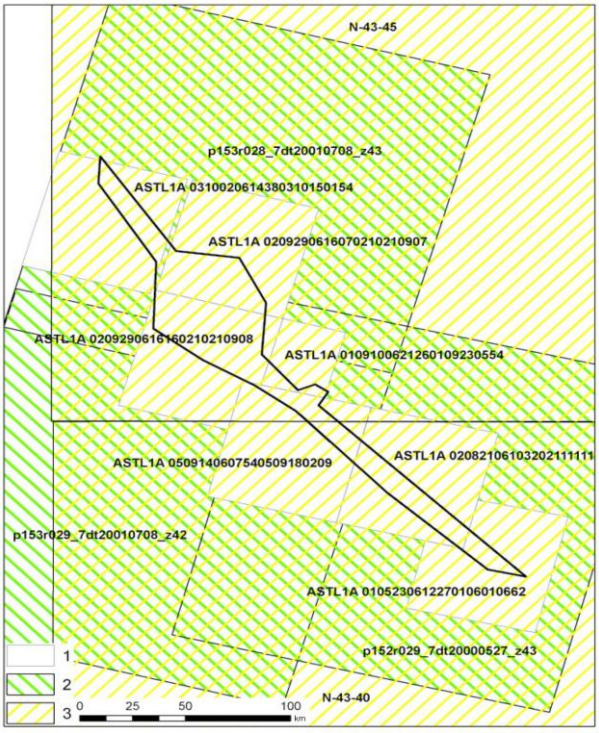

Figure 3. Scheme of coverage of the work area with space data. 1 – ASTER data; 2 – Landsat ETM+ data; 3 – mosaics based on Landsat ETM+ data

Remote sensing analysis has identified shear zones, dikes, and acidic intrusions that define key structural elements of the study area. These features show a clear spatial relationship with the Akbakai and Ashiktas deposits, underscoring their geological significance. Overall, the results demonstrate the effectiveness of satellite imagery in mapping structural and lithological controls on mineralization.

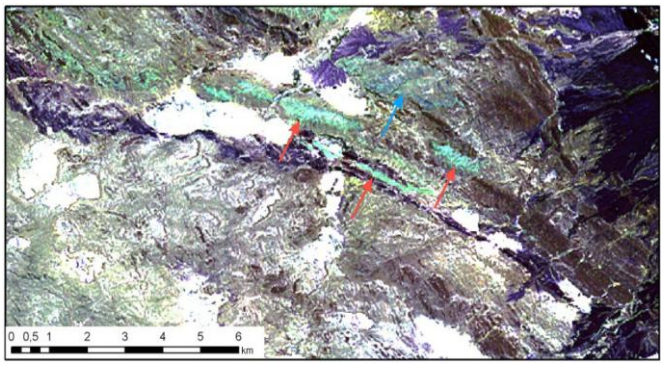

Figure 4. Dikes (shown by red arrows) and stem (shown by blue arrow) of acidic composition in Landsat ETM+ image processing materials

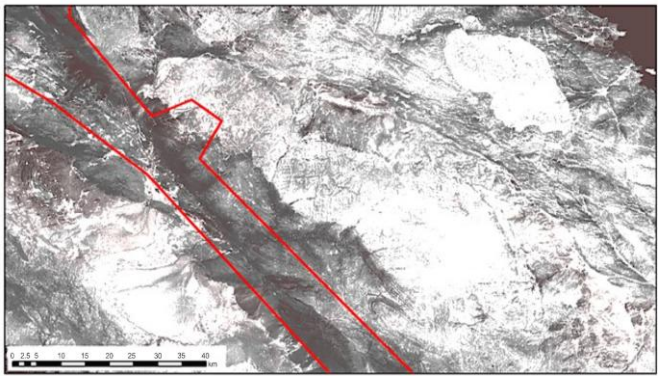

Figure 5. Bodies of sosdvig intrusions of acidic composition near the northeastern boundary of the work area in the materials of processing of Landsat ETM+ images by the «Iron oxides» method

3.4. Integration model

Synthesis of field, geological-geophysical and cosmogeological data shows that the formation of the Shu-Ile suture and its ore potential is plume-tectonic in nature. Based on the results of the studies, linear and ring structures that determine the localization and position of the area intrusive bodies in the mapped zone are clearly identified (Figure 6).

Role of mantle plumes. The data obtained from the performed studies indicate that the mantle plume, which led to the splitting of the Rodinia megacontinent and the isolation of the continent of Kazakhia in the Neoproterozoic, was active during the Paleozoic. The active plume led to the formation of ring structures and sutural zones, within which the corresponding geologic structures and geologic formations developed. Linear structures of different ranks were channels of upwelling solutions that enriched the crust with metals. Comparison of the proposed model with currently existing global analogs (the Hawaiian Plume) confirms its adequacy.

3.5. Practical significance

Plume-tectonic model of geodynamics of Kazakhstan can serve as a reliable theoretical basis explaining the formation of geological structures, and allows to predict new promising areas for mineral prospecting [17]. Ring zones of geosaturas are a system of deep faults and crushing zones. They serve as channels for the penetration of magmatic melts, create conditions for the formation of derivative magmas in the Earth's crust and their ore derivatives for the formation of ore deposits (Figure 7).

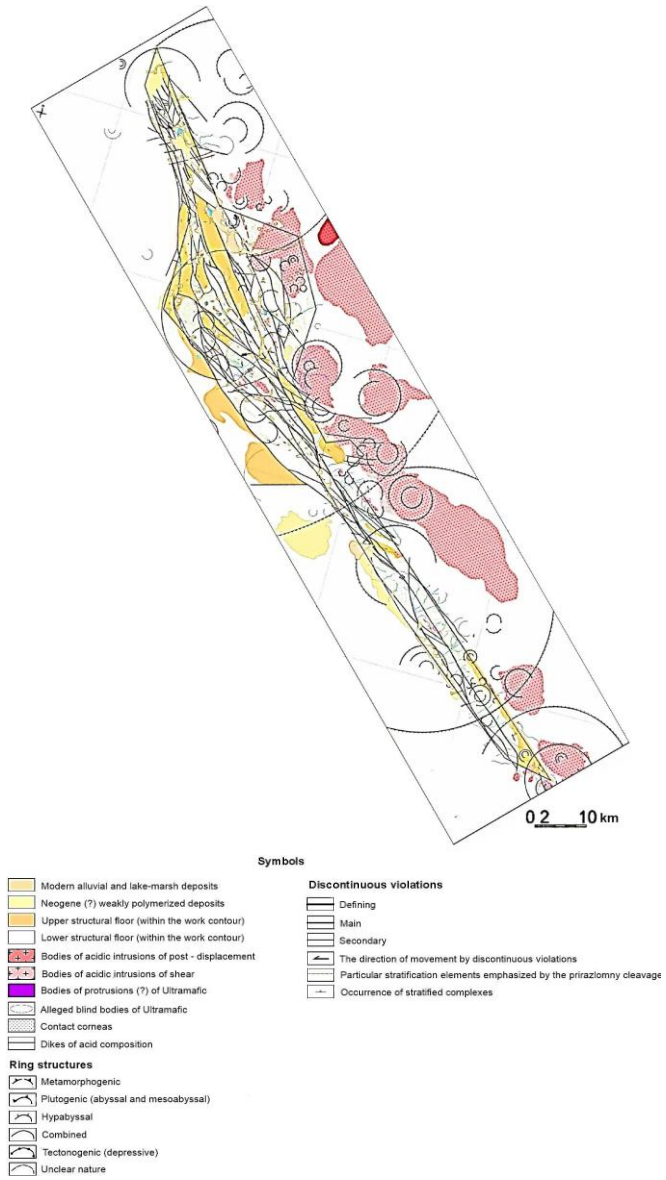

Figure 6. Spatial and structural scheme of the Jalaiyr-Naiman zone. M: 1:200 000

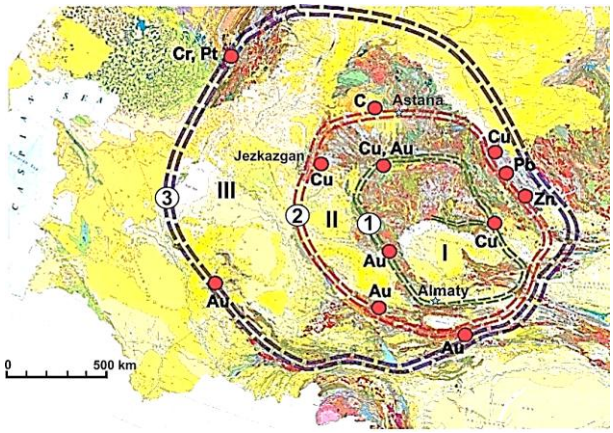

Figure 7. The location of metallogenic belts with the largest mineral deposits along geosuture zones (1, 2, 3) between ring structures (I, II, III) (by Baibatsha, 2020)

Thus, the plume-tectonic model provides both a genetic explanation of ore-bearing structures and a practical framework for guiding mineral exploration in Kazakhstan.

4. Conclusions

The study of the geological structure of the Shu-Ile ore zone in Kazakhstan based on the concept of plume-tectonics allowed us to create an adequate geological model of geodynamics to understand the complex processes that determined the geological evolution of this region. Based on the integration of geologic mapping, geophysical studies and remote sensing data, it was possible to confirm that mantle plumes played a key role in the formation of the tectonic structure and mineral potential of the Shu-Ile suture. These processes not only formed the unique lithospheric architecture of the region but also became a determining factor in the concentration of economically significant mineral deposits, including gold, copper and uranium. This approach allows us to rethink the geological history of the region, going beyond the traditional models of plate tectonics, which are often insufficient to explain the complex structural and mineral features of the territory and are not confirmed by the practice of geological exploration.

The main tectonic elements of the Shu-Ile zone, such as ring structures, linear deep faults and tectonic flow zones, area intrusive bodies, which led to the formation of economic minerals, were identified and characterized. The resulting survey data correlated with geophysical anomalies and remote sensing data to develop a holistic model linking mantle processes to crustal mineralization processes, providing a favorable context for mineral formation in the Shu-Ile Zone and understanding the relationship between deep-seated processes and metallogeny. This approach deepens our understanding of the geological evolution of Kazakhstan and enriches the science of plume-tectonics, providing a concrete example of its successful application in a region with high tectonic and mineralogical complexity. The proposed theoretical ideas about the geodynamics of the Shu-Ile zone are of practical importance in predicting promising areas for prospecting.

Author contributions

Conceptualization: ABB, MKK; Data curation: SER, AKA; Formal analysis: ABB, MKK, SER, WY; Funding acquisition: MKK; Investigation: ABB, MKK, WY, YTB; Methodology: ABB, MKK, SER; Project administration: MKK; Resources: ABB, MKK, SER, YTB; Software: SER, AKA; Supervision: ABB; Validation: ABB, MKK; Visualization: ABB, MKK; Writing – original draft: ABB; Writing – review & editing: ABB, MKK. All authors have read and agreed to the published version of the manuscript.

Funding

This research has been funded by the Science Committee of the Ministry of Science and Higher Education of the Republic of Kazakhstan of AP27511149 «Geological and mineralogical studies of granitoids of Kazakhstan as sources of rare metals to replenish their resources».

Acknowledgements

The authors express their sincere gratitude to the editor and anonymous reviewers for their constructive comments and valuable suggestions, which have significantly improved the quality of this manuscript.

Conflicts of interest

The authors declare no conflict of interest.

Data availability statement

The original contributions presented in this study are included in the article. Further inquiries can be directed to the corresponding author.

References

[1] Pirajno, F. (2000). The Earth's Internal Structure and Convection in the Mantle. *Ore Deposits and Mantle Plumes, 1-58.* http://dx.doi.org/10.1007/978-94-017-2502-6_11

[2] Baibatsha, A.B. (2020). Geotectonics and geodynamics of the paleozoics of Kazakhstan from the position of plume-tectonics. *International Journal of GEOMAT, 19(71), 194-202.* https://doi.org/10.21660/2020.71.31100

[3] Baibatsha, A., Vyazovetsky, Y., Kembayev, M., Rais, S., & Agaliyeva, B. (2024). On the use of remote sensing data to study the geological structure and forecast mineral resources of the Shu-Ile suture. *Mining of Mineral Deposits, 18(4), 56-70.* https://doi.org/10.33271/mining18.04.056

[4] Baibatsha, A.B. (2016). New geodynamic model of the development of the territory of Kazakhstan. *International Geological Congress IGC-35, 194-203*

[5] Baibatsha, A. (2017). Relationship of Paleozoides and Mineral Deposits of Kazakhstan with the Paleozoic Superplume. *SGEM, 17(11), 479-486.* https://doi.org/10.5593/sgem2017/11/S01.061

[6] Dosmukhamedov, N., Kaplan, V., Zholdasbay, E., Argyn, A., Kuldeyev, E., Koishina, G., & Tazhiev, Y. (2022). Chlorination Treatment for Gold Extraction. *Sustainability, 14(17), 11079.* https://doi.org/10.3390/su141711019

[7] Koshkin, V.Ya. (2008). Paleozoites of the western part of the Ural-Mongolian belt. *Geology and Subsoil Protection, (3), 2-10*

[8] Potseluev, A.A., & Ananyev, Y.S. (2012). Remote sensing methods of geological research. *Tomsk: STT*

[9] Yuen, D.A. Shigerenori, M., Shun-Ichiro, K. & Windley, B.F. (2007). Superplumes: Beyond Plate Tectonics. *Netherlands, Springer*

[10] Chen, X., Qu, W., Han, S., Eleonora, S., Yang, N., Chen, Z., & Wang, Z. (2010). Re–Os geochronology of Cu and W–Mo deposits in the Balkhash metallogenic belt, Kazakhstan and its geological significance. *Geoscience Frontiers, 1(1), 115-124.* https://doi.org/10.1016/j.gsf.2010.08.006

[11] C Chen, X., Wang, Z., Chen, Z., Seitmuratova, E., Han, S., Zhou, Q., & Ye, B. (2015). SHRIMP U–Pb, Ar–Ar and fission-track geochronology of W–Mo deposits in the Balkhash Metallogenic Belt (Kazakhstan), Central Asia, and the geological implications. *Journal of Asian Earth Sciences, 110, 19-32.* https://doi.org/10.1016/j.jseaes.2014.07.016

[12] Li, G., Cao, M., Qin, K., Evans, N.J., Hollings, P., & Seitmuratova, E.Y. (2016). Geochronology, petrogenesis and tectonic settings of pre- and syn-ore granites from the W-Mo deposits (East Kounrad, Zhanet and Akshatau), Central Kazakhstan. *Lithos, 252-253, 16-31.* https://doi.org/10.1016/j.lithos.2016.01.023

[13] Joachim, R.R., & Christensen, U.R. (2007). Mantle Plums. *Springer Science & Business Media*

[14] Shen, P., Pan, H.D., Seitmuratova, E. et al. (2016). U-Pb zircon and geochemical constraints on the Nurkazgan Cu–Au deposit in Kazakhstan. *Journal of Asian Earth Sciences, (116), 232–248.* https://doi.org/10.1016/j.jseaes.2015.11.018

[15] Abdulin, A.A. (1980). Geology of the Shu-Ile region. *Alma-Ata: Nauka*

[16] Zhao, D. (2009). Deep mantle plumes and their geological implications. *Earth and Planetary Science Letters, (287), 1-12*

[17] Gao, J., Klemd, R., Zhu, M., Wang, X., Li, J., Wan, B., Xiao, W., Zeng, Q., Shen, P., Sun, J., Qin, K., & Campos, E. (2018). Large-scale porphyry-type mineralization in the Central Asian metallogenic domain: A review. *Journal of Asian Earth Sciences, 165, 7-36.* https://doi.org/10.1016/j.jseaes.2017.10.002

Шу-Іле рудалы зонасының геодинамикасы: геофизикалық, геохимиялық және космогеологиялық әдістердің интеграциясы

А.Б. Байбатша[1], М.К. Кембаев[1*], С.Е. Раис[1], В. Ян [2], А.К. Амантаев[1], Е.Т. Биякышев[1]

[1]*Satbayev University, Алматы, Қазақстан*
[2]*Хьюстон университеті, Техас, АҚШ*

**Корреспонденция үшін автор: m.kembayev@satbayev.university*

Аңдатпа. Мақалада қазіргі заманғы геофизикалық, геохимиялық әдістер мен Жерді қашықтықтан зондылау технологияларын қолдана отырып, Шу-Іле металлогениялық зонасын кешенді зерттеу нәтижелері келтірілген. Зерттеудің мақсаты жаңа геодинамикалық тәсілдер мен көпсалалы геологиялық деректерді біріктіру негізінде кен нысандарын зона шегінде орналасу заңдылықтарын белгілеу болып табылды. Жұмыстың көкейтестілігі күрделі геологиялық жағдай мен біршама оңай барланған ресурстардың сарқылуы жағдайында алтын, полиметалдар мен ілеспе элементтерді қоса алғанда, пайдалы қазбалар кенорындарының негізделген болжамды модельдерін құру қажеттілігімен анықталады. Зерттеу барысында гравиметрия, магниттік түсірілім, электромагниттік зондылау және қашықтықтан зондылау деректері, сондай-ақ кен түзілімдерінің геохимиялық сипаттамалары талданды. Бұл деректер далалық геологиялық байқаулар нәтижелерімен, стратиграфиялық және тектоникалық құрылымдармен салыстырылды. Кешенді талдау мантия мен жер қыртысының белсенді өзара әрекеттесу аймақтарын бөліп көрсетуге мүмкіндік берді, олар терең ақаулар, субвертикал өткізгіш құрылымдар және тектоникалық босаңсыған зоналар түрінде білінеді, олар кен түйіндерінің қалыптасуында шешуші рөл атқарады. Геофизикалық және геохимиялық белгілердің жиынтығы негізінде алтын-сульфидті және полиметалды минералдануды болжаудың жаңа тәсілі ұсынылды. Ол терең құрылымдарды модельдеуді және олардың кенді минералдануының беткі көріністеріне әсер ету дәрежесін бағалауды қамтиды. Алынған нәтижелер маңызды қолданбалы мәнге ие: оларды геологиялық барлау жұмыстарының бағыттарын оңтайландыру, бұрғылау ұңғымалары бағдарламаларының тиімділігін арттыру және қаржылық шығындарды азайту үшін пайдалануға болады. Ұсынылған әдістемені Орталық Азияның басқа металлогениялық провинцияларында сәтті қолдануға болады, бұл орындалған жұмыстың әмбебаптығы мен практикалық маңыздылығын көрсетеді.

Негізгі сөздер: *геодинамика, геофизикалық ауытқылар, кенжасаушы флюидтер, космогеологиялық карталау, мантия плюмдері.*

Геодинамика рудной зоны Шу-Иле: интеграция геофизических, геохимических и космогеологических методов

А.Б. Байбатша[1], М.К. Кембаев[1*], С.Е. Раис[1], В. Ян [2], А.К. Амантаев[1], Е.Т. Биякышев[1]

[1]*Satbayev University, Алматы, Казахстан*
[2]*Хьюстонский университет, Техас, США*

**Автор для корреспонденции: m.kembayev@satbayev.university*

Аннотация. В статье представлены результаты комплексного изучения Шу-Иле металлогенической зоны с применением современных геофизических, геохимических методов и технологий дистанционного зондирования Земли. Цель исследования заключалась в установлении закономерностей размещения рудных объектов в пределах зоны на основе новых геодинамических подходов и интеграции многопрофильных геологических данных. Актуальность работы определяется необходимостью создания обоснованных прогнозных моделей месторождений полезных ископаемых, включая золото, полиметаллы и сопутствующие элементы, в условиях усложнённой геологической обстановки и исчерпания легкоразведанных ресурсов. В ходе исследований были проанализированы данные гравиметрии, магнитной съёмки, электромагнитных зондирований и данных дистанционного зондирования, а также геохимические характеристики рудоносных формаций. Эти данные были сопоставлены с результатами полевых наблюдений, стратиграфическими и тектоническими построениями. Комплексный анализ позволил выделить зоны активного взаимодействия мантии и земной коры, проявляющиеся в форме глубинных разломов, субвертикальных проводящих структур и тектонически ослабленных зон, которые играют ключевую роль в формировании рудных узлов. На основе совокупности геофизических и геохимических признаков предложен новый подход к прогнозированию золотосульфидной и полиметаллической минерализации. Он предполагает моделирование глубинных структур и оценку степени их влияния на поверхностные проявления рудной минерализации. Полученные результаты имеют важное прикладное значение: они могут быть использованы для оптимизации направлений геологоразведочных работ, повышения эффективности буровых программ и минимизации финансовых затрат. Предложенная методология может быть успешно применена и в других металлогенических провинциях Центральной Азии, что подчёркивает универсальность и практическую значимость выполненной работы.

Ключевые слова: *геодинамика, геофизические аномалии, рудообразующие флюиды, космогеологическое картирование, мантийные плюмы*.

Publisher's note

All claims expressed in this manuscript are solely those of the authors and do not necessarily represent those of their affiliated organizations, or those of the publisher, the editors and the reviewers.

SATBAYEV UNIVERSITY

Engineering Journal of Satbayev University

Volume 147 (2025), Issue 4, 37-42

https://doi.org/10.51301/ejsu.2025.i4.06

Creation of a complex for the production of heat and electric power based on the geothermal waters of the Zharkent depression

M.K. Absametov, V.D. Vyalov, D.K. Adenova*, A.M. Baikadamova

Institute of Hydrogeology and Geoecology named after U.M.Akhmedsafin, Almaty, Kazakhstan

**Corresponding author: adenovadinara@gmail.com*

Abstract. The object of this study is renewable energy sources in the Republic of Kazakhstan, with an emphasis on the geothermal resources of the Zharkent field. Geothermal energy is a promising direction in ensuring energy independence and sustainable development, especially in the context of the need to decarbonize the economy and reduce dependence on fossil fuels. The objective of this work is to develop and scientifically substantiate an integrated complex for the production of heat and electricity based on the geothermal resources of the Zharkent field. The study included an analysis of the hydrogeothermal characteristics of the field, an assessment of the energy potential of existing geothermal wells, and a selection of the most efficient technologies, including binary geothermal units, heat pump systems and direct heat supply systems. A feasibility study of the proposed solutions was carried out considering the climatic, geological and infrastructural features of the region. The research results can be applied in the development of pilot projects in the field of geothermal energy, as well as within the framework of the state strategy for the transition to a «green» economy. The proposed complex is capable of increasing the energy sustainability of the Zhetysu region and becoming an example for the implementation of similar solutions in other regions of Kazakhstan.

Keywords: *Zharkent depression, geothermal waters, geothermal technology park.*

Received: 26 May 2025
Accepted: 15 August 2025
Available online: 31 August 2025

1. Introduction

Geothermal energy resources, like other types of renewable energy sources, make it possible to satisfy virtually any consumer in terms of energy potential and quality. However, in economic terms, they can only compete with non-renewable energy resources in the area of electricity production and meeting medium and low potential heat needs. In the future, it is expected that geothermal resources will be widely used for the extraction of rare earth metals and gases, the production of biomass for agriculture, thermal processing of oil horizons, and so on [1-4].

The scope of application and efficiency of using geothermal energy resources of a particular field depend on their energy potential, total reserves and well flow rates, chemical composition, mineralization and aggressiveness of water, the presence of a consumer and its remoteness, temperature and hydraulic regimes of wells, the depth of aquifers and their characteristics, as well as a number of other factors [5-8].

Therefore, exploitation of geothermal sources should be based on prior geological investigation in order to avoid significant financial risk in the event of further capital expenditure. In order to determine whether a particular location has the potential to supply geothermal heat for industrial and domestic needs, a preliminary search is necessary. This feature is one of the main differences between geothermal energy and other renewable energy sources [9-12].

Nowadays, geothermal energy is used in two main directions - heat supply and generation of electrical energy. A number of technologies and efficient equipment have been developed for obtaining both thermal and electrical energy separately and for their combined production [13-15]. In the Russian Federation, combined schemes are being developed for using geothermal sources [16-20] as a heat carrier for heating water at thermal power plants, which provides quite noticeable savings in organic fuel and increases the efficiency of converting low-potential energy. Such combined schemes allow the use of heat carriers with initial temperatures of 70-80ºC for the production of electricity, which is significantly lower than those currently accepted (150ºC and higher) [11-12].

At the St. Petersburg Polytechnic Institute, hydro-steam turbines have been created, the use of which at a geothermal power plant (GeoTPP) will allow an increase in the useful capacity of double-circuit systems (second circuit - water vapor) in the temperature range of 20...200ºC by an average of 22% [4-6].

The efficiency of thermal waters is significantly increased when used in combination. At the same time, in various technological processes it is possible to achieve the most complete realization of the thermal potential of water, including the residual one, and also to obtain valuable components of water (iodine, bromine, lithium, cesium, table salt, Glauber's salt, boric acid and many others) for their industrial use.

mabsametov@mail.ru; valeriy.vyalov@mail.ru; adenovadinara@gmail.com; ainurchuk90@mail.ru
Engineering Journal of Satbayev University. eISSN 2959-2348. Published by Satbayev University

Technical and economic analysis shows that with modern technology for extracting subsurface heat, systems with a borehole depth of up to 3 km are economically justified. The thermal potential of 90% of geothermal waters at this depth does not exceed 100ºC. In this case, geothermal heat supply is predominant, as a result of which the replacement of organic fuel is greater than in the production of electricity [1-10].

2. Materials and methods

The Zharkent geothermal basin is located in the southeast of Kazakhstan, in the Almaty region, near the city of Zharkent, not far from the border with China. Geographically, it is located within the Ili depression, at the foot of the Zhungar Alatau ridges. This region is characterized by active tectonics, high geothermal anomalies and the presence of thermal water outlets, which makes it promising for the development of geothermal resources for both heat supply and balneological use and possible electricity generation [1-2].

There are several wells located in the Zharkent geothermal basin that are of interest for use as an energy source [1-2]. At the first stage, two promising geothermal wells were identified – 1PT and 3T (Figure 1), for which research was conducted on obtaining heat and electricity [2].

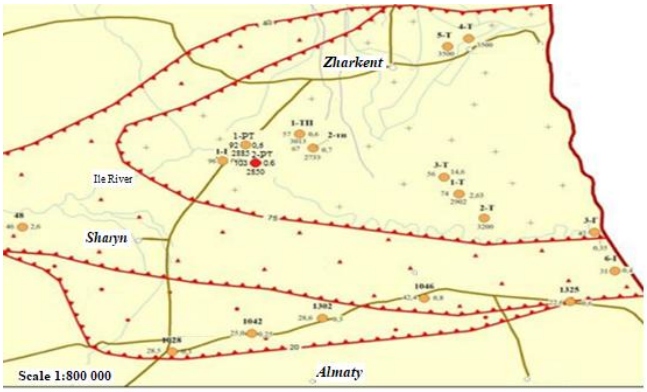

Figure 1. Location of thermal wells in the Zharkent depression

The wells are located 45 km apart and have the same flow rate of 40 kg/s. The water temperature in well 1PT is 92°C, and in well 3T it is 66°C. Both wells penetrate thermal horizons at depths of 1200 to 1800 m within the Zharkent geothermal basin. The reservoirs are represented by fractured sedimentary and volcanogenic-sedimentary rocks. The waters are characterized by medium mineralization (up to 2 g/l) and are of the hydrocarbonate-sodium type. Temperature differences are probably due to the heterogeneity of the geothermal gradient and the depth of the aquifers. The wells are intended for use in heat supply and balneology.

The temperature of geothermal waters in the Zharkent field (from 66°C to 92°C) is considered insufficient for traditional steam turbine plants operating on water vapor. In such conditions, the most effective solution is the use of binary geothermal technology. The essence of binary technology is the use of two working environments (geothermal water and organic working fluid).

Stages of the process flow chart:

1. Supply of geothermal water from the well to the heat exchanger;
2. In the heat exchanger geothermal water heats the secondary liquid which evaporates;
3. Vapors of the organic liquid are fed to the turbine where they rotate the generator and generate electricity;
4. After leaving the turbine the steam cools and turns back into liquid in the condenser closing the cycle;
5. Condensed working fluid returns to the heat exchanger;
6. The spent thermal water is either reused for heating or returned to the reservoir through injection wells (reinjection) which minimizes the environmental impact.

Chemical analyses were carried out according to the scheme of mineral waters. The analysis of the chemical composition of geothermal waters was carried out according to the methods adopted for the classification and assessment of mineral waters, both for drinking and balneological use [2-5].

The purpose of this study is to investigate the possibility of complex (cascade) development of the thermal energy potential of two wells of the Zharkent geothermal field. The main topic of the study is a comparative analysis of the two well options, as well as a brief overview of the chemical composition and possible limitations that may be imposed on the technological process.

Selection and justification of optimal technologies for the production of electricity and heat based on existing geothermal wells of the Zharkent geothermal water field.

For low enthalpy wells such as 3T and 1PT, connecting them by pipeline will not be justified, the pressure and temperature losses over such a distance will outweigh any increase increase in net energy production, in relation to the cost of pumping and the cost of pipelines.

3. Results and discussion

The temperature of the reservoir in the Zharkent field is too low to support the operation of a conventional geothermal power plant. The only practically feasible option for producing electricity from a geothermal flow with a temperature of 70-96°C is binary technology [5, 15].

In recent decades, the production of electricity using binary cycle technology has become increasingly popular. This technology is reliable and has virtually no impact on the environment, and in addition, it allows the use of liquids from less hot thermal sources by heating the working fluid with a lower boiling point (Figure 2).

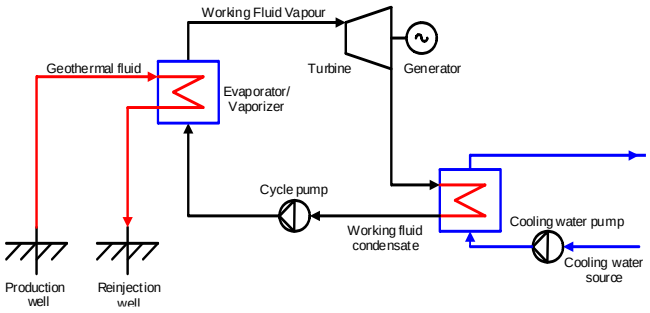

Figure 2. Scheme of electricity production using binary technology

Binary technology is generally divided into two categories: the Organic Rankine Cycle (ORC) and the Kalina Cycle. Since the Kalina cycle is more preferable for geothermal fluid with a temperature of 100-140ºC, it was not considered further. ORC technology is the most common form of power generation from low enthalpy reservoirs [6].

The first observation was to model the 1PT well in a system for maximum power production. In addition, a heating plant was added as a waste heat recovery unit, using waste heat from electricity production. Initially, it was obvious that these two wells could not simultaneously provide both maximum electricity production and sufficient heat supply, however, the waste heat could be used as a base load for district heating or for other purposes with the addition of an oil/gas/coal fired water heater, or for hot water supply for a swimming pool, spa, or other low temperature applications.

The available maximum geothermal energy under different conditions is shown in Table 1.

Table 1. Maximum heat extraction from geothermal water

Name	Well 1 PT with max. electric energy production	Well 1PT without power generation	Well 3T
T at the entrance, °C	62	92	70
T at outlet, °C	40	40	40
Flow rate, dm^3/s	40	40	40
Thermal power, kW	3.681	8.714	5.02

Each well has its own technological scheme for providing heat to the district heating network.

Well 1PT is capable of providing heating water at a temperature of 75ºC without using a post-heating boiler. Figure 3 shows a diagram for maximum heat supply to the district heating network from well 1PT, where the calculated supply temperature is 75ºC.

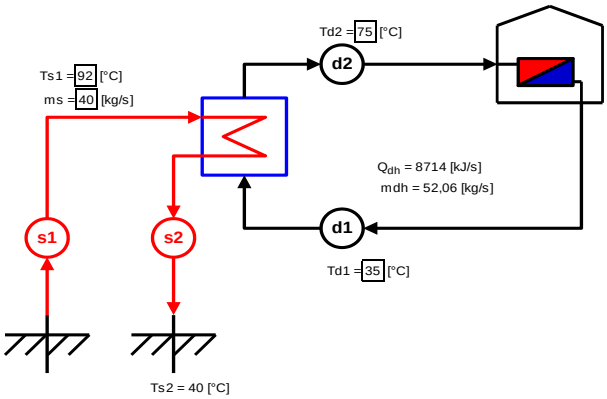

Figure 3. Technological scheme of thermal energy production from well 1PT

However, due to the extremely high demand on cold days, it will certainly be more economical to install a secondary heating boiler. There are two ways to use a secondary heating boiler in a heating system:

– to increase the temperature above 75ºC when necessary.

– when the flow in the network is increased, use the boiler to maintain the supply temperature at 75ºC.

Figure 4 shows a diagram for maximum heat supply to the district heating network from well 3T. A secondary heating boiler must be added to the system as the geothermal water temperature is 70ºC.

The power that can be extracted from a geothermal source depends largely on the heating system used. For example, if a room has 90/70ºC type systems installed, the geothermal energy utilization will be much less. On the other hand, using a geothermal resource for other uses (non-heating) will result in increased energy extraction.

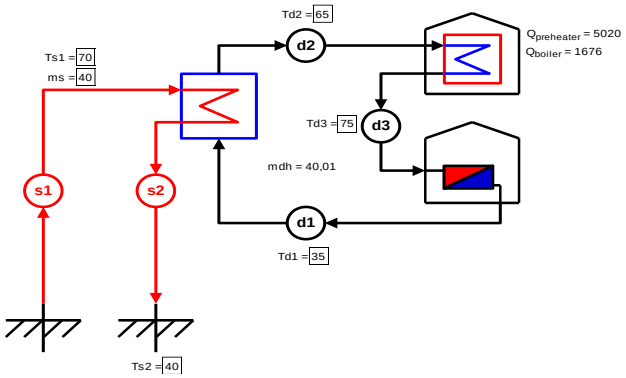

Figure 4. Technological scheme of thermal energy production from well 3T

If domestic hot water is supplied by a system, it is estimated that 10% of the total mass flow will be required.

Vegetables, fruits, spices and flowers are the most common species grown in greenhouses heated using geothermal energy. The optimal growing temperature depends on the plant species, for example, tomatoes are grown at a temperature of 20-21ºC, roses at a temperature of 20-25ºC. The design load of greenhouses is calculated based on a set of requirements for air temperature, natural cooling, lighting and air conditioning. This needs to be further investigated considering detailed information regarding weather conditions, the number of daylight hours, and the plant species grown [6].

The use of geothermal energy in hydrotherapy and other bathing establishments is very effective. The water in swimming pools often has a temperature of 26-29ºC, and in baths 38-42ºC. The heat load for geothermal energy use therefore depends on many factors such as conductive and convective heat exchange and heat transfer between the pool and the environment. Outdoor air temperature, evaporation rate, precipitation, system type (closed or other) also play an important role in this design.

The determination of the thermal energy and hydrogeodynamic potential of thermal waters was based on the study of hydrogeological and geothermal data. Based on the available factual materials on geology, hydrogeology and geothermy, an assessment of regional and operational reserves of thermal waters is given below [9, 11].

Natural heat reserves should be understood as heat contained in groundwater, and operational reserves should be understood as the amount of heat that can be obtained by a technically and economically rational reservoir structure under a given mode during the entire estimated service life [7].

Natural heat reserves of thermal waters are determined based on natural reserves and average temperature (Table 2).

Table 2. Calculated parameters and natural heat reserves of thermal waters of the Zharkent basin

Age of water-bearing rocks	Natural reserves of thermal waters, billion m^3	Estimated temperature, °C	Natural heat reserves, 10^{12} calories
Neogene	86.9	15	1303.5
Paleogene	26.7	35	934.5
Cretaceous	54.1	50	2705
Jurassic	37.7	60	2262
Triassic	42	75	3150
Total			10355

Regional exploitable heat reserves of thermal waters are determined based on Regional exploitable reserves and average temperature as shown in Table 3.

Table 3. Regional exploitable heat reserves of the Zharkent basin

Age of water-bearing rocks	Regional operational reserves, m^3/day	Estimated temperature, °C	Operating heat reserves, 10^3 kcal/day
Neogene	368452.3	15	5526784.5
Paleogene	210836.6	35	7379281
Cretaceous	108164.5	50	5408225
Jurassic	63344.6	60	3800676
Triassic	68049.1	75	5103682.5
Total			27218649

The carrier of geothermal energy is underground water, which compares favorably with all types of energy raw materials due to its widespread occurrence, constant renewability, large reserves, accessibility of obtaining it using modern technical means and the possibility of their comprehensive use.

To generate electricity, a steam-water mixture with a temperature of over 100ºC is used.

Using heat pumps with low energy consumption, water with a temperature of 30-40ºC can be heated to a high temperature suitable for heating, and vice versa, water with a temperature of 70-90ºC can be used to obtain artificial cold in absorption refrigeration machines [8].

The thermal energy productivity of geothermal wells 1-PT and 3-T is determined by the formula:

$$G = 365 \cdot Q \cdot c \cdot \gamma_g \cdot \left(T_m - T_f\right) \cdot 10^{-6}, \quad (1)$$

where G heat energy productivity, Gcal/year; Q is water flow rate, t/day; c is specific heat capacity of water, 1000 kcal/tºC; γ_g is water density during well operation, t/m^3; T_m is water temperature at the wellhead, ºC; T_f is final temperature after use, ºC.

For well 1-PT G is equal to 74.17×10^3 Gcal/year. For well 3-T G is equal to 35.64×10^3 Gcal/year.

The total thermal capacity of the two wells is therefore $G_{total} = 109.81 \times 10^3$ Gcal/year.

This value is equivalent to the combustion of more than 16 thousand tons of standard fuel per year.

Thus, the calculations show that the total thermal energy productivity of wells 1-RT and 3T is 109.81 thousand Gcal/year, which is equivalent to burning more than 16 thousand tons of standard fuel per year. This confirms the high energy potential of the Zharkent geothermal field, sufficient for local heat supply and partial electrification of facilities, as well as for organizing balneological and agro-industrial complexes. Given the high degree of resource sustainability, low greenhouse gas emissions and low operating costs, the use of geothermal energy in this region is a popular area of sustainable energy development. The introduction of binary power plants and heat pumps further expands the possibilities of efficient utilization of low-potential heat. All this makes the Zharkent field a promising object for the implementation of projects within the framework of green energy in Kazakhstan.

4. Conclusions

This article presents the results of a preliminary justification of the possibility of complex (cascade) development of the thermal energy potential of two wells of the Zharkent geothermal field in the Almaty region of the Republic of Kazakhstan.

The wells are ready for operation and require limited restoration work. The cost of drilling a well usually accounts for 50-60% of the cost of a power plant, but in this case, it is not considered. The distance between wells makes it difficult to use them together for economic reasons.

In this paper, two options for using these wells were studied:

1. The maximum power generation for well 1PT, W_{clean} = 265 kWe. Well 3T does not meet the requirements for generating electricity from a geothermal power plant, the water temperature is very low. But thanks to the high pressure, it is possible to obtain electricity from micro hydroelectric power plants. By adding a waste heat recovery unit to the power plant at well 1PT, it is possible to produce 3.7 MW of thermal energy from waste heat after electricity generation.

2. The maximum production of thermal energy without electricity for district heating needs or other applications is 8.6 MW (thermal energy) and 5 MW (thermal energy) for wells 1PT and 3T, respectively.

The first option can be practically implemented with an internal rate of return on investment in 10 years. Also, when adding a waste heat recovery unit to feed the district heating network, the internal rate of return on investment will be 270% for such a unit separately, since it can be used to preheat water for the district heating system (the costs of the afterheating boiler, heating main and district heating system are not taken into account).

The practical implementation of the second option is possible with an internal rate of return on investment in the range of 270-333% after 10 years of operation. Both alternatives are practically feasible. Electricity production has a slower payback period but is feasible from an environmental perspective.

Thermal energy production is a very profitable option when used as a base load preheating element for a district heating system. In the Zharkent depression, several promising areas have been identified that meet the parameters for their practical use: Usekskaya, Priiliyskaya, Neftebaza.

Author contributions

Conceptualization: MKA, VDV, DKA; Data curation: MKA, VDV; Formal analysis: DKA, VDV; Funding acquisition: MKA; Investigation: AMB; Methodology: VDV; Project administration: MKA; Resources: VDV; Software: AMB; Supervision: MKA; Validation: AMB; Visualization: VDV, AMB; Writing – original draft: VDV; Writing – review & editing: DKA. All authors have read and agreed to the published version of the manuscript.

Funding

This research was funded by the Science Committee of the Ministry of Science and Higher Education of the Republic of Kazakhstan, grant number BR21882211.

Acknowledgements

The authors express their sincere gratitude to the editor and anonymous reviewers for their constructive comments and valuable suggestions, which have significantly improved the quality of this manuscript.

Conflicts of interest

The authors declare no conflict of interest.

Data availability statement

The original contributions presented in this study are included in the article. Further inquiries can be directed to the corresponding author.

References

[1] Bondarenko, N.M., Zhevago, V.S. & Kan, M.S. (1981). Thermal anomalies of groundwater in Kazakhstan. *Alma-Ata: «Science» of the Kazakh SSR*

[2] Report of JSC «Kazakh Institute of Oil and Gas». (2006). Pilot project for exploration work on geothermal waters, including the survey of 40 wells that have discovered geothermal waters and the preparation of a feasibility study for their use. *Astana*

[3] Dzhakelov, A.K. (1993). Formation of underground waters of the Chu-Sarysu artesian basin, their resources and prospects for use. *Almaty: Gylym. Retrieved from*: https://search.rsl.ru/ru/record/01000594988?ysclid=mc1swfof7n833755399

[4] Sagin, J., Adenova, D., Tolepbayeva, A. & Poryadin, V. (2017). Underground water resources in Kazakhstan. *International Journal of Environmental Studies, 74(3), 386-398.* https://dx.doi.org/10.1080/00207233.2017.1288059

[5] Gleick, P.H. (1998). The human right to water. *Water Policy, 1*(5), *487-503*. https://doi.org/10.1016/S1366-7017(99)00008-2

[6] Ingrao, C., Strippoli, R., Lagioia, G. & Huisingh, D. (2023). Water scarcity in agriculture: An overview of causes, impacts and approaches for reducing the risks. *Heliyon, 9(8), e18507*. https://doi.org/10.1016/j.heliyon.2023.e18507

[7] Tikhonov, A.N., Shvetsov, P.F. & Dvorov, I.M. (1990). Study and use of geothermal resources in the USSR. Fundamental and applied hydrothermy: Materials of the visiting session of the Scientific Council of the USSR Academy of Sciences on geothermal research. *Alma-Ata: Science*

[8] Butuzov, V.A., Tomarov, G.V. & Shetov, V.Kh. (1989). Geothermal heat supply system using solar energy and heat pumps. *Nauka Publishing House, Moscow*

[9] Unfried, K., Kis-Katos, K. & Poser, T. (2022). Water scarcity and social conflict. *Journal of Environmental Economics and Management, 113, 102633*. https://doi.org/10.1016/j.jeem.2022.102633

[10] Boguslavsky, E.I. (1995). Evaluation of technical and economic parameters and indicators of geothermal heat supply systems in various conditions of Russia. *International symposium «Problems of geothermal energy*

[11] Arutyunyants, R.R., & Gokhberg, L.K. (1983). Justification of the search for thermal waters in the Alma-Ata artesian basin to determine the prospects and scale of their practical use for health resort purposes. *Report «Geominvod»*

[12] Borisova, E.A. (2014). History of the development of conflicts over water resources in Central Asia in the post-Soviet period. *East (Oriens), Series «International Relations», 2, 80-86*

[13] Nachtnebel, H.P. (2000). The Danube river basin environmental programme: plans and actions for a basin wide approach. *Water Policy, 2(1-2), 113-129*. https://doi.org/10.1016/S1366-7017(99)00025-2

[14] Bishop, K., Lyon, S.W. & Dahlke, H.E. (2012). The relationship between land use and water. *Eos, Transactions American Geophysical Union, 93(28), 259*. https://doi.org/10.1029/2012EO280004

[15] Rosenfeld, L.M. (1952). Thermodynamic cycles of dynamic heating using the temperature difference of the cold season. *Reports of the USSR Academy of Sciences, 82(3), 45-56*

[16] Svalova, V.B. (2009). Geothermal resources of Russia and their complex use. *International Scientific Journal for Alternative Energy and Ecology, 7(75)*

[17] Gareev, A.M., Farkhutdinov, A.M., Farkhutdinov, I.M. & Cherkasov, S.V. (2014). Current state and prospects for the use of thermal power waters of the Russian Federation (on the example of the Khankalskoe deposit). *Bulletin of the Bashkir University, 19(3), 1-8*

[18] Farkhutdinov, A.M., Khamitov, I.Sh., Cherkasov, S.V., Mintsaev, M.Sh., Zaurbekov, Sh.Sh., Shaipov, A.A. & Labazanov, M.M. (2017). Thermal groundwaters of the east circulausian artesian basin: economic aspects of use on the example of the Khankalskoe deposit. *Bulletin of Tomsk Polytechnic University. Georesources Engineering, 328(1), 50-61*

[19] Dakik, B.A. (2025). Geothermal energy: potential, problems and development prospects. *Young Scientist, 25(576), 27-36*

[20] Charity, M.N., Ujah, C.O., Asadu, C.O., Kallon, D.V.V. (2025). Exploring geothermal energy as a sustainable source of energy: A systemic review. *Unconventional Resources, (6), 100149.* https://doi.org/10.1016/j.uncres.2025.100149

Жаркент бойының геотермалдық суларының негізінде жылу және электр энергиясын өндіру кешенін құру

М.К. Абсаметов, В.Д. Вялов, Д.К. Аденова*, А.М. Байкадамова

У.М. Ахмедсафин атындағы Гидрогеология және геоэкология институты, Алматы, Қазақстан

**Корреспонденция үшін автор: adenovadinara@gmail.com*

Аңдатпа. Бұл зерттеу объектісі Жаркент кен орнының геотермалдық ресурстарына баса назар аудара отырып, Қазақстан Республикасындағы жаңартылатын энергия көздері болып табылады. Геотермалдық энергетика – энергетикалық тәуелсіздік пен тұрақты дамуды қамтамасыз етудің перспективалық бағыты, әсіресе экономиканы декарбонизациялау және қазба отындарына тәуелділікті азайту қажеттілігі жағдайында. Бұл жұмыстың мақсаты Жаркент кен орнының геотермалдық ресурстары негізінде жылу және электр энергиясын өндірудің кешенді кешенін әзірлеу және ғылыми негіздеу болып табылады. Зерттеу кен орнының гидрогеотермиялық сипаттамаларын талдауды, қолданыстағы геотермиялық ұңғымалардың энергетикалық әлеуетін бағалауды және бинарлы геотермиялық қондырғыларды, жылу сорғы жүйелерін және тікелей жылумен жабдықтау жүйелерін қоса алғанда, ең тиімді технологияларды таңдауды қамтиды. Аймақтың климаттық, геологиялық және инфрақұрылымдық ерекшеліктерін ескере отырып, ұсынылған шешімдердің техникалық-экономикалық негіздемесі жасалды. Зерттеу нәтижелері геотермалдық энергетика саласындағы пилоттық жобаларды әзірлеуде, сондай-ақ «жасыл» экономикаға көшудің мемлекеттік стратегиясы аясында қолданылуы мүмкін. Ұсынылып отырған кешен Жетісу өңірінің энергетикалық тұрақтылығын арттыруға және Қазақстанның басқа аймақтарына ұқсас шешімдерді енгізуге үлгі болуға қабілетті.

Негізгі сөздер: *Жаркент ойпаты, геотермалдық сулар, геотермалдық технопарк.*

Создание комплекса производства тепловой и электрической энергии на основе геотермальных вод Жаркентской впадины

М.К. Абсаметов, В.Д. Вялов, Д.К. Аденова*, А.М. Байкадамова

Институт гидрогеологии и геоэкологии им. У.М. Ахмедсафина, Алматы, Казахстан

**Автор для корреспонденции: adenovadinara@gmail.com*

Аннотация. Объектом настоящего исследования выступают возобновляемые источники энергии в Республике Казахстан, с акцентом на геотермальные ресурсы Жаркентского месторождения. Геотермальная энергия представляет собой перспективное направление в обеспечении энергетической независимости и устойчивого развития, особенно в условиях необходимости декарбонизации экономики и снижения зависимости от ископаемых видов топлива. Целью данной работы является разработка и научное обоснование интегрированного комплекса по производству тепловой и электрической энергии на основе геотермальных ресурсов Жаркентского месторождения. В процессе исследования проведен анализ гидрогеотермальных характеристик месторождения, оценен энергетический потенциал существующих геотермальных скважин, а также осуществлён выбор наиболее эффективных технологий, включая бинарные геотермальные установки, теплонасосные системы и системы прямого теплоснабжения. Проведено технико-экономическое обоснование предложенных решений с учётом климатических, геологических и инфраструктурных особенностей региона. Результаты исследования могут быть применены при разработке пилотных проектов в сфере геотермальной энергетики, а также в рамках государственной стратегии перехода к «зелёной» экономике. Предлагаемый комплекс способен повысить энергетическую устойчивость Жетысуской области и стать примером для внедрения аналогичных решений в других регионах Казахстана.

Ключевые слова: *Жаркентская впадина, геотермальные воды, геотермальный технопарк.*

Publisher's note

All claims expressed in this manuscript are solely those of the authors and do not necessarily represent those of their affiliated organizations, or those of the publisher, the editors and the reviewers.

CONTENTS

Alimzhanova A.M., Sakhova B.T., Terlikbaeva A.Zh., Mukhametzhanova A.A., Maldybaev G.K., Seidakhmetova N.M., Vorotilo S.A., Koishina G.M.
THERMODYNAMIC CALCULATIONS AND CONSTRUCTION OF ELLINGHAM AND PHASE STABILITY DIAGRAMS FOR THE W-Ti-C-Co SYSTEM..... 1
Kakimov U.K., Kaipova A.A.
THERMOMECHANICAL PROCESSING OF HSLA STEELS: OVERVIEW..... 9
Sarsembekov T.K., Chepushtanova T.A., Merkibayev Ye.S., Yanko T.B.
DISTRIBUTION OF NIOBIUM DURING CHLORINE PROCESSING OF VARIOUS TITANIUM-CONTAINING FEEDSTOCKS..... 16
Nizamova A.T., Rasulov A.Kh., Maxmadiyev D.R.
ASSESSMENT OF INDUSTRIAL WASTE DISPOSAL PRACTICES IN THE MINING SECTOR OF UZBEKISTAN..... 23
Baibatsha A.B., Kembayev M.K., Rais S.E., Yan W., Amantayev A.K., Biyakyshev Y.T.
GEODYNAMICS OF THE SHU-ILE ORE ZONE: INTEGRATION OF GEOPHYSICAL, GEOCHEMICAL AND COSMOGEOLOGICAL METHODS..... 30
Absametov M.K., Vyalov V.D., Adenova D.K., Baikadamova A.M.
CREATION OF A COMPLEX FOR THE PRODUCTION OF HEAT AND ELECTRIC POWER BASED ON THE GEOTHERMAL WATERS OF THE ZHARKENT DEPRESSION... 37

МАЗМҰНЫ

Алимжанова А.М., Сахова Б.Т., Терликбаева А.Ж., Мухаметжанова А.А., Малдыбаев Г.К., Сейдахметова Н.М., Воротыло С.А., Койшина Г.М.
W–Ti–C–Co ЖҮЙЕСІ ҮШІН ЭЛЛИНГЕМНІҢ ФАЗАЛЫҚ ТҰРАҚТЫЛЫҚ ДИАГРАММАСЫ МЕН ФАЗАЛЫҚ БАСЫМДЫҚ ДИАГРАММАСЫН ҚҰРУ ЖӘНЕ ТЕРМОДИНАМИКАЛЫҚ ЕСЕПТЕУЛЕР..... 1
Какимов У.К., Каипова А.А.
HSLA БОЛАТТАРЫН ТЕРМОМЕХАНИКАЛЫҚ ӨҢДЕУ: ШОЛУ……. 9
Сарсембеков Т.К., Чепуштанова Т.А., Меркібаев Е.С., Янко Т.Б.
ХЛОРЛАУ ӨҢДЕУ ПРОЦЕСІНДЕ НИОБИЙДІҢ ӘРТҮРЛІ ТИТАНДЫ ҚҰРАМДЫ ШИКІЗАТТАРДА ТАРАЛУЫ..... 16
Низамова А.Т., Расулов А.Х., Махмадиев Д.Р.
ӨЗБЕКСТАННЫҢ ТАУ-КЕН СЕКТОРЫНДАҒЫ ӨНЕРКӘСІПТІК ҚАЛДЫҚТАРДЫ КӘДЕГЕ ЖАРАТУ ТӘЖІРИБЕСІН БАҒАЛАУ..... 23
Байбатша А.Б., Кембаев М.К., Раис С.Е., Ян В., Амантаев А.К., Биякышев Е.Т.
ШУ-ІЛЕ РУДАЛЫ ЗОНАСЫНЫҢ ГЕОДИНАМИКАСЫ: ГЕОФИЗИКАЛЫҚ, ГЕОХИМИЯЛЫҚ ЖӘНЕ КОСМОГЕОЛОГИЯЛЫҚ ӘДІСТЕРДІҢ ИНТЕГРАЦИЯСЫ..... 30
Абсаметов М.К., Вялов В.Д., Аденова Д.К., Байкадамова А.М.
ЖАРКЕНТ БОЙЫНЫҢ ГЕОТЕРМАЛДЫҚ СУЛАРЫНЫҢ НЕГІЗІНДЕ ЖЫЛУ ЖӘНЕ ЭЛЕКТР ЭНЕРГИЯСЫН ӨНДІРУ КЕШЕНІН ҚҰРУ..... 37

СОДЕРЖАНИЕ

Алимжанова А.М., Сахова Б.Т., Терликбаева А.Ж., Мухаметжанова А.А., Малдыбаев Г.К., Сейдахметова Н.М., Воротыло С.А., Койшина Г.М.
ТЕРМОДИНАМИЧЕСКИЕ РАСЧЕТЫ И ПОСТРОЕНИЕ ДИАГРАММ ФАЗОВОЙ СТАБИЛЬНОСТИ ЭЛЛИНГХЕМА И ФАЗОВОГО ДОМИНИРОВАНИЯ ДЛЯ СИСТЕМЫ W–Ti–C–Co…….……. 1
Какимов У.К., Каипова А.А.
ТЕРМОМЕХАНИЧЕСКАЯ ОБРАБОТКА СТАЛЕЙ HSLA: ОБЗОР ……...…..… 9
Сарсембеков Т.К., Чепуштанова Т.А., Меркибаев Е.С., Янко Т.Б.
РАСПРЕДЕЛЕНИЕ НИОБИЯ ПРИ ХЛОРНОЙ ПЕРЕРАБОТКЕ РАЗЛИЧНОГО ТИТАНСОДЕРЖАЩЕГО СЫРЬЯ……..……...… 16
Низамова А.Т., Расулов А.Х., Махмадиев Д.Р.
ОЦЕНКА ПРАКТИКИ УТИЛИЗАЦИИ ПРОМЫШЛЕННЫХ ОТХОДОВ В ГОРНОДОБЫВАЮЩЕМ СЕКТОРЕ УЗБЕКИСТАНА……..…. 23
Байбатша А.Б., Кембаев М.К., Раис С.Е., Ян В., Амантаев А.К., Биякышев Е.Т.
ГЕОДИНАМИКА РУДНОЙ ЗОНЫ ШУ-ИЛЕ: ИНТЕГРАЦИЯ ГЕОФИЗИЧЕСКИХ, ГЕОХИМИЧЕСКИХ И КОСМОГЕОЛОГИЧЕСКИХ МЕТОДОВ……..…… 30
Абсаметов М.К., Вялов В.Д., Аденова Д.К., Байкадамова А.М.
СОЗДАНИЕ КОМПЛЕКСА ПРОИЗВОДСТВА ТЕПЛОВОЙ И ЭЛЕКТРИЧЕСКОЙ ЭНЕРГИИ НА ОСНОВЕ ГЕОТЕРМАЛЬНЫХ ВОД ЖАРКЕНТСКОЙ ВПАДИНЫ…….. 37

Учредитель: Satbayev University

Регистрация:
Министерство информации и общественного развития Республики Казахстан
№ KZ19VPY00056529 от 30.09.2022

Официальный сайт: https://vestnik.satbayev.university/index.php/journal/

Основан в августе 1994 г. Выходит 6 раз в год

Адрес редакции:
г. Алматы, ул. Сатпаева,
22 тел.: 292-63-46